

# Report on the Harmonised SOPs on high throughput approaches for hazard assessment of ENMs

## DELIVERABLE 5.2

<b>Due date of Deliverable:</b>	31.12.2022
<b>Actual Submission Date:</b>	27.05.2023
<b>Responsible partner:</b>	UiB, Norway
<b>Report Author(s):</b>	Mihaela Roxana Cimpan, Ivan Rios-Mondragon, Håkon van Ta, Ole-Bendik Hofshagen, Medhusja Nalliah (UiB); Naouale El Yamani, Elise Runden-Pran, Maria Dusinska, Eleonora Longhin (NILU); Valerie Fessard, Julia Varet (ANSES); Sivakumar Murugadoss, Peter Hoet (KUL); Ivana Vinkovic Vircek (IMI); Michael Burgum, Shareen Doak (SU); Anita Sosnowska, Natalia Bulawska, Tomasz Puzyn (QSARL).
<b>Reviewed by:</b>	
<b>Nature:</b>	R (Document, report)
<b>Dissemination Level:</b>	PU (Public)
<b>Call:</b>	H2020-NMBP-13-2018
<b>Topic:</b>	Risk Governance of nanotechnology
<b>Project Type:</b>	Research & Innovation Action (RIA)
<b>Name of Lead Beneficiary:</b>	NILU, Norway
<b>Project Start Date:</b>	1 January 2019
<b>Project Duration:</b>	50-Months



## Document History

<i>Version</i>	<i>Date</i>	<i>Authors/ who took action</i>	<i>Comment</i>	<i>Modifications made by</i>
<i>0.1</i>	03-05-2023	Mihaela Roxana Cimpan, Ivan Rios-Mondragon, Håkon van Ta and Ole-Bendik Hofshagen (UiB)	First Draft	
<i>0.2</i>	23-05-2023	Mihaela Roxana Cimpan (UiB)	Draft sent to WP partners, leader and PMO	Anita Sosnowska (QSARL), Naouale El Yamani, Eleonora Longhin, Maria Dusinska (NILU)
<i>1.0</i>	27-05-2023	Eleonora Longhin (PMO, NILU)	Submitted to Commission	



## Abstract

Adoption of high throughput screening (HTS) and high content analysis (HCA) methods in the hazard assessment of engineered nanomaterials (ENMs) allows the testing of large numbers of different materials, over a range of concentrations, time points, and cell types, in order to rapidly evaluate multiple toxicological endpoints. HTS/HCA approaches offer several advantages aside from their speed, including reduced inter-experimental variation, and both time and cost savings.

**The aim of Task 5.2** was to assess the reliability, reproducibility, and suitability of HTS and HCA methods for the hazard assessment of ENMs, and thus, to speed up the transition towards a reliable, robust, and cost-efficient hazard and risk assessment. For this purpose, traditional and alternative *in vitro* assays, including impedance-based methods, were compared in an interlaboratory testing, by addressing the same endpoints and using the same cell lines, ENMs, controls, exposure conditions and protocols established in WP4 and WP5.

Task 5.2 has built upon Task 5.1, by making use of the Standard Operating Procedures (SOPs), results and conclusions drawn in this task. First, the reliability of the methods was evaluated. Then, the reproducibility of the methods employed in Task 5.2 was assessed. For this, the results obtained in the two round robins, RR1 & RR2, in Task 5.1, were also used.

One of the main sources of uncertainties in nanotoxicity assessment is represented by ENM interferences with testing systems. To address this, impedance-based methods that are label-free and thus, less prone to interferences were employed. Another important advantage of such methods is monitoring of cells in real-time, which allows the identification of relevant concentrations and timepoints for further in-depth mechanistic studies. Impedance-based monitoring gives information about cell proliferation, adhesion, and viability and by coupling it with live microscopy, a more complete image of cellular behaviour during ENM exposure can be obtained. Furthermore, CV, an electrochemical method, was adapted for the first time for the assessment of ENM-induced oxidative stress in a label-free manner (UiB) and a mathematical model to interpret the results was developed (HVL).

The data obtained, the methods and the biological models are also feeding into NanoHarmony activities for further evaluation and into inter-laboratory comparisons (ILCs), to support the activities of the OECD Working Party on Manufactured Nanomaterials (WPMN) and other standardization bodies. This activity forms the basis of SOPs to be taken forward as guidance documents, to ensure the translation of the scientific data generated into risk management tools underpinning a human risk assessment framework.

## TABLE OF CONTENTS

Document History.....	2
Abstract .....	3
TABLE OF CONTENTS.....	4
List of Abbreviations .....	8
1. Introduction .....	10
2. Background.....	11
2.1 Cytotoxicity methods employed in Task 5.2 .....	12
2.1.1 Impedance-based label-free nanotoxicity testing .....	13
2.1.2 Cyclic voltammetry for label-free assessment of ENM-induced oxidative stress .....	15
2.1.2 High Content Analysis.....	17
2.1.3 Alamar Blue and WST-1 assays.....	18
2.2 Genotoxicity methods employed in Task 5.2.....	18
2.2.1 COMET assay.....	18
2.2.2 Micronucleus assay .....	19
2.2.3. The $\gamma$ H2AX assay.....	19
3. Methodology.....	20
3.1 Literature review conducted to select methods for interlaboratory testing .....	20
3.2 Cell types and ENMs employed in Task 5.2.....	21
3.3 Impedance-based testing of ENM toxicity on adherent cells (UiB).....	23
3.3.1 Cell culture.....	23
3.3.2 Nanomaterials and dispersion protocols .....	24
3.3.3 ENM characterization in exposure media.....	25
3.3.4 Impedance-based toxicity testing using the xCELLigence system .....	26
3.3.5 16-well E-plate preparation and treatment.....	27
3.4 Impedance-based flow cytometry (IFC) (UiB).....	28
3.4.1 U937 cell culture and testing by IFC.....	28
3.5 3D Microvasculature formation in a microfluidic chip (UiB) .....	29
3.5.1 Fabrication of the microfluidic chip.....	29
3.5.2 Setup of the microfluidic system.....	32
3.5.3 Bubble trap fabrication.....	33



3.6. Cyclic Voltammetry to Monitor Total Antioxidant Capacity of In-Vitro Biological Models Exposed to Nanomaterials (UiB) .....	33
3.6.1 Electrode configuration.....	33
3.6.2 Oxidative potential of ENMs in Hank’s balanced salt solution.....	33
3.6.3 Data Analysis .....	34
3.6.4 Modelling of results from electrical impedance-based methods and CV.....	34
3.7. HCA assessment of cell count, nuclear size, nuclear intensity, caspase-3 intensity, and $\gamma$ H2AX intensity (ANSES) .....	34
3.8. COMET assay (NILU).....	35
3.9 <i>In Vitro</i> Micronucleus Assay Round Robin (SU, ANSES).....	36
4. Results.....	37
4.1 Results of the literature review .....	37
4.2 Impedance-based label-free monitoring of cell proliferation and viability (xCELLigence system) (UiB, NILU) .....	38
4.2.1 Hydrodynamic diameter and Zeta potential of ENMs.....	38
4.2.2 Impedance-based measurements using the xCELLigence system.....	39
4.3 Cell viability assessed by Impedance-based Flow Cytometry (UiB).....	45
4.3.1 IFC of U937-cells exposed to nano-CuO (Plasmachem).....	45
4.3.2 IFC of U937-cells exposed to nano-ZnO (Sigma) .....	46
4.4 Microfluidic system (UiB).....	48
4.4.1 Fabrication of the microfluidic chip.....	48
4.4.2 Optimal cell ratio to co-culture HULEC-5a and Fibroblast.....	48
4.5. Results from the colorimetric tests (NILU, KUL, INIC, ANSES) .....	50
4.5.1. Dispersion protocol .....	50
4.5.2. Overview of colorimetric methods, cell lines and exposure conditions.....	51
4.5.3. RR1 and RR2 Summary of data (NILU, KU Leuven, INIC) .....	52
4.5.4. Comparison of the methods between partners (RR1 & RR2 data in Task 5.1).....	52
4.5.5. Summary of data obtained with colorimetric methods in Task 5.2.....	58
4.5.6. Comparison of the data obtained with each method and compilation of all RRs data including task 5.2 data.....	60
4.5.7. Test for possible ENM-induced interferences.....	60
4.5.8. Advantages and disadvantages of colorimetric tests.....	61
4.5.9. Recommendations regarding colorimetric methods used in T 5.1 and T 5.2 .....	62

4.5.10 Conclusion on the results from the colorimetric tests.....	62
4.6. High Content Analysis (HCA) of cell count, nuclear size, nuclear intensity, caspase-3 intensity, and DNA double strand breaks .....	63
4.6.1. Results from HCA analysis in A549 cells: Negative and positive controls .....	63
4.6.2. CuO: Results from HCA analysis in A549 cells .....	66
4.6.3. WC/Co: Results from HCA analysis in A549 cells .....	69
4.6.4. NM-300K and its diluent: Results from HCA analysis in A549 cells .....	72
4.6.5. TiO <sub>2</sub> (JRC): Results from HCA analysis in A549 cells .....	77
4.6.6. ZnO (Sigma): Results from HCA analysis in A549 cells.....	80
4.6.7. ZnO NM-111 (JRC): Results from HCA analysis in A549 cells .....	83
4.6.8. Nanocyl 7000 and its diluent: Results from HCA analysis in A549 cells.....	86
4.6.9. Conclusion HCA Analysis.....	90
4.7 Genotoxicity testing using the Comet assay (NILU) .....	91
4.7.1 <i>In Vitro</i> comet Assay data from RR1 and RR2 (DELIVERABLE D5.1) also included in T5.2 .	91
4.7.2 <i>In Vitro</i> comet Assay data from Task 5.2 (NILU data) .....	92
4.7.3. Categorization of the ENMs following the NanoREG2 approach .....	93
4.7.4 Test for interferences .....	93
4.7.5 Advantages and disadvantages.....	94
4.7.6. Recommendations.....	94
4.7.7. Statistical Analysis .....	95
4.7.8 Conclusion regarding the Comet Assay medium-throughput format.....	95
4.8 Micronucleus Test – results obtained by ANSES.....	95
4.8.1. Aim of task 5.2 regarding the micronucleus assay.....	95
4.8.2. Development of an SOP for task 5.2: SOP for a micronucleus assay on TK6 cells using cytochalasin B in a 12-well plate format. ....	96
4.8.3 Cytotoxicity, RICC and micronuclei analysis of TK6 cells.....	97
4.8.4. Comparison of micronucleus data gathered in the 12-well plate format in the absence of cytochalasin B, manual counting versus automated scoring. ....	99
4.8.5. Results for Task 5.2: micronucleus assay on TK6 cells using cytochalasin B in a 12-well plate format. ....	102
4.9. Micronucleus Assay - Results from Swansea University regarding Task 5.2.....	107
4.9.1. <i>In vitro</i> micronucleus assay data generated by Swansea University using the ANSES 12-well format SOP on mononucleated TK6 cells.....	107

4.9.2. In <i>vitro</i> cytokinesis-blocked micronucleus assay data generated by Swansea University using the ANSES 12-well SOP with additional cytochalasin B step added.....	108
4.9.3. Comparison of data obtained from both partners (ANSES and SU) following the SOP from T5.1 and T5.2.....	109
4.9.4. Tests for interferences .....	112
4.9.5. Statistical Analysis .....	113
4.9.6. Conclusion regarding task 5.2 and the micronucleus assay in a high throughput format. ....	113
5. Results analysis .....	113
5.1. Comparison of the Impedance-based method (xCELLigence) with the HCA testing for cell proliferation and viability assessment (QSAR Lab).....	113
5.1.1. Presentation of data, summary of data, data analysis, and evaluation .....	114
5.1.2. Conclusion on the comparison of impedance-based method with HCA testing for cell proliferation and viability assessment.....	116
5.2. Repeatability testing of the Impedance-based method (xCELLigence): Data from UiB, NILU, and CEA (QSAR lab) .....	117
5.2.1. Summary of results .....	117
5.2.2. Conclusion on repeatability testing of the impedance-based method .....	117
5.3 SOPs.....	119
6. Final conclusions .....	119
7. References.....	121
ANNEX 1 .....	128

## List of Abbreviations

3D	Three-dimensional
AA	Ascorbic acid
AB	Alamar Blue
AC	Alternating current
ANSES	French Agency for Food, Environmental and Occupational Health & Safety
BSA	Bovine serum albumin
CA	Comet Assay
CCM	Cell culture medium
CE	Counter Electrode
CFE	Colony forming efficiency
CI	Cell index
CNT	Carbon nanotube
CuO	Copper oxide
CV	Cyclic voltammetry
DLS	Dynamic light scattering
DMEM	Dulbecco's modified Eagle's medium
DSB	Double strand breaks
DSE	Delivered sonication energy
EC	Effective concentration
EDTA	Ethylenediaminetetraacetic acid
ENM	Engineered nanomaterial
FBS	Foetal bovine serum
FC	Foldchange vs control
Fpg	Formamidopyrimidine DNA glycosylase
HDD	Hydrodynamic diameter
HCA	High content analysis
HTS	High throughput screening
HVL	Høgskulen på Vestlandet
IFC	Impedance-based flow cytometry
ILC	Inter-laboratory comparison





INT	Interference controls
JRC	Joint Research Centre
KUL	Catholic University of Leuven
LMWA	Low-molecular-weight antioxidant
MWCNT	Multi-walled carbon nanotube
N <sub>2</sub>	Nitrogen
NC	Negative control
NCI	Normalized cell index
NILU	Norwegian Institute for Air Research
OECD	Organization for Economic Cooperation and Development
PBS	Phosphate-buffered saline
PC	Positive Control
PDI	Poly dispersity index
PDMS	Polydimethylsiloxane
PS	Penicillin Streptomycin
RE	Reference Electrode
RR	Round Robin
SBs	Strand Breaks
SD	Standard deviation
SOP	Standard operating procedure
SPSF	Standard project submission form
SU	Swansea University
TAC	Total antioxidant capacity
UA	Uric Acid
UiB	University of Bergen
WE	Working Electrode
WPMN	Working Party on Manufactured Nanomaterials
QSARL	QSAR Lab Ltd.
ZP	Zeta potential



## 1. Introduction

This deliverable represents the outcome of the RiskGONE Task 5.2 “*Report on the harmonised SOPs on high throughput approaches for hazard assessment of ENMs*”. The demand for reliable high-throughput and high-content testing systems to assess the toxicity of engineered nanomaterials (ENMs), both at an initial screening level and at a more in-depth mechanistic level, is urgent due to the rapid development of new and more complex ENMs and their applications.

The aim was to provide high throughput screening (HTS) and high content analysis (HCA) *in vitro* assays that are reliable, robust, cost-efficient, and ecologically friendly for nanomaterial-related hazard assessment, having also in view their applicability for regulatory OECD testing.

This aim has been accomplished by comparing *in vitro* assays that assessed the same cellular endpoints using the same biological models, ENMs and exposure conditions. The first step was to conduct a thorough literature review and analysis of HTS/HCA methods used in nanotoxicity testing, which is presented in this deliverable.

The heterogeneity and increasing complexity of ENMs severely limit the feasibility of producing general toxicity protocols to address hazard assessment. Moreover, ENMs have been shown to often interfere with testing systems, which enhances the uncertainty regarding their biological effects (Kroll et al. 2012, Seiffert et al. 2012, Vinkovic et al. 2015, Ostermann et al. 2020). This leads to an increasing and urgent demand for reliable, robust and validated protocols for testing ENM toxicity, which are essential for the environmental, and implicitly human health-related hazard and risk assessment (Collins et al. 2016, Fadeel et al. 2018). So far, no consensus has been established regarding models and tests to assess the *in vitro* toxicity of ENMs and at present no clear regulatory guidelines on testing and evaluation are available (Drasler et al. 2017).

HTS techniques aim at accurately assessing and predicting the toxicity of large numbers of ENMs in a timely manner and with savings in labour costs are clearly needed. HTS is defined as the use of automated tools to facilitate rapid execution of a large number and variety of biological assays that may include several substances in each assay (Collins et al. 2016). HTS was introduced in the pharmaceutical and chemical industries as a rapid way of evaluating effects of many novel compounds. Another central tool in pharmaceutical industry, now widely used in various research areas, is represented by HCA, which combines automated image acquisition and powerful algorithms designed to quantify and extract a maximum of information from a population of cells. HCA generates great quantities of data for a multitude of cellular aspects, frequently based on changes in fluorescence intensity and distribution of intracellular targets, allowing researchers to characterise and quantify biological responses at the level of the individual cell as well as for whole cell populations. Advantages and challenges pertaining to HTS/HCA approaches in ENM safety evaluation have been previously identified and comprehensively summarised (Collins et al., 2016).

Provided that reliable toxicity metrics will be established, the HTS/HCA approach can generate large and valuable data sets and facilitate the hazard ranking of ENMs, through the generation of database(s) with all reported effects on human health. One of the main priorities in nanotoxicology is the development of new or adaptation of existing instruments and methods and are not distorted by ENM-caused interferences with assay components and/or testing systems (Dusinska et al. 2015, Guadagnini et al. 2015). Some of the most encountered interferences are with fluorescent markers, which could be adsorbed onto ENMs preventing the markers from being available to bind to cellular structures of interest. In some cases, ENMs fluoresce themselves and/or are able to act as fluorescence quenchers. Moreover, a general drawback of fluorescence-based assays is that a good quantification of fluorescence is difficult to obtain. During handling through multiple steps in traditional toxicity assays cells can become

permanently modified and damaged. Such assays are oftentimes time-consuming, labour-intensive, and complex (Ceriotti et al. 2007). Another drawback of many traditional methods is that they can only evidence effects at a specific point in time and thus do not give an overview of the biokinetic behaviour and of the real-time interactions between biological structures and toxicants over time (Ceriotti et al. 2007). The need for label-free detection methods that can monitor the cells in real-time has therefore emerged, especially in nanotoxicity studies.

For the initial high-throughput toxicity screening, the electrical impedance-based monitoring of cells that allows for *real-time and label-free cell* assessment of proliferation, viability and adhesion of adherent cells, while minimizing the possibility of ENM interference, was employed by UiB (Cimpan et al. 2013). The electrical impedance method uses the electrical characteristics of cells to monitor cellular behavior continuously over longer time intervals, up to two weeks. For single cells, impedance-based flow cytometry (IFC) was used (UiB). The impedance-based screening is time-, manpower- and cost- efficient and does not require chemical reagents, which makes it more eco-friendly compared to traditional methods. Furthermore, a *microfluidic-chip impedance-based system* combined with live-imaging was developed to mimic the dynamic *in vivo* exposure to ENM dispersions (UiB) (Ruzycka et al. 2019).

Traditional colorimetric methods for assessing cytotoxicity were included for evaluation in T5.2. These were represented by Alamar blue and WST-1, which test cellular metabolic activity (NILU, KUL).

Cell proliferation and viability were also evaluated by HCA in T5.2 using the cell count, nuclear size, and nuclear intensity assessment (ANSES).

To assess oxidative stress in a label-free manner, UiB has established cyclic voltammetry (CV) for nanotoxicity testing using human lung cancer A549 epithelial cells. Mathematical models were developed to interpret the results of CV and of impedance-based testing on adherent cells, the latter incorporating the kinetics of cellular response to ENMs (HVL).

Genotoxicity is an essential part of the safety assessment of ENMs, therefore genotoxicity endpoints need to be included in ENMs' hazard and risk assessment. These were addressed in Task 5.2 by using methods with high throughput potential, i.e., the COMET assay (NILU) and the micronucleus assay (SU, ANSES), as well as by HCA  $\gamma$ H2AX testing (ANSES).

The ENMs were dispersed following the Standard Operating Procedures (SOPs) developed in WP4, as well as the NANOGENOTOX protocol for a subset of ENMs. The Hydrodynamic diameter was measured at the beginning and end of exposure using the Dynamic light scattering (DLS) method.

Task 5.2 has built upon Task 5.1, by making use of the SOPs, results and conclusions drawn in this task. *Additionally, the reliability and the reproducibility of the methods employed in Task 5.2 was assessed. For this, the results obtained in the two round robins, RR1 & RR2, in Task 5.1, were also used.*

## 2. Background

The literature review conducted by all partners to identify promising HTS and HCA methods, as well as methods with HTS and HCA potential for ENM-related hazard assessment, produced an insufficient number of high-quality peer-reviewed publications based on the GuideNano scoring system (Fernandez-Cruz et al. 2018) to allow a proper selection of methods. Furthermore, some of the methods were not available at the partners' laboratories. It was therefore decided to proceed with the interlaboratory comparison using the partners' methods for cytotoxicity and genotoxicity evaluation. The backgrounds for the methods selected for interlaboratory comparison with regard to reliability and reproducibility, as well for new methods developed in RiskGONE, are presented below.

The methods were compared based on the biological endpoints. Both the HTS and HCA methods were grouped in two main categories: Cytotoxicity and Genotoxicity methods (Tables 1 and 2).

**Table 1 - Cytotoxicity methods grouped according to endpoint**

Method (partner)	Endpoints addressed	HTS / HCA
Bioimpedance (UiB)	Proliferation, viability	HTS
Cell count (ANSES)	Proliferation, viability	HCA
Nuclear intensity	Proliferation, viability	HCA
Nuclear size	Proliferation, viability	HCA
WST-1 (KUL)	Metabolic activity	HTS
Alamar blue (NILU)	Metabolic activity	HTS

**Table 2 – Genotoxicity methods**

Method (partner)	Endpoints addressed	HTS / HCA
COMET assay (NILU)	DNA breaks	HTS
Micronucleus assay (SU and ANSES)	DNA damage	HTS
Micronucleus assay +/- cytochalasin (ANSES and SU)	DNA damage	HTS
$\gamma$ H2AX (ANSES)	Double strand breaks	HCA

## 2.1 Cytotoxicity methods employed in Task 5.2

There is a wide range of methods that can be used to investigate the cytotoxic effects of chemicals and other test substances, including ENMs. These methods are based on diverse principles and cell functions, e.g., membrane integrity assessed by label-free assays, such as impedance-based flow cytometry (Ostermann et al. 2020), and by colorimetric assays, such as trypan blue exclusion, neutral red uptake, LDH release; cellular proliferation in a population, which also reflects cell death, such as the label-free impedance-based monitoring (Cimpan et al. 2013) and relative population doubling; the ability to survive and form colonies by the colony forming efficiency assay (CFE), and cellular metabolic competence (Riss et al., 2016, 2019).

Metabolically active cells maintain a reducing environment within their cytosol. This reducing capacity is utilized in colorimetric or fluorometric redox indicators, and their conversion that can be measured spectrophotometrically. These methods include those with tetrazolium salt-based assays such as MTT and WST-1, and the Alamar Blue (AB) assay.

Within the H2020 RiskGONE project, the cytotoxicity/cellular metabolic activity of cells exposed to different ENMs was analysed through a battery of HTS/HCA tests by impedance-based real-time

monitoring and several colorimetric methods in order to evaluate the suitability of the methods for nanotoxicity testing, as well as identifying the most robust testing system(s). Both adherent (A549) and suspension cells (TK6) were used in these assays. Interference controls were included.

A method paper has been published by NILU TEAM in a Frontier special issue where the use of colorimetric assays, especially the AB assay, for ENMs testing was addressed (Longhin et al. 2022). This paper provides support to a sound safety assessment of ENMs by providing a detailed procedure that can be tested among different laboratories as a step forward toward standardisation of this method having in view the possibility to submit to OECD a standardized and validated published procedure as a standard project submission form (SPSF). The same is envisioned for the impedance-based label-free monitoring of adherent cells established at UiB for ENM testing as a label-free, less prone to interference and eco-friendly method.

Before task 5.2 started, Task 5.1 was conducted with the aim to develop robust assays as well as to deliver robust SOPs to study the toxicity of nanomaterials by conducting several round-robins (RR1 & RR2) amongst partners. Several ENMs were tested, and several partners joined one or both RRs and provided data within Task 5.1 which were reported in Deliverable 5.1. For task 5.2, NM300K and NM111 were to be tested following the developed SOPs within 5.1.

### 2.1.1 Impedance-based label-free nanotoxicity testing

Electrical impedance-based assays that measure the electrical properties of cells are label-free and represent a reliable alternative with the potential to become a method of choice for the initial screening of ENMs' toxic effects. They take advantage of the passive properties of an object, which occur when the object is composed of dissipative elements, such as ohmic resistors or conservative elements such as capacitances and inductances. It measures how much objects, such as cells, impede a flow of electrical current. Proliferation, growth, morphology, and adhesion can be measured by applying an electric source to an electrode covered by cells, and measuring how the cells impede the current. By using alternating current (AC) information about the properties of the cells as a function of signal frequency is obtained. Cell membranes are insulating structures with an abundance of negatively charged molecules on the inside as compared to the outside, which give rise to the resting potential of the membrane. When a time-oscillating electric field is applied, a change in the charge distribution will ensue, with charged molecules trying to follow the electric field. The polarisation effect depends on frequency and gives rise to  $\alpha$ -,  $\beta$ - and  $\gamma$  dielectric dispersions (Pliquett 2010) (Fig. 1).

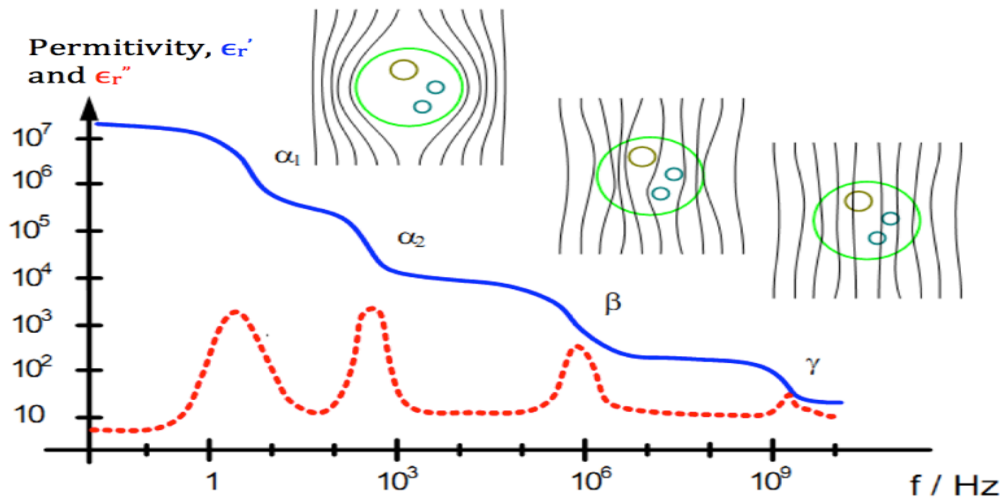


Fig. 1. Dispersion types. The higher frequencies allow easier passage of current through the cell. The real dielectric number  $\epsilon_r'$  is shown in blue, while the imaginary part  $\epsilon_r''$  is shown in red.  $\alpha$ -dispersion has an active cell-membrane effect. In  $\beta$ -dispersion, the passive cell membrane-capacitance is observed. The  $\gamma$ -dispersion is due to polarisation of the medium in the cell (water, salts, proteins). Figure adapted by Pliquett from Schwan and Kay (1957).

For a cell placed between two electrodes, there is a relationship between the different dispersions and the polarisation of the cell (Fig. 2). At low frequencies, a lateral movement of ions along insulating membranes takes place, giving rise to  $\alpha$ -dispersion. As a result, a high polarisation of the membrane is obtained together with a high permittivity. Impedance measuring at low frequencies gives information about the size of the cell (Cheung et al. 2010). When frequency is increased, the charged molecules cannot follow the electric field anymore, because of its rapid fluctuation, leading to a decrease in the capacitance of the membrane. Between 100 kHz and 10 MHz the rapid depolarisation known as  $\beta$ -dispersion can be observed and measurements within this range can give information about membrane properties (Prodan et al. 2008, Pliquett 2010). At very high frequencies (1GHz),  $\gamma$ -dispersion occurs as a result of the polarisation of water, salts and proteins in the cell.

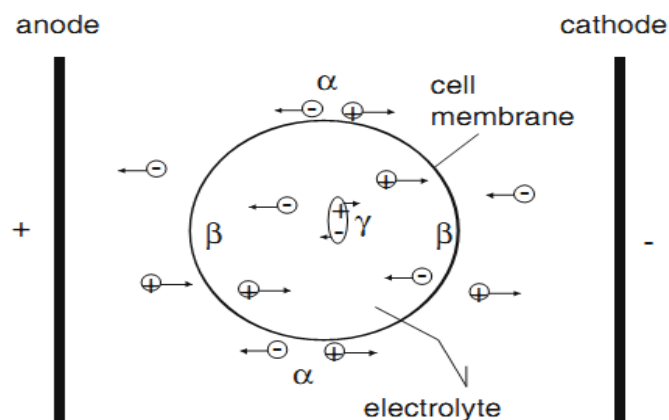


Fig. 2. Polarisation mechanisms for a cell situated between two electrodes. Movement of ions along the cell membrane gives  $\alpha$  a-dispersion.  $\beta$ -dispersion occurs as the cell membrane is depolarised. The  $\gamma$ -dispersion is recognised as polarisation of macromolecules (Pliquett, 2010).

Impedance-based methods have an advantage when compared to traditional methods because they allow “*in situ*” real-time recordings without the use of markers, as well as monitoring of the dynamics in cell growth and viability (Hondroulis et al. 2010). For this, the xCELLigence system (Agilent Technologies, Santa Clara, CA, USA) was used in WP5 to monitor the effects of ENMs on adherent cells (UiB). For cells in suspension, the microfluidic chip-based impedance flow cytometer (IFC) Ampha Z30 (Amphasys AG) has been introduced by UiB for nanotoxicity testing in human cells in suspension (Ostermann et al. 2020). Furthermore, a bioimpedance- and live-microscopy-based microfluidic system and microfluidic impedance-based chips have been designed and produced (UiB) for testing and recording of adherent cells and biomimetic biological structures, such as co-cultures, lung-on-a-chip and microvasculature-on-a-chip, in real-time under dynamic exposure. The system is currently being optimised and throughput has been increased.

### 2.1.2 Cyclic voltammetry for label-free assessment of ENM-induced oxidative stress

To assess the putative oxidative stress induced by ENMs, CV was implemented in WP5 (UiB). CV is a label-free method, which can be used to assess the redox-properties of biofluids by applying an electrical potential in a cyclic manner and measuring the resulting current as electrons are transferred in a redox reaction. Because most low-molecular-weight antioxidants (LMWAs) are reducing agents that scavenge ROS and quench them by electron donation, measuring a sample's total reducing power by CV can reveal the LMWA activity in the sample (Chevion et al. 2000). The oxidative scan is crucial for evaluating the total antioxidant capacity (TAC) because it gives critical details about the antioxidant content of the sample. As it can be seen in Figure 3, the anodic peak current,  $i_{pa}$ , describes the antioxidant's reducing power, and the anodic peak potential,  $E_{pa}$ , characterizes the specific antioxidant measured. Together, they provide information on what antioxidants are present, their inherent capacity of reducing other substances, and their concentrations. The  $i_{pa}$  increases linearly with concentration and can thus, be used to estimate the antioxidant concentration (Psotova et al. 2001). The resulting micro-scale currents make it possible to track even minute changes in antioxidant capacity. When a voltage is applied to the working electrode, it becomes sufficiently positive or negative to oxidise or reduce the molecule of interest. In the case of an oxidative scan, the current increases until it reaches the  $i_{pa}$ , then decreases as the reduced state of the molecule of interest depletes at the anodic surface.

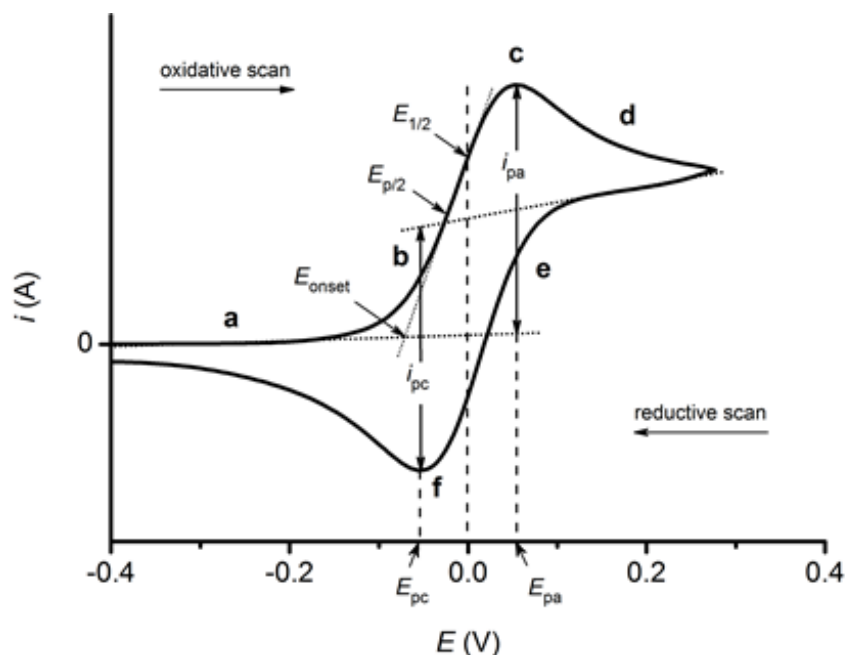


Fig. 3. Typical cyclic voltammogram where  $i_{pc}$  and  $i_{pa}$  show the cathodic and anodic peak current, respectively.  $E_{pc}$  and  $E_{pa}$  show the cathodic and anodic peak potential, respectively.

A cyclic voltammogram's oxidative scan is heavily reliant on the antioxidants present in the sample, as they donate electrons at their oxidation potential. As a result, the integrated value of the oxidative scan can be presented as the sample's total antioxidant capacity. This method of evaluating antioxidant capacity, however, does not determine which specific antioxidants are present. Various antioxidants can be distinguished by the anodic peak potential at which they are oxidised. The potency of the antioxidants determines the potential for oxidation. For example, ascorbic acid (AA) is a more effective antioxidant than uric acid (UA) and is oxidised at a potential that is about 40 mV lower than UA (Chevion et al. 1997). In more complex biological samples where several antioxidants may contribute to the overall current, it has been proposed that the TAC may prove more useful when monitoring changes in antioxidant content than  $I_{pa}$  (Chevion et al. 1999). Because antioxidants are depleted during oxidative stress and CV is very sensitive to changes in antioxidant concentration, this approach has been demonstrated to be capable of tracking oxidative stress (Chevion et al. 1997). For electrochemically reversible couples when both the oxidized and reduced form is stable in solution and does not readily react with other species and can therefore be oxidized/reduced to its original state, the redox potential ( $E^\circ$ ) for the couple is the midpoint between  $E_{pc}$  and  $E_{pa}$ . Figure 4 shows a schematic representation of a traditional electrochemical cell and a commercial screen-printed electrode. CV typically employs a three-electrode configuration: the working, counter and reference electrodes. The oxidation/reduction reaction takes place at the working electrode. A potentiostat is used to apply a working electrode potential that is a function of the reference electrode potential. The working electrode's most significant properties are that it is inert to redox reactions and that it has a clean surface. The purpose of the reference electrode is to have a stable and well-defined equilibrium potential. This is extremely valuable since it serves as a reference against which the other electrodes are measured. Silver wires fed into a glass tube filled with electrolyte solution are commonly used as a reference electrode. The electrical current begins to flow when a voltage is provided to the working electrode and a redox reaction occurs. The counter electrode completes the circuit, allowing the current to be measured (Elgrishi et al. 2018).



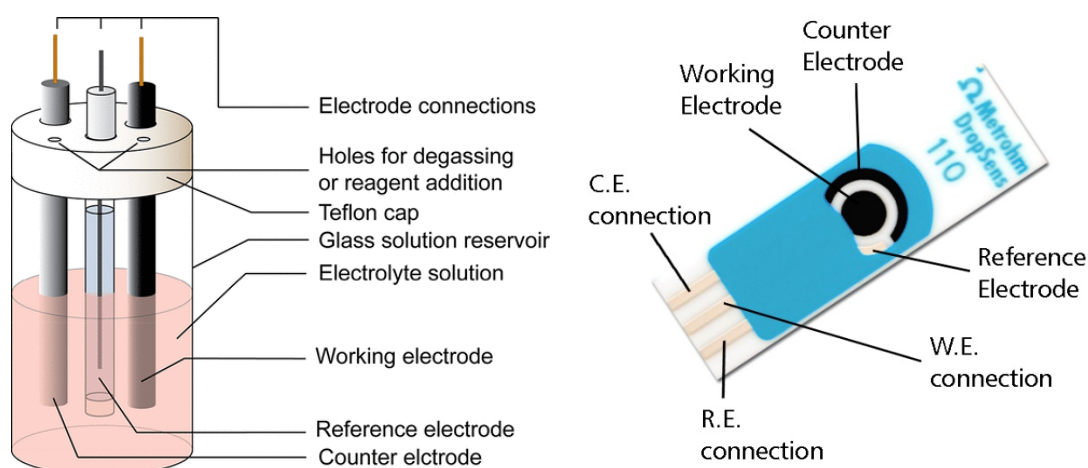


Fig. 4. Traditional electrochemical cell (left) and commercial screen printed electrode (right).

The microfluidics system, CV, and IFC were part of the R&D within task 5.2 and were not included in the interlaboratory comparison. Only the impedance-based method for adherent cells performed with the xCELLigence system (Agilent) (Cimpan et al. 2013) was included in the interlaboratory comparison of methods.

### 2.1.2 High Content Analysis

From its debut in the mid-1990s, developments in cellular imaging have rendered HCA an important tool for understanding biological processes induced by diverse xenobiotic molecules. Originally an approach used almost exclusively in the pharmaceutical industry to screen potential drug candidates aimed at specific targets, this technology is now widely used by researchers in many disciplines to study a wide range of cellular responses.

Combining automated image acquisition and powerful algorithms designed to quantify and extract a maximum of information from individual cells, HCA generates great quantities of data for a large number of cellular characteristics, including changes in fluorescence intensity and distribution of intracellular targets, as well as detailed information on cellular and nuclear morphology. The speed of analysis, the multiparametric nature of the analysis, combined with the quantity and quality of data, make HCA an efficient and powerful approach to study a wide range of cellular processes and responses. The miniaturization of cellular toxicity assays greatly increases the number of ENMs that can be analyzed within a single assay. In addition, automated image analysis and quantification of markers of cellular toxicity in individual cells makes HCA a powerful tool for the evaluation of the mechanisms of toxicity of ENMs. Limitations associated with the time required for the dispersion protocol do not allow high throughput screening. The use of an HCA approach, however, generates multiparametric data for a number of cellular parameters in individual cells. While the approach is not high throughput, the use of HCA generates a high content of data. High content imaging represents a promising approach in the prediction and evaluation of ENM toxicity. Combined with complementary HTS methods, HCA provides valuable information on the mechanistic pathways involved in toxicity and cellular responses.

High Content Analysis is perfectly adapted for the testing and quantification of markers of cytotoxicity, genotoxicity, oxidative stress, etc. providing that the appropriate controls are in place to evaluate possible interference artifacts with certain ENMs. A large number of ENMs can be tested in a single assay, and multiple markers of cellular toxicity pathways can be analyzed with individual cells, thereby allowing the correlation of toxicity endpoints. The results obtained from the HCA methodology in this project were reliable and reproducible.

All methods and cellular toxicity markers were developed prior to the start of the RiskGONE project. Apart from additional controls to assess ENM interference, no considerable modifications were made to existing HCA protocols.

### 2.1.3 Alamar Blue and WST-1 assays

Cytotoxic methods such as **AlamarBlue®** measure cytotoxicity through a colorimetric response to the intracellular reducing metabolism of living cells. The conversion of resazurin (oxidised form) to resorufin (reduced form) results in colorimetric and fluorescence changes; resazurin is blue and non-fluorescent whereas resorufin is red and highly fluorescent. As other colorimetric methods also AlamarBlue may be prone to interference thus additional control should be included as previously suggested (Guadagnini et al. 2015).

Tetrazolium salts, such as MTT (3-(4,5-dimethyl-2-thiazolyl)-2,5-diphenyl-2H-tetrazolium bromide), XTT (2,3-bis-(2-methoxy-4-nitro-5-sulfophenyl)-2H-tetrazolium-5-carboxanilide), and **WST-1** (2-(4-iodophenyl)-3-(4-nitrophenyl)-5-(2,4-disulfophenyl)-2H-tetrazolium), are widely employed to assess cellular metabolic activity, by utilizing their cellular reduction to formazan products. However, tetrazolium-based assays can be perturbed by the presence of reducing chemicals, such as dithiothreitol or mercaptoethanol, L-cysteine or L-ascorbic acid, as well as by interferences with ENMs (Almutary et al. 2016, Scarcello et al. 2020).

## 2.2 Genotoxicity methods employed in Task 5.2

Genotoxicity is crucial when assessing the safety of ENMs and thus genotoxicity endpoints need to be evaluated for hazard and risk assessment. These include gene mutation, DNA damage (strand breaks and specific DNA lesions such as DNA oxidation), chromosomal damage (clastogenicity, micronucleus assay) and numerical chromosomal damage (aneuploidy). Moreover, high throughput modifications of available genotoxicity assays such as comet assay allow to investigate a high number of ENMs in much shorter time than standard assays.

### 2.2.1 COMET assay

The comet assay (CA), or single cell gel electrophoresis, is a method for detection of DNA damage in cells with a nucleus. The method is widely used for detection of strand breaks (SBs) as well as specific DNA lesions, such as oxidized purines and pyrimidines by inclusion of specific enzymes (in this case Fpg, (formamidopyrimidine DNA glycosylase) protein, that detects preferably oxidized base lesions). The assay is considered a useful method for genotoxicity testing *in vitro* as well as *in vivo*. The SOP was provided by NILU to all participating partners; ANSES, KU Leuven, IMI, SU, LIST and NILU. During RR1 in Task 5.1, the main focus was the harmonization of the critical steps in the SOP between the partners, and with the COST Human Comet project. Additional PCs suitable for alkylation and oxidatively damaged DNA were included and tested by all the partners. Possible interference of the ENMs with the CA test is

a matter of concern. To investigate this aspect, interference controls (INT) have been added to the experiments. Interference was assessed by mixing non exposed cells (negative control, NC) with ENMs at the highest exposure concentration used (e.g., 100 µg/mL), right before cells embedding in agarose. This aims at checking for the creation of “artificial” DNA breaks induced by ENMs after exposure and resulting in increased DNA migration during electrophoresis. After RR1, discussions took place among the partners about the interference possibilities and a review of the literature on this issue was performed. Based on this discussion and review work, in RR2 in Task 5.1 more conditions were to be considered to assess potential ENM interference in the CA. These possible types of interference were described in D5.1 and by El Yamani et al. (El Yamani et al. 2022).

The *in vitro* comet assay has been miniaturized to allow many more samples to be analysed in a single experiment. Thus, 12 mini-gels are applied to one slide instead of the one or two gels as in the original procedure; or 96 mini-gels can be placed on a GelBond film (Azqueta et al. 2013; Gutzkow et al. 2013). Automated image analysis systems are also available (e.g., Metafer from Metasystems, Germany). To increase its sensitivity and to detect diverse types of lesions, the assay has been modified by the inclusion of a digestion with lesion-specific enzymes after the lysis step; thus, otherwise undetectable base damage is converted into a-basic sites and single SBs are introduced (Dušinská and Collins 1996). The most used enzymes are endonucleases specific for DNA base oxidation, namely Fpg (Dušinská and Collins 1996).

Within RiskGONE project, a method paper has been published by NILU TEAM where they addressed the use of miniaturised version of comet assay for ENMS testing (El Yamani et al. 2022). The method paper is to help the standardization of this test and support sound safety assessment of ENMs, by providing a detailed procedure that can be tested among different laboratories. Eventually, the standardized and validated procedure of the comet assay is to be submitted to the OECD as a standard project submission form (SPSF).

### 2.2.2 Micronucleus assay

The micronucleus assay is a robust assay commonly used by toxicologist to assess the potential genotoxicity of chemicals. Micronuclei are chromosomes or fragments of chromosome found in the cytoplasm of cells during interphase. Micronuclei represent chromosomal damages that have been transmitted to daughter cells, and as such micronucleus formation requires cell division. This assay has been standardised by OECD with two guidelines related to *in vivo* (OECD TG474) and *in vitro* (OECD TG487) assays. In the *in vitro* set-up, cells are treated in the absence or presence of the substance of interest for 1.5 to 2 cell cycles. After treatment, cells are counted to ensure cell division occurred and mononucleated cells are analysed for the presence of micronuclei. A variant of the micronucleus assay consists of the use of cytochalasin B to block cytokinesis and in this set-up, binucleated cells are analysed for the presence of micronuclei. The micronucleus assay in the presence of cytochalasin B is regarded as more integrative since it ensures that cell analysis is limited to those that have undergone cell division in the presence of the test substance.

### 2.2.3. The $\gamma$ H2AX assay

The C-termini phosphorylated histone protein,  $\gamma$ H2AX, has been proposed as a potential biomarker of DNA double strand breaks (DSB) caused by genotoxicants. After DSB formation large numbers of  $\gamma$ H2AX molecules accumulate around the break site, making possible their detection. The importance of this biomarker arises from the fact that DSB are considered the most critical kind of DNA damage, initiating genomic instability and, potentially, leading to cancer (O’Driscoll & Jeggo 2006).

Two types of methods are often used for  $\gamma$ H2AX detection, those counting foci or other  $\gamma$ H2AX-containing structures in images of cells and tissues (by immunofluorescence microscopy), and those measuring overall  $\gamma$ H2AX protein levels (by immunoblotting or flow cytometry). Although both methods are currently used, counting  $\gamma$ H2AX foci is several orders of magnitude more sensitive, and allows the distinction between pan-nuclear staining and focus formation, and it is this approach that is being employed in efforts to develop high throughput techniques (Bonner et al. 2008). However, counting  $\gamma$ H2AX foci is usually done manually by microscopy, which is time-consuming and cumbersome. Therefore, efforts are being made to improve this method, based on microscopy techniques, such as imaging modalities in cell culture and in tissues, and computer-assisted approaches.

### 3. Methodology

#### 3.1 Literature review conducted to select methods for interlaboratory testing

We performed a literature search to identify original, peer-reviewed research publications on nanotoxicology where HTS and HCA methods had been used to assess cyto- and genotoxicity. The search was carried out on three different databases of scientific publications (PUBMED, SCOPUS and EMBASE) using the following key words for the queries:

"High content screening", "High content imaging", "High content analysis", "High throughput screening", "High throughput imaging", "High throughput analysis", nano\*, cytotox\*, genotox\*, "adverse effect", "adverse outcome", "oxidative stress", ROS, lysosom\*, inflammation.

The literature search was grouped by endpoints and each endpoint search was assigned to a specific partner. The syntax of the search queries is listed below (grouped by endpoint).

#### Query syntax for Endpoints

##### Cytotoxicity (UiB)

("High content screening" OR "High content imaging" OR "High content analysis") AND nano\* AND cytotox\*

("High throughput screening" OR "High throughput imaging" OR "High throughput analysis") AND nano\* AND cytotox\*

##### Genotoxicity (NILU & SU)

("High content screening" OR "High content imaging" OR "High content analysis") AND nano\* AND genotox\*

("High throughput screening" OR "High throughput imaging" OR "High throughput analysis") AND nano\* AND genotox\*

##### Adverse Outcome Pathway (KUL & IMI)

("High content screening" OR "High content imaging" OR "High content analysis") AND nano\* AND ("adverse effect" OR "adverse outcome")

("High throughput screening" OR "High throughput imaging" OR "High throughput analysis") AND nano\* AND ("adverse effect" OR "adverse outcome")

##### Oxidative Stress (KUL)



("High content screening" OR "High content imaging" OR "High content analysis") AND nano\* AND ("oxidative stress" OR ROS)

("High throughput screening" OR "High throughput imaging" OR "High throughput analysis") AND nano\* AND ("oxidative stress" OR ROS)

#### Lysosomal dysfunction (KUL)

("High content screening" OR "High content imaging" OR "High content analysis") AND nano\* AND lysosom\* AND toxic\*

("High throughput screening" OR "High throughput imaging" OR "High throughput analysis") AND nano\* AND lysosom\* AND toxic\*

#### Inflammation (ANSES)

("High content screening" OR "High content imaging" OR "High content analysis") AND nano\* AND inflammation

("High throughput screening" OR "High throughput imaging" OR "High throughput analysis") AND nano\* AND inflammation

The filters “NOT review[pt]”, “humans[mh]” and “english[la]” were used in PUBMED to obtain original, species specific and English language studies.

Next, each scientific publication obtained in the search results was manually evaluated to corroborate the relevance to the search. Relevant publications were then scored taking into consideration the guidelines of the GuideNano scoring system (Fernandez-Cruz et. al. 2018) to objectively assess the quality of the studies. The threshold for publication acceptance was a Q score  $\geq 0.8$ , which indicates that publications are of high-quality regarding study design and characterization of nanomaterials.

### 3.2 Cell types and ENMs employed in Task 5.2

The selected cytotoxicity and genotoxicity assays were performed on A549 human epithelial lung cancer cell line and/or the TK6 lymphoblast cell line (see Table 3) and exposed to a set of common ENMs (see Table 4) under common exposure conditions for each biological endpoint assessed and type of assay utilized. The exposure conditions are specified below for each method.

**Table. 3. Cell types tested per endpoint**

Method (partner)	Endpoints addressed	Cell type tested
<b>Cytotoxicity</b>		
Bioimpedance (UiB)	Proliferation, viability	A549
Cell count (ANSES)	Proliferation, viability	A549
Nuclear intensity	Proliferation, viability	A549
Nuclear size	Proliferation, viability	A549
WST-1 (KUL)	Metabolic activity	A549 & TK6
Alamar blue (NILU)	Metabolic activity	A549 & TK6
<b>Genotoxicity</b>		
COMET assay (NILU)	DNA breaks	A549 & TK6
Micronucleus assay (SU and ANSES)	DNA damage	TK6
Micronucleus assay +/- cytochalasin (ANSES and SU)	DNA damage	TK6
$\gamma$ H2AX (ANSES)	Double strand breaks	A549

### ENMs selected for cyto- and geno-toxicity testing

The ENMs selected for use in the *in vitro* experiments are summarized in Table 4. The ERM numbers correspond to the unique RiskGONE ENM identifiers, are defined by the NanoCommons research infrastructure project, which established the European Registry of Materials as a means to increase the interoperability of datasets related to individual ENMs. To be able to use the results obtained in task 5.1, ENMs from RR1&RR2 were employed (see below). To be able to compare the methods and utilize results from previous projects, widely used ENMs with known cytotoxic effects were added in Task 5.2 (see below).

From RR1: ZnO from Sigma (ERM00000063) and TiO<sub>2</sub> from JRC (ERM00000064).

From RR2: CuO (ERM00000088), Nano Tungsten (ERM00000089) and MWCNTs (ERM00000325).

Specific for Task 5.2: Ag NM-300K (JRC- Fraunhofer), ZnO NM-111 (JRC)

For interlaboratory reproducibility testing of impedance-based nanotoxicity testing: Ag NM-300K (JRC-Fraunhofer), ZnO NM-110 (JRC), SiO<sub>2</sub> NM-200 (JRC).

At least four concentrations of each ENM (1- 100  $\mu$ g/mL) were tested in each method. In addition to the toxicity testing, possible interferences of ENMs with the test methods were carefully checked.

Particle characterization of the ENMs in the relevant test medium was performed in WP4 and was reported in the deliverable D4.1, Report on the RRs for physico-chemical characterisation of ENMs.

**Table 4. Overview of the selected ENMs (identifications and specifications) and dispersion protocols**

ERM identifiers	ID	Name	CAS	type	Supplier	Supplier code	Batch	Core	RR	Dispersion protocol
ERM00000063	ERM 00000063	ZnO	1314-13-2	NPO_1542	Sigma Aldrich	721077	MKCJ-4155	ZnO	RR1 & T5.2	Vortexing
ERM00000064	JRCNM01005a	TiO <sub>2</sub>	13463-67-7	NPO_1486	JRC	JRCNM 01005a		TiO <sub>2</sub>	RR1 & T5.2	DeLoid
ERM00000088	ERM 00000088	CuO 40nm	1317-38-0	NPO_1544	PlasmaChem			[Cu]=0	RR2	DeLoid
ERM00000089	ERM 00000089	Nano Tungsten Carbide/ Cobalt Powder	12718-69-3	ENM_9000257	NanoAmor	5561HW		[Wc]-[Co]	RR2 & T5.2	Nanogenotox
ERM00000325	ERM 00000325	MWCNT 3wt% AQUACYL 0303-NC7000		NPO_354	Nanocyl	AQUACYLTM AQ0303		Carbon	RR2 & T5.2	Vortexing
NM-300K					JRC-Fraunhofer			Ag	T5.2	Nanogenotox
NM-110					JRC			ZnO	T5.2	Nanogenotox
NM-111					JRC			ZnO	T5.2	Nanogenotox
NM-200					JRC			SiO <sub>2</sub>	T5.2	Nanogenotox

### 3.3 Impedance-based testing of ENM toxicity on adherent cells (UiB)

#### 3.3.1 Cell culture

Human lung carcinoma epithelial cells (A549) and human monoblastoid cells (U937) were purchased from ATTC (Manassas, USA). **For the interlaboratory comparison of methods investigating proliferation and viability, only the common cell line A549 and the xCELLigence RTCA SP instrument (Agilent, Santa Catalina, CA, USA) system were used.** The U937 cells were used for Impedance flow cytometry, which was not included in the interlaboratory comparison, as this was a part of R&D in WP5, i.e., establishing new methods, that have not yet reached the maturity level to be considered for OECD regulatory purposes.

The cells were cultured in T75 flasks (Nunc, Roskilde, Denmark) in Duplecco's modified eagle medium (DMEM) supplemented with 10% FBS and 1% P/S Sigma-Aldrich in an incubator at 37°C and 5% CO<sub>2</sub>.

A549 cells were passaged at approximately 80% confluency by trypsinization, i.e., the flask was washed twice with phosphate buffered saline (PBS) before adding 2 mL of trypsin-verse EDTA (Sigma-Aldrich). The cells were incubated for 5 min before the cell suspension was mixed with 8 mL of completed culture medium, then transferred to a 15 mL tube, which was centrifuged at 250 g for 5 min. The supernatant was discarded and afterwards the cell pellet was resuspended in 10 mL CCM. Trypan blue 0.4% was

used to assess the viability of the cells. Cells in passage 4-15 with viability higher than 90% were used for testing.

Human monoblastoid U937 cells are non-adherent and fast growing. Half of the medium in the flask was removed and fresh CCM was added. every other day to maintain a density of 100 000 – 200 000 cells/mL. The cells were regularly counted, and their viability tested by trypan blue 0.4%. Cells with viability higher than 90% were used for testing.

### Trypan blue exclusion test of cell viability

A volume of 10  $\mu$ L of trypan-blue 0.4% (ThermoFisher, Waltham, MA, USA) and 10  $\mu$ L of cell suspension were placed in a 500  $\mu$ L Eppendorf tube and thoroughly mixed. Out of the mixture, 10  $\mu$ L were pipetted to both chambers of an Invitrogen Countess chamber (ThermoFisher, Waltham, MA, USA). The automatic cell counter was then used to count cells and assess cell viability.

### 3.3.2 Nanomaterials and dispersion protocols

An overview of the ENMs and the dispersion protocols is given in Table 4. A 130-Watt probe sonicator (VCX130, Vibra-Cell, 130W, Sonic & Materials, Newtown, USA) was used at 22% amplitude of the maximum amplitude, equipped with a 12.8 mm probe with a replaceable tip to prepare particle dispersions. The sonicator was calibrated to ensure that the desired energy was delivered to the systems. The power ( $P$ ) was found to be 6.1919 J for the DeLoid-protocol (DeLoid 2017) and 8.41 J for the NANOGENOTOX-protocol (Jensen et al. 2011). By implementing the referenced critical delivered sonication energy ( $DSE_{cr}$ ) and Equation 1 the sonication time ( $t_{cr}$ ) needed to disperse the ENMs was calculated.

$$t_{cr} = \frac{DSE_{cr}}{P} V \quad (1)$$

$t_{cr}$  = critical sonication time (s)

$DSE_{cr}$  = Referenced delivered sonication energy (J/mL)

$P$  = Sonicator power (J/s)

$V$  = Volume of dispersion (mL)

### DeLoid-protocol

A mass of 15 mg of ENM powder was carefully weighed in a 20 mL scintillation vial by using a disposable plastic antistatic spatula. MilliQ water was added drop-by-drop to the glass scintillation vial while tilting and swirling the vial, so that a concentration of 5 mg/mL was reached. After swirling the vial containing ENM and milliQ water, the sonication started. Without touching the sides of the vial, the tip of the sonicator probe was placed inside the vial. The tip was submerged at 2/3 of the height of the vial carefully, not touching the bottom. The ENM was then sonicated according to the  $DSE_{cr}$ -values specified in the LIST-protocol. The amount of time calculated as necessary to sonicate the dispersion was 19 sec for CuO, 93,5 sec for TiO<sub>2</sub> (Sigma-Aldrich) and 156,2 sec for TiO<sub>2</sub> (JRC). To protect it against light, the dispersion was sealed and covered with aluminum foil.

### NANOGENOTOX-protocol

A mass of 15.36 mg of ENM powder was weighed in a 20 mL scintillation vial by using a disposable plastic antistatic spatula. The vial was tilted at a 45° angle and tapped gently on the side to gather the



material. A volume of 30  $\mu\text{L}$  EtOH (96%) was added drop-by-drop onto the raw material and mixed gently. A volume of 970  $\mu\text{L}$  of 0.05% BSA water was added slowly to avoid foaming. Lastly, an additional 5 mL of 0.05% BSA water was added slowly along the walls of the vial to collect any powder that might have deposited on the walls. A stock concentration of 2.56 mg/mL was made. The vial was sealed with a cap and placed on ice for at least 5 min, while the sonicator was prepared. The sonicator probe was carefully submerged in the scintillation so that to avoid touching any of the sides. The ENM dispersion was sonicated according to the  $\text{DSE}_{\text{cr}}$ -values specified in the NANOGENOTOX-protocol. The time calculated to sonicate the WC-Co dispersion was 2 sec. Afterwards, the dispersion was sealed with a cap and covered with aluminum foil and placed on ice to rest.

#### **Vortexing: Multi-Walled Carbon Nano Tubes (AQUACYL 3 wt. % NC7000) dispersion by vortexing**

The MWCNT (AQUACYL 3 wt. % NC7000) were provided by Nanocyl (Sambreville, Belgium). The MWCNT (AQUACYL 3 wt. % NC7000) dispersion was a pitch-black dense viscous solution, which was vortexed vigorously for 30 sec. An intermediate suspension was made by extracting a quantity of 1 mL of stock dispersion and diluting it at 1:6 ration in the proprietary dispersant (1 mL AQUACYL 3 wt.% dispersion + 5 mL Dispersant). Thus, a concentration of 5 mg/mL was obtained.

#### **Vortexing: Zinc Oxide (ZnO)**

ZnO was provided by Sigma-Aldrich (Darmstadt, Germany) as a powder suspension. The density of the ZnO bottled in suspension was estimated at 240 mg/mL. A volume of 1 mL was removed from the bottle and the ZnO suspension was vortexed vigorously for 30 sec. before further dilution in cell culture medium and before cell exposure.

#### **Preparation of ENM dispersions in cell culture medium**

The ENM to be tested was dispersed in a 15 mL tube cell culture medium at required concentrations by adding fresh vortexed ENM dispersions to complete the cell culture medium. The tube with the solution was then rotated in the tube rotator ISB3 (Bibby Scientific, Staffordshire, England) at 40 rpm for 2 minutes and mixed with a pipet. When multiple concentrations were prepared, a high concentration tube (100  $\mu\text{g}/\text{mL}$  or 50  $\mu\text{g}/\text{cm}^2$ ) was used for serial dilution. In each dilution series step, the solution was mixed by pipetting and vortexed for 5 seconds. Before exposure to cells, the solution was mixed by pipetting.

### **3.3.3 ENM characterization in exposure media**

#### **Dynamic light scattering**

Dynamic light scattering (DLS) using a Zetasizer Nano ZSP (Malvern Instruments, Malvern, England) was employed to measure the hydrodynamic diameter (HDD) of the batch dispersions and of ENMs in complete cell culture medium. For the latter, the highest exposure concentration (100  $\mu\text{g}/\text{mL}$ ) was used. Three measurements of the HDD and polydispersity index (PDI) were performed for each sample at the beginning and end of exposure to ENM dispersions.

#### **Zeta potential**

The Zeta potential (ZP) was measured for the ENMs dispersed in complete CCM (with 10% FBS and 1% P/S). In a prewetted folded capillary zeta cell (DTS1070, Malvern Instrument), 800  $\mu\text{L}$  of the highest ENM concentration used in experiments (100  $\mu\text{g}/\text{mL}$  which corresponds to 50  $\mu\text{g}/\text{cm}^2$ ) was pipetted.

The ZP was measured using a Zetasizer Nano ZSP at the temperature corresponding to that used during ENM exposure in the toxicity tests.

### 3.3.4 Impedance-based toxicity testing using the xCELLigence system

For the interlaboratory comparison of methods assessing proliferation and viability, the following ENMS were used: ZnO from Sigma (ERM00000063), TiO<sub>2</sub> from JRC (ERM00000064), CuO (ERM00000088), Nano Tungsten (ERM00000089), MWCNTs (ERM00000325), Ag NM-300K (JRC), and ZiO NM-111 (JRC).

For interlaboratory reproducibility testing of impedance-based nanotoxicity testing, the following set of sENMs were used by UiB and NILU: Ag NM-300K (JRC- Fraunhofer), ZnO NM-110 (JRC) and NM-200 (JRC). As NILU or other partners in RiskGone, other than UiB, do not possess an xCELLigence system, the instrument was transported to NILU and training was provided by UiB to NILU colleagues. The results obtained by UiB and NILU were also compared with those obtained in the FP7 project NANoREG by CEA (Commissariat à l'Énergie Atomique) for the same set of ENMs.

The impedance-based measurements were performed using an xCELLigence RTCA SP instrument (Agilent, Santa Catalina, CA, USA) with 16-well E-plates for label-free, real-time monitoring of A549 cell proliferation, adherence and viability. This is achieved by measuring the difference in impedance at the gold-plated electrodes that cover 70-80% of the bottom of the wells onto which cells are seeded. The experiments using xCELLigence followed three main steps: preparation of the E-plate, seeding of cells and exposure of A549 cells to ENM dispersions.

The xCELLigence (RTCA) instrument measures the electrical impedance under static exposure conditions. For each timepoint, the software provides the measured impedance as a Cell Index (CI), which is a nondimensional quantity. In both the presence and absence of cells, the CI is a measurement of electrical impedance normalized by a frequency factor,  $Z_n$  (equation 2):

$$CI = \frac{Z_t - Z_0}{Z_n} \quad (2)$$

Where  $Z_t$  = Impedance at time t

$Z_0$  = Impedance at time 0 (background)

$Z_n$  = Frequency factor

Increase of cell proliferation and attachment are indicated by a rise in the CI, whereas detachment, loss of membrane integrity, and cell death are indicated by a reduction in the CI.

All the experiments were done in triplicates or duplicates and in three independent experimental repetitions. In these experiments, A549 cells were exposed to ENMs after an initial seeding and proliferation for 24 h in the E-plates. The CIs were normalized to the value measured right before the cells were exposed to the ENMs, i.e., at 24 h after seeding. The normalization is given as equation 3; the normalization was performed to correct for possible differences in cell numbers between the wells at the time of exposure.

$$NCI = \frac{CI_t - CI_{med}}{CI_{t=24}} \quad (3)$$

$CI_t$  = Cell Index at timepoint t.

$CI_{med}$  = Cell index of the referenced medium, without cells.

$CI_{t=24}$  = Cell index at timepoint 24-hours, last timepoint before exposure of cells to ENM

In order to evidence the interference that the ENMs might have with impedance-based readings, the CI of wells containing cell culture medium with the highest concentration of ENMs (i.e., 100 µg/mL) was also measured. The calculation of NCI gives real time information about whether there is a proliferation or decrease of viability of cells.

The fold-change vs control (FC) represents the ratio between the cells exposed to ENMs and control cells at the measured timepoints. The FC was calculated for the cells at 48 h after seeding, i.e., 24 h after exposure to ENMs. The FC is given in **equation 4** and the FC of control = 1. Consequently, FC > 1 at a specific concentration of ENM solution indicates increase of proliferation/viability compared to the control and FC < 1 indicates a decrease.

$$FC = \frac{CI_{t=24}}{CI_{control}} \quad (4)$$

$CI_{t=48}$  = Cell index of exposed cells at timepoint t = h.

$CI_{control}$  = Cell index of control group at timepoint t = 48 h.

For every experiment, the cells were seeded and left to attach to the electrode surface and proliferate for 24 h before exposure to ENMs. After 24h, the cells were exposed to five different concentrations of ENMs (2, 10, 20, 50, 100 µg/mL).

### 3.3.5 16-well E-plate preparation and treatment

The 16-well E-plates were prepared by filling the sides around each well with sterile water to maintain humidity in the E-plate while inside the incubator. Then 100 µL of fresh complete DMEM was pipetted into each well and then kept at room temperature for 30 min, before placing them in the xCELLigence RTCA SP for a background measurement. The seeding of the cells happened immediately after the background measurement. A549 cells were added to each well resulting in a density of 25.000 cells/cm<sup>2</sup> (5.000 cells/well) for a total volume of 200 µL in each well. For the wells without cells, complete medium alone was added. The plate was then incubated at 37°C at 5% CO<sub>2</sub> for 30 min before insertion into the xCELLigence system located in an incubator with the same parameters. The CI was measured every 15 min for the next 24 h.

After 24 h, the E-plate was taken out of the xCELLigence system, 100 µL of cell culture medium were removed and replaced by the ENM dispersions in complete cell culture medium at different concentrations. In the wells not containing any cells and the control group, 100 µL of fresh complete medium were added. In the wells with cells, 100 µL of ENM dispersions at concentrations 1, 2, 5, 10, 25 and 50 µg/cm<sup>2</sup> (corresponding to 2, 10, 20, 50, and 100 µg/mL) were added. For ENM interference

control, 100  $\mu\text{L}$  of the highest concentration (100  $\mu\text{g}/\text{mL}$ ) were added in wells with medium only (without cells). Then the CI was measured every 15 min for an additional 24 h. Each measurement was performed in duplicate and repeated at least three times. The plate layout for the experiments is shown in Figure 5.

#### 16-well plate layout:

	1	2	3	4	5	6	7	8
A	M	M+100	C	2	10	20	50	100
B	M	M+100	C	2	10	20	50	100

<b>M: DMEM only (no cells)</b>	<b>C: Cells only (control)</b>
<b>M+100: DMEM with NM at 100 <math>\mu\text{g}/\text{mL}</math> (no cells)</b>	<b>X: Cells + NM at concentration X</b>

Fig. 5: Overview of the 16-well plate experimental showing the contents of the wells.

### 3.4 Impedance-based flow cytometry (IFC) (UiB)

The Ampha Z30 (Amphasys AG, Lucerne, Switzerland) was used, which is an impedance flow cytometer for single-cell characterization without optical components that assess cellular size, membrane capacitance, and cytoplasm resistance (UiB) (Ostermann et al. 2020). The ENMs which showed the highest cytotoxicity according to the xCELLigence data were ZnO, CuO and MWCNT. Therefore, these ENMs were picked to be tested for toxicity by impedance-based flow cytometry. The MWCNT could not be used with the AmphaZ 30 because they caused frequent clogging of the analysis chip, which did not allow the cells to pass through. Thus, the tests were finally run with ZnO and CuO. The cells were exposed to the ENMs at five different concentrations (2, 10, 20, 50, 100  $\mu\text{g}/\text{mL}$ ).

IFC was not included in the interlaboratory method comparison, as it is in an earlier stage with regards to standardization than the testing performed for adherent cells with the xCELLigence system.

#### 3.4.1 U937 cell culture and testing by IFC

The U937-cells were seeded at a cell density of 100.000 cells/mL in a 6-well plate in 2 mL of complete DMEM medium (with 10% FBS and 1% PS) and kept in an incubator at 37°C and 5% CO<sub>2</sub> for 24 h. After 24 h, the 6-well plate was centrifuged at 250 g for 5 min. Optical microscopy was used to ensure that the cells did not float. From each well, 1 mL of supernatant medium was carefully removed, then 1 mL of ENM dispersions were added and final concentrations of 1, 2, 5, 10, 25 and 50  $\mu\text{g}/\text{cm}^2$  (corresponding to 2, 10, 20, 50, and 100  $\mu\text{g}/\text{mL}$ ) were obtained. The plate was then incubated for an additional 24 h period.

Prior to cell collection, the AmphaZ30 device was rinsed and cleaned using Ampha Clean (Amphasys AG, Lucerne, Switzerland) and EtOH. The 6 well plate was centrifuged at 250 x g for 5 min and then the supernatant was removed and replaced by 1 mL of PBS in each well. Cells were resuspended and pipetted into centrifuge tubes. The tubes with cells and PBS were centrifuged at 250 x g for 5 min after which the supernatant was removed and replaced with 100  $\mu\text{L}$  of PBS. In each tube, 400  $\mu\text{L}$  of sucrose

buffer were added to ensure a 1:4 PBS/sucrose ratio. A 20 x 20  $\mu\text{m}$  channel chip was employed in measurements. To avoid clogging, the chip was rinsed with MilliQ water regularly.

Cells heated at 70 °C for 30 min served as positive control for necrosis. To test for possible ENM interferences, the highest ENM concentration (100  $\mu\text{g}/\text{mL}$ ) was added to cell-free medium, as well as to negative and positive cell controls. The impedance-based measurements were made using the Ampha Z30 IFC (Amphasys AG, Switzerland) and were carried out at 0.5, 2, 6, and 12 MHz. The ENMs and cell debris were excluded at the chosen settings, the trigger level of 0.02 V excluded any noise by a good margin. Additional curve detection further excludes random noise as noise does not follow the same time-dependent pattern as cells do.

A total of 10.000–20.000 cells per sample were analysed using the AmphaSoft 2.0 (Amphasys AG, Switzerland). The 6 MHz-frequency was found to be optimal for assessing plasma membrane permeability. A gate for viable cells (intact cell membrane) was created in AmphaSoft 2.0 using the negative control and then applied to all samples within one exposure experiment. The viable cells within the gate were presented as a percentage of the total number of cells, which was used for further analysis.

### 3.5 3D Microvasculature formation in a microfluidic chip (UiB)

The aim was to develop a 3D microvasculature structure in a microfluidic chip. For this, the ideal cell density was determined for the co-culture of HULEC-5a cells (ATTC, Manassas, USA) with fibroblasts (Innoprot, Spain) to form in vitro angiogenesis on a chip, and to construct a chip that imitates the endothelial barrier found in a human blood vessel.

#### 3.5.1 Fabrication of the microfluidic chip

The design of the chip was conceived with the intent of constructing a model that physiologically is as close to the in vivo vascular biology as possible. Therefore, the pattern consists of specific channels with dimensions that will later be lined with cells. The layout of the microvasculature chip constructed in this thesis is presented in Figure 5, and the design was created using LayoutEditor software. The chip consisted of three channels: One “big”, central channel with diamond-shaped chambers and two smaller channels (cross section 100x100  $\mu\text{m}$ ) on each side. The two outer channels were interconnected to the diamond chambers at the edges (see Figure 6). The middle channel accommodated the capillary network formation. The capillary network formation was induced by co-culturing fibroblast and endothelial cells embedded in fibrin gel. The outer channels are meant for lining with endothelial cells to mimic the endothelial lining found in an artery and vein.

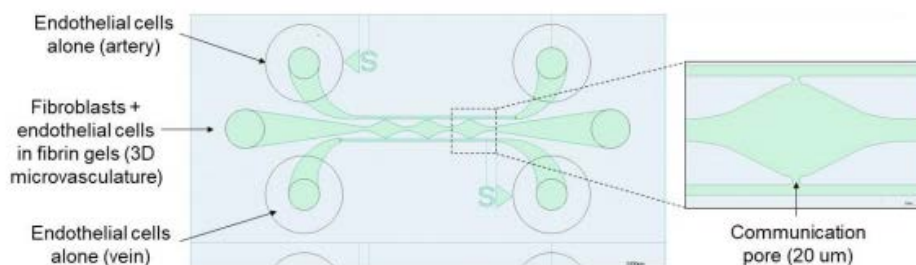


*Fig. 6: Top view of the design of the microvasculature chip.* The microfluidic chip consisted of three channels, where the middle channel was for co-culturing endothelial cells with fibroblasts in a fibrin gel to induce in vitro angiogenesis, while the outer two channels were for culturing endothelial cells, thereby creating endothelial lining.

The outer channel lined with endothelial cells will mimic the function of the artery and vein in a mammalian body: transport biological molecules to the microvascular network, in this case formed by self-assembly of microvessels by endothelial cells co-cultured with fibroblasts in the diamond chamber. In this study, the channels were mainly utilized to perfuse nutrients to the cells. They can also be utilized to perfuse drugs and other substances and therefore can be served as a nanotoxicity assay by perfusing nanoparticles. The fluid that is injected into the side channels can also perfuse through the semipermeable capillary network (Figures 7 and 8).

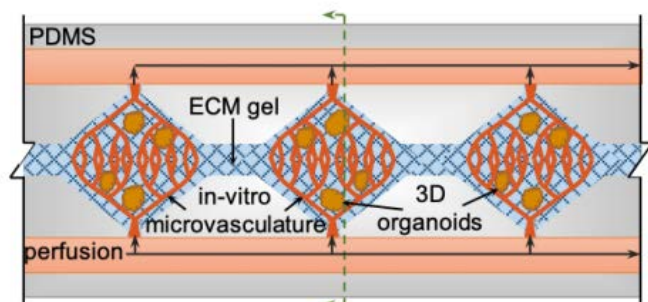


*Fig. 7: A top view of the microvasculature chip. The diamond chambers compartmentalized the formation of the capillary network, while the outer channels provided nutrients to the cells.*

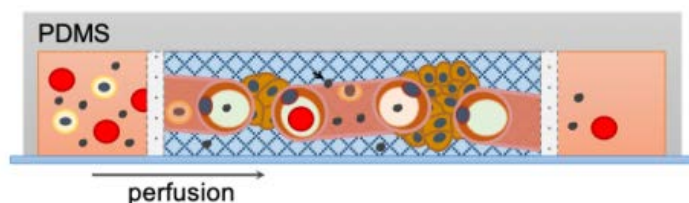


*Fig. 8. Cross-section of the chip. The network is semipermeable; thus nutrients or other substances provided by the side channels can flow through it (depicted with an arrow). Illustration is adapted from Ruzicka et al. 2019.*

Photolithography was used to fabricate the master for the microfluidic chip using the above-mentioned chip design (Figure 5). Photolithography is a technique used to transfer a pattern onto a substrate, a Silicon wafer coated with photosensitive resist. The method utilizes electromagnetic radiation, UV-light in this case, to transfer the pattern from an optical mask (photomask) to the photosensitive resist on the substrate. This is done by coating the wafer with a photoresist. Then, the photomask with the preferred pattern is placed on top of the coated wafer and exposed to light. The photomask blocks out light according to the predefined features, like an object casting a shadow. After the light exposure, the wafer undergoes a series of chemical treatments to remove only exposed or unexposed parts of the photoresist depending on the type of resist used: in positive photoresists, the exposed area of the wafer is “washed away” by exposure to UV radiation, whereas with a negative photoresist the exposed area undergoes UV radiation-mediated cross-linking, so it stays on the wafer while the unexposed areas are washed away (Leng 2013). In this thesis, a negative photoresist was used to transfer the chosen pattern from a photomask. The silicon master utilized in this thesis was fabricated in a clean room. A silicon wafer (University Wafers, South Boston, Massachusetts, USA) was cleaned with isopropanol. The wafer was then incubated in a piranha solution (7:3 ratio of sulfuric acid to 30% hydrogen peroxide) for 45 min. The wafer was thereafter cleaned with MilliQ water and acetone and blown dry with N<sub>2</sub>-gun. Afterwards, the wafer was coated with a thin layer (approximately 100 μm) of negative photoresist SU-

8 2100 (MicroChem Corporation, Westborough, Massachusetts, USA) by spinning it for 10 seconds at 500 rpm followed by 30 seconds at 3000 rpm. Next, the coated wafer was placed on a hot plate (PZ 28-2 ET, Harry Gestigkeit GMBH, Düsseldorf, Germany) for 5 min at 65°C and then 30 min at 95°C. The coated wafer together with the photo mask (JD Photo Data, Hitchin, United Kingdom) were placed in a mask aligner (SUSS MicroTec, Garching, Germany). An I-line mask aligner filter (Omega Optical, LLC, Brattleboro, USA) was placed on top to block wavelengths of 360 nm and below, since the filter allows for sharper and straighter feature walls of the resist. The setup was thereafter exposed to UV light through the mask and the optical filter for 60 s. The wafer was then placed on a hot plate for 5 min at 60°C and then at 75°C for 50 min. Unexposed resist was then stripped away using SU8 2100 developer (MicroChem Corporation, Westborough, Massachusetts, USA) in a water bath sonicator for 5 min. Afterwards, the wafer was rinsed carefully in isopropanol and MilliQ H<sub>2</sub>O. The wafer was thereafter carefully dried using an N<sub>2</sub> gun.

**The casting of the chip (PDMS)** The microfluidic chip was casted by using the Si-master with the patterned design and Polydimethylsiloxane (PDMS). The PDMS was made by mixing the base elastomer and curing agent thoroughly together in a 10:1 ratio. The mixture was placed in a vacuum chamber to remove bubbles that formed during stirring. The master was placed in a casting system made of Teflon with a polycarbonate lid on top. The polycarbonate lid had been O<sub>2</sub> plasma-treated using a low-pressure plasma system (Diener electronics GmbH & Co. KG, Ebhausen, Germany) for 1 min (0.3 bar, 60 W) before mounting it in the casting system. Small tubes (channel spacers) were inserted through the polycarbonate lid to create inlet and outlet holes in the chip. The degassed PDMS was pipetted carefully into the assembled casting system via the polycarbonate lid, then cured at 65°C for 6 h. After the curing step, the PDMS chip was cut, and edges were cleaned up. Any remaining fragments on the chip were removed using adhesive tape (scotch tape). Furthermore, the chip was fused together with a glass coverslip to seal off the engravements left by the SI-master. The fusion was executed by rinsing the PDMS chip in isopropanol followed by double distilled water (ddH<sub>2</sub>O). Then the glass cover slip (50mm\*20mm Decker glass) was sonicated in pure isopropanol for 5 min at 21°C (power intensity of 50%) and rinsed in 70% isopropanol and ddH<sub>2</sub>O as well. Both the chip and cover slip were dried using a N<sub>2</sub> gun. Thereafter the chip and cover slip were O<sub>2</sub> plasma-treated (1 minute, 0.3 bar, 60W), and permanently fused together by gently pressing the cover slip onto the PDMS chip with the engraved pattern.

**Cell ratio for microvasculature formation.** The formation of new blood vessels involves proliferation and sprouting of endothelial cells from the endothelium of the pre-existing vasculature. The sprouting and formation of vessel is dependent on fibroblast-derived ECM and growth factors. Thus, fibroblast play a critical role in vasculature formation. Several researchers have successfully replicated in vivo angiogenesis in vitro, and one of the 41 methods was to co-culture endothelial cells with fibroblasts. The condition for replicating vasculature is dependent on cell types, thus, finding the optimal cell ratio for co-culturing is the first step in construction a microvasculature on a chip. Two different cell ratio conditions were tested in three different media in order to find the proper cell condition to implement for growing cells in ECM (fibrin gel) for the experiments with microfluidic chip. The different conditions were seeded in an imaging chamber and immunostained so the samples could be imaged by utilizing confocal fluorescence microscopy. The ratios tested in this study are 1:1 and 1:2 Human Pulmonary Fibroblasts cells to HULEC-5a (in total  $1 \times 10^6$  cells per 30  $\mu$ l gel was seeded per ratio condition). Each of the ratio conditions was assessed in duplicate wells and cultured with either complete EGM-2 medium the first two days after cell seeding then with EGM-2 medium without VEGF and FGF, or complete MCDB131 medium with 10%FBS. The fibroblasts and HULEC-5a were first trypsinized, then the required amount of fibroblast cells and HULEC-5a were combined in a falcon tube and centrifuged at 900 rpm for 3 min. Afterwards, the supernatant was removed, the cell pellet was suspended in a 2:1:1 mixture

of 20 mg/ml Fibrinogen:2XPBS:8mM CaCl<sub>2</sub>/4mM MgCl<sub>2</sub> in water (Fibrin-cell solution). To create the gel, thrombin was added to the fibrin-cell solution and the solution was quickly pipetted in the imaging chamber slide. The amount of thrombin added to create the gel was either 2.5 U/ml or 5.0 U/ml. The seeded cells were left to grow in an incubator at 37°C perfused with 5% CO<sub>2</sub> for 7 days, adding fresh medium every other day. After incubation, each well was fixed with 4% PFA in 2mM CaCl<sub>2</sub>-PBS for 20 min at RT inside a chemical fume hood. The PFA was then replaced with sterile PBS to wash for 1 h at RT. After washing, the cells were permeabilized with 0.05% Tween 20 in PBS for 1 h. The sample was again washed with PBS after permeabilization and left with blocking solution (4% BSA/4% FBS in PBS) ON at 4°C to reduce nonspecific bindings. The next day the samples were immunostained with primary antibodies. The sample was incubated with primary antibodies at 4°C ON. This primary antibody solution consisted of 2.5% VE-Cadherin diluted in PBS containing 0.5% blocking solution. After ON incubation of the primary antibodies, the sample was 42 washed with PBS thrice; the last two washes were incubated for 30 min at RT each. After the PBS washes, secondary antibody solution of 10 µg/ml donkey anti-mouse ATTO647 (Sigma-Aldrich, St. Louis, Missouri, USA) was added to each well and incubated ON at 4°C. After 24 hours of incubation, the sample was washed with PBS twice; each wash was incubated with PBS for 30 min. Thereafter actin green (ThermoFisher, Waltham, Massachusetts, USA) staining was performed by adding a solution of actin green diluted in PBS containing 0.5% blocking solution to each well and incubated at RT for 1 hour. The sample was again washed with PBS twice; this time each wash was incubated for 15 min. Lastly, nuclei staining was performed using DAPI solution (1:1000 dilution in PBS) and left ON at 4°C. The DAPI solution was then replaced with PBS to wash the sample, and thereafter the sample was left with PBS at 4°C until imaging.

### 3.5.2 Setup of the microfluidic system

The microfluidic system consisted of a microscope equipped with a DSD2 unit and a Zyla 5,5 sCMOS camera, enclosed in an environmental chamber to maintain the temperature at 37°C (see Figure 9).

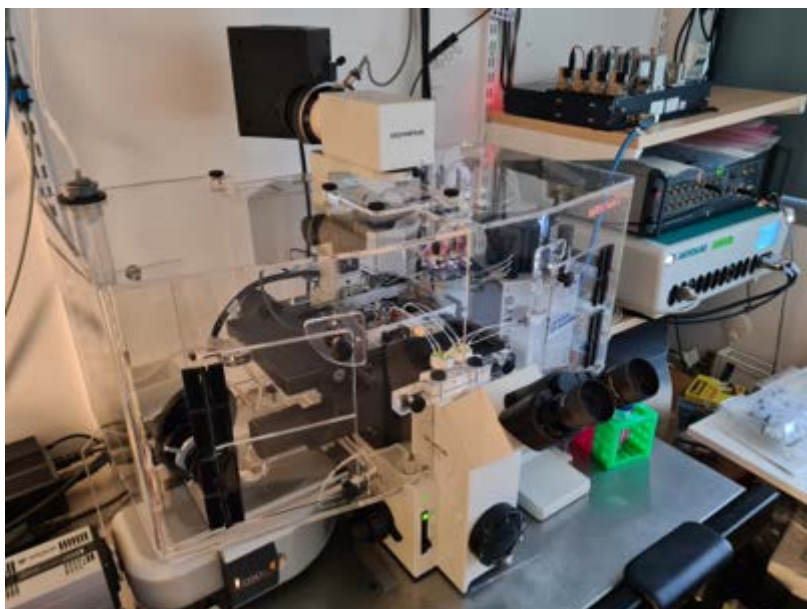


*Fig. 9. Microfluidic setup* consisting of a microscope, DSD2 unit and camera enclosed in an environmental chamber. Inside the chamber there is a microscope-stage for the microfluidic chip, the tubing-system containing reservoirs and CO<sub>2</sub>-tubes and the peristaltic pump.



### 3.5.3 Bubble trap fabrication

A bubble trap was fabricated to prevent air bubbles being dragged inside the microfluidic chip, which dislodge and damage the cells. Two discs (3.3 cm diameter by 6 mm thickness) of polyvinyl chloride (PVC) were CNC-machined using a compact CNC machine (Wegstr, Czech Republic) based on a layout designed on Cut2D software (Vectric, UK). One of the PVC discs contained a long serpentine microfluidic network (0.2 x 0.2 x 15 mm) and the other disc five vent channels (1 x 2 x 15 mm). Both discs were interfaced by a micro-porous, hydrophobic PTFE membrane (Darwin Microfluidics, France) and fastened together. This trap works by allowing excess gas trapped in the cell culture medium flowing through the serpentine channel to pass through the micro-porous PTFE membrane towards the opposing disc with air vents opened to the atmosphere.

## 3.6. Cyclic Voltammetry to Monitor Total Antioxidant Capacity of In-Vitro Biological Models Exposed to Nanomaterials (UiB)

To our knowledge, CV is being established for the first time for nanotoxicity testing by UiB. This is part of the R&D in WP5 and was therefore not included in the interlaboratory method comparison. A set of ENMs produced by Applied Nanoparticles in Barcelona was used, as these were well dispersed and characterized, allowing for a better comparison of the ENMs' oxidative effects. Cells were not used in the CV experiments.

### 3.6.1 Electrode configuration

The choice of electrodes is essential for a thorough analysis of electrochemical phenomena. Three electrodes are utilized in the voltametric cell assembly for CV:

- **The working electrode (WE)**, which carries out the electrochemical event of interest.
- **The counter electrode (CE)**, which completes the electrical circuit so that current flows between WE and CE when potential is applied at WE.
- **The reference electrode (RE)**, which has a well-defined and stable potential and therefore is used as a reference point against which the other potentials are measured.

Three different electrode setups were used to track the oxidation of AA at concentrations varying from 50-500  $\mu\text{M}$  in cell culture medium without cells:

- 1) Traditional glassy carbon WE / Pt CE / Ag RE (PalmSens, The Netherlands)
- 2) Screen printed (SP) electrodes with the configuration C / Pt / Ag (Metrohm Autolab, The Netherlands)
- 3) SP electrodes with the configuration C / C / Ag (Metrohm Autolab, The Netherlands)

Using a scan rate of 100 mV/s, the CV was performed in the range of -0.5 V to 1.2 V.

To find the optimal scan rates for measuring small changes in the availability of ascorbic acid, cyclic voltammetry was performed between -0.5 and 1.2 V using either PBS with 250  $\mu\text{M}$  L-AA or DMEM with 10% FBS and 4 concentrations of L-AA: 0, 100, 250 and 500  $\mu\text{M}$ . Five different scan-rates were tested: 100, 150, 200, 300 and 400 mV/s. Initial measurements were performed using a traditional Glassy Carbon/Pt/Ag electrode, before moving on to using screen-printed C/Pt/Ag electrodes.

### 3.6.2 Oxidative potential of ENMs in Hank's balanced salt solution

The ENMs' intrinsic redox characteristics and their oxidative abilities were evaluated using a multiplexed potentiostat (PalmSens) and disposable screen-printed Carbon/Carbon/Ag electrodes. The CV for the

ENMs was performed in Hank's Balanced Salt Solution with  $\text{Ca}^{2+}$  and  $\text{Mg}^{2+}$  (HBSS) at 0, 10 and 30 min after addition of ENMs with and without 250  $\mu\text{M}$  L-AA, by applying an electrical voltage sweep from -1 V to 1.2 V and measuring the resulting current as electrons are transferred in a redox reaction. Experiments were performed using either pure L-AA or L-AA from dissolved over-the-counter Vitamin-C tablets. 150  $\mu\text{L}$  of each prepared sample was pipetted directly on top of each of the C/C/Ag SP electrodes. To prevent light-induced degradation of L-AA, a cover was placed on top of the system shortly after the samples were pipetted on top of the electrodes. For the resulting voltammograms, the peak height and area under the curve were measured. The area under the curves were found by integrating the CV voltammograms using MATLAB (Mathworks) with the help of Assoc. Prof. Emil Cimpan (Western Norway University of Applied Sciences, HVL). The interpretation of the results using the program developed at HVL is ongoing and therefore the results are not presented in this Deliverable.

### 3.6.3 Data Analysis

Data from the xCELLigence studies, CV and IFC (Ampha Z30) were analysed using the IBM SPSS statistical software tool (version 26.0) [43]. For multiple sample comparisons, a One-Way ANOVA with a Tukey Post Hoc test was employed, and for paired comparisons of independent samples, the independent sample test (t-test) was performed ( $p \leq 0.05$  denotes statistical significance with a 95 % confidence interval).

### 3.6.4 Modelling of results from electrical impedance-based methods and CV

A mathematical model was developed by HVL that takes into consideration the speed of the FC change. The calculation was performed in Matlab by integrating the derivative of the FC vs control over the entire exposure period to ENMs. The interpretation of the results is ongoing.

## 3.7. HCA assessment of cell count, nuclear size, nuclear intensity, caspase-3 intensity, and $\gamma\text{H2AX}$ intensity (ANSES)

A549 cells were seeded in black 96-well plates (plates purchased from Sigma Aldrich, Saint-Quentin-Fallavier, France) at a density of 25 000 cells per  $\text{cm}^2$ . 24h after seeding, cells were treated for 24 h with the various nanomaterials at concentrations ranging from 1 - 100  $\mu\text{g}/\text{mL}$ . Staurosporine (Sigma Aldrich, Saint-Quentin-Fallavier, France) 0.8  $\mu\text{M}$  was used as a positive control for apoptosis while 0.2 mM methyl methanesulfonate (MMS) (Sigma Aldrich, Saint-Quentin-Fallavier, France) was used as a positive control for DNA double strand breaks. Following treatment, cells were washed with PBS and fixed 10 min with 4% formaldehyde in PBS. Cells were then washed with PBS and permeabilised with PBS Triton 0.2% for 10 min and non-specific sites were blocked with a solution of PBS Tween 0.05% + BSA 1% for 30 min. Cells were then incubated for 2 h at room temperature with primary antibodies (rabbit anti-active caspase-3 (Abcam, Paris, France) and mouse anti- $\gamma\text{H2AX}$  (Abcam) diluted in PBS Tween 0.05% + BSA 1% at 1:1500 and 1:2000 respectively. After three washes in PBS Tween 0.05%, cells were incubated for 1 h in the dark with fluorescent-labelled secondary antibodies (goat anti rabbit IgG (Alexa Fluor® 647) and goat anti mouse IgG (Alexa Fluor® 488) Abcam) diluted at 1:2000 in PBS Tween 0.05% + BSA 1%. Subsequently, DNA was stained with DAPI (Sigma) 1 $\mu\text{g}/\text{mL}$  in PBS Tween 0.05% and cells were rinsed with PBS. Fluorescence was measured with an Arrayscan VTI HCS Reader (Thermo Scientific, Waltham, MA USA). For each well, 8 fields (20 $\times$  magnification) were analyzed. Cell counts were performed using nuclear DAPI labelling.

Potential sources of interference with HCA, including autofluorescence and non-specific interactions of nanomaterials with antibodies, were evaluated. For interference testing, fluorescence measurements in

wells stained with DAPI only, DAPI + primary antibodies, and DAPI + secondary antibodies were performed. The median raw value from measures for interference at each wavelength (DAPI staining only or DAPI plus the various antibodies) was subtracted from raw value obtained with the specific staining (DAPI, primary and secondary antibodies) for active caspase-3 and  $\gamma$ H2AX intensities. This was done for each NM and for each concentration tested. Since HCA analyses require nuclear staining (DAPI, Hoechst ...) for cell identification, evaluation of interference in the DAPI channel was not possible. For HCA analysis, two independent experiments were performed and, for each experiment, the median intensity of three technical replicates was expressed relative to that of the media control. For interference tests, only one well was used. The parameters studied included cell counts, average nuclear size, nuclear intensity, active caspase-3 intensity and  $\gamma$ H2AX intensity.

### 3.8. COMET assay (NILU)

The CA, or single cell gel electrophoresis, is a method for detection of DNA damage in cells with a nucleus. The method is widely used for detection of strand breaks (SBs) as well as specific DNA lesions, such as oxidized purines and pyrimidines by inclusion of specific enzymes that detects preferably oxidized base lesions, in this case Fpg, which is a formamidopyrimidine glycosylase protein. The assay is considered a useful method for genotoxicity testing *in vitro* as well as *in vivo*. An SOP was provided by NILU in Task 5.1, which preceded Task 5.2, to all participating partners: ANSES, KU Leuven, IMI, SU, LIST and NILU. The results and conclusions drawn in T5.1 were included and taken into consideration in Task 5.2 and are therefore presented below. Moreover, the T 5.1 results from RR1 and RR2 were used in the reproducibility testing of the CA.

During RR1 in T5.1, the main focus was the harmonization of the critical steps in the SOP between the partners, and with the COST Human Comet project. Additional PCs suitable for alkylation and oxidatively damaged DNA were included and tested by all the partners.

Possible interferences of the ENMs with the CA test is a matter of concern. To investigate this aspect, interference controls (INT) have been added to the experiments. In RR1, the interference was assessed by mixing non exposed cells (negative control, NC) with ENMs at the highest exposure concentration used (e.g., 100  $\mu$ g/mL), right before cells embedding in agarose. This aims at checking for the creation of “artificial” DNA breaks induced by ENMs after exposure and resulting in increased DNA migration during electrophoresis.

After RR1, more discussion took place among the partners about the interference possibilities and a review of the literature on this issue was performed. Based on this discussion and review work, in RR2 several conditions needed to be considered to assess potential ENM interference in the CA. These possible types of interferences were individuated as follows:

- Inhibition/interaction with the Fpg activity
- Quenching /autofluorescence during quantification of signals
- Direct/physical interference of nanoparticles with DNA (after washing steps)
- creating additional breaks or adducts
- interfering by reducing or blocking the DNA migration during electrophoresis

To assess all these possible types of interference the following interference controls were prepared:

- For inhibition/interaction with Fpg activity: NC and PC for Fpg samples were trypsinized after exposure and the cells were mixed with the ENMs immediately before embedding in agarose

- Physical interference:

- o NC cells and ENMs were mixed just before embedding into agarose like in RR1
- o PC cells and ENMs were mixed just before embedding into agarose.

This last control is meant to check for possible reduced or hindered DNA migration into the agarose gel as a consequence of ENMs still being present in the gel.

The CA SOP was applied on the human lymphoblastoid cells TK6 and the human lung epithelial cells A549. Five ENMs in total were tested in RR1 and RR2, as described in Deliverable 5.1, with 3 or 24 h exposure times. Each partner provided data for 2-3 independent experiments for each ENM, cell line and time point.

The inclusion of potassium bromate ( $\text{KBrO}_3$ ) as PC gave inconsistent data. Several trial studies have been conducted in parallel to identify the best condition for  $\text{KBrO}_3$ . A data entry template for the RiskGONE instance of the eNanoMapper database was tailored and harmonized with partner NMBP13 project Gov4Nano.

### 3.9 *In Vitro* Micronucleus Assay Round Robin (SU, ANSES)

The description of the method and SOP can be found in D 5.1. The assay was performed using TK6 cells. Task 5.1 aimed at developing robust assays to study the toxicity of nanomaterials and round-robins were organised amongst partners to evaluate various Standard Operating Procedures (SOPs). It has been shown that ENMs could interfere with the micronucleus assay at several levels. Indeed, it has been shown that cytochalasin B, by blocking the actin cell cytoskeleton formation could prevent uptake of nanomaterials, and consequently reduce their potential genotoxic effects (Magdolenova et al. 2012). Therefore, it has been suggested to either use the micronucleus assay in the absence of cytochalasin B or to add cytochalasin B after 1.5 to 2 cell cycle long treatment with the nanomaterials. Other interferences of nanomaterials have been reported. For example, it has been shown that nanomaterial presence can hinder the micronuclei analysis and therefore influence the scoring of micronuclei (Fernández-Bertólez et al., 2021). Moreover, it has been suggested that the presence of aggregates/agglomerates of particles may influence the operator that would not work blind anymore (Kaiser et al., 2011). During task 5.1, the micronucleus assay was chosen as part of a round robin to evaluate the potential genotoxicity of selected nanomaterials. A SOP was developed by an OECD expert working group during the project *Development of the Guidance Document on the Adaptation of the "In Vitro micronucleus assay (OECD TG 487) TGs for Testing of Manufactured Nanomaterials"*, that was discussed amongst partners. One aspect of this SOP aimed at developing a common protocol to assess micronuclei in TK6 cells using cytochalasin B with large scale cultures in flasks. Within task 5.1, the SOP was successful for some partners. However, ANSES did not manage to have it working and faced 2 main issues: a low percentage of binucleated cells (only around 20%) as well as difficulties in scoring due to the absence of a cytospin step and the lack of spreading of the cell cytoplasm. Importantly, this SOP required a lot of cells, medium and reagents while ANSES had an internal SOP for the micronucleus assay on TK6 cells using a 12-well plate format, allowing a higher throughput but in the absence of cytochalasin B. Therefore, ANSES generated data for the micronucleus assay in the absence of cytochalasin B but in a higher throughput manner, while the other partners used the SOP on a micronucleus assay using cytochalasin B but with a lower throughput. TK6 cells were grown in RPMI 1640 medium containing 10 % Horse serum, 100 U/mL Penicillin and 100 ug/mL Streptomycin. ANSES added sodium pyruvate (1 mM), as recommended per supplier to have a cell cycle of ~13 hours. At SU, the TK6 cell cycle time was observed between 12-14 hours, grown in RPMI 1640 medium containing 10 % Horse serum and 1% L-glutamine.

Data gathered at ANSES indicated that TiO<sub>2</sub> did not show any cytotoxicity with TK6 cells after 24h incubation, as assessed both by Trypan Blue dye exclusion and by the Relative Increase in Cell Counts (RICC) (Figure 1). ZnO treatment induced a dose dependent increase in cytotoxicity from 5 µg/mL and analysis of the RICC showed a dose dependent decrease suggesting a reduction in cell number upon ZnO treatment. Importantly, 20 µg/mL ZnO was too cytotoxic (more than 50% as recommended in the OECD guideline), and therefore analysis of micronuclei was not performed. WC/Co treatment was not cytotoxic but showed a small decrease in RICC as shown in Figure 3. The positive control MMS did not display cytotoxicity as assessed by Trypan Blue dye exclusion. However, MMS induced a cytostatic effect, illustrated by a reduced RICC, which is due to cell cycle arrest in G2/M (Islaih et al., 2005).

## 4. Results

### 4.1 Results of the literature review

The literature search (PUBMED, SCOPUS and EMBASE) to identify original, peer-reviewed research publications on nanotoxicology where high-throughput and high-content methods had been used to assess cyto- and genotoxicity provided the results presented in Table 6. Each scientific publication obtained in the search results was manually evaluated to corroborate the relevance to the search. Relevant publications were then scored taking into consideration the guidelines of the GuideNano scoring system (Fernandez-Cruz, et. al., 2018) to objectively assess the quality of the studies. The threshold for publication acceptance was a Q score  $\geq 0.8$ , which indicates that publications are of high-quality regarding study design and characterization of nanomaterials. We obtained a low number of high-quality peer-reviewed publications (Table 1) even though we had widened our criteria for selection of HTS publications. This is, to include methods not only performed entirely in a high-throughput setting, but also with a high-throughput potential.

The pool of papers was too low to provide a solid basis for the identification of the most reliable, reproducible and promising HTS and HCA methods for nanotoxicity testing. Furthermore, some of the methods in those papers were not available at the partners' laboratories, making impossible the interlaboratory comparison. It was therefore decided that the methods available at the Task 5.2 partners' laboratories will be compared.

The methods were grouped according to the biological endpoints they addressed and then compared for reliability. In this respect, ENM interferences were also accounted for. Each group of methods employed common cell line(s), ENMs, exposure conditions, concentrations, and exposure times.

The methods were also evaluated for reproducibility, making use of the results from RR1&RR2 in T5.1. Moreover, results from the NANoREG project were also used for the reproducibility evaluation of the impedance-based nanotoxicity testing (xCELLigence system).

**Table 5. Number of HTS/HCA publications with a GuideNano Q score  $\geq 0.8$ : Publications are sorted according to endpoint.**

Endpoint	Nr. of HTS publications		Nr. of HCA publications	
	Total	Q score $\geq 0.8$	Total	Q score $\geq 0.8$
<b>Cytotoxicity</b>	8	4	14	2
<b>Genotoxicity</b>	17	13	1	1
<b>Adverse outcome pathway</b>	10	5	10	3
<b>Oxidative stress</b>	0	0	11	6
<b>Lysosomal dysfunction</b>	0	0	4	1
<b>Inflammation</b>	-	-	-	-

## 4.2 Impedance-based label-free monitoring of cell proliferation and viability (xCELLigence system) (UiB, NILU)

### 4.2.1 Hydrodynamic diameter and Zeta potential of ENMs

The hydrodynamic diameter (HDD) and polydispersity index (PDI) of the ENM dispersions in complete DMEM cell culture medium and in miliQ water (stock dispersion) were measured using DLS (Zetasizer Nano ZSP, Malvern Instruments) and the overview is given in Table 6. These parameters were determined for the highest exposure concentration (100  $\mu\text{g}/\text{mL}$ ) shortly after preparation at 0h (time of exposure) and 24 h after exposure, which corresponds to the end of ENM exposure duration.

**Table 6: Hydrodynamic diameter (HDD) and Polidispersity index (PDI) of ENMs in Stock (milliQ) and complete DMEM cell culture medium**

Samples	DLS			
	Mean hydrodynamic diameter $\pm$ SD [nm]		PDI $\pm$ SD	
	0h	24h	0h	24h
<b>CuO (Plasmachem)</b>				
DMEM	765,4 $\pm$ 51,9	112,1 $\pm$ 38,5	0,881 $\pm$ 0,030	0,291 $\pm$ 0,083
STOCK (milliQ)	2764	25630	1	0,581
<b>MWCNT (NanoCyl)</b>				
DMEM	2280 $\pm$ 337,9	3342 $\pm$ 454,9	0,353 $\pm$ 0,153	0,328 $\pm$ 0,032
STOCK (milliQ)	293,2	271,3	0,354	0,276
<b>WC/co (NanoAmor)</b>				
DMEM	341,3 $\pm$ 17,9	622 $\pm$ 405,6	0,502 $\pm$ 0,019	0,666 $\pm$ 0,173
STOCK (milliQ)	667,5	429,2	0,693	0,377
<b>TiO<sub>2</sub> (Sigma)</b>				
DMEM	824,7 $\pm$ 116,7	1174,7 $\pm$ 122,2	0,779 $\pm$ 0,080	0,833 $\pm$ 0,046
STOCK (milliQ)	2349	-	1	-
<b>TiO<sub>2</sub> (JRC)</b>				
DMEM	415,2 $\pm$ 13,40	413,0 $\pm$ 16,65	0,364 $\pm$ 0,029	415,2 $\pm$ 13,40
STOCK (milliQ)	1857	-	0,359	1857
<b>ZnO (Sigma)</b>				
DMEM	1129 $\pm$ 194,9	997,5 $\pm$ 231,0	0,567 $\pm$ 0,142	1129 $\pm$ 194,9
STOCK (milliQ)	533,9	-	0,313	533,9
<b>ZnO NM-110 (JRC)</b>				
DMEM	255.0 $\pm$ 1.8	237.1 $\pm$ 4.9	0.123 $\pm$ 0.013	0.129 $\pm$ 0.001
STOCK (milliQ)		233.9 $\pm$ 0.6		
<b>ZnO NM-111 (JRC)</b>				
DMEM	237.2 $\pm$ 1.6	238.9 $\pm$ 3.4	0.166 $\pm$ 0.004	0.141 $\pm$ 0.006
STOCK (milliQ)		244.3 $\pm$ 1.9		
<b>SiO<sub>2</sub> NM-200 (JRC)</b>				
DMEM	274.8 $\pm$ 14.8	167.0 $\pm$ 0.7	0.466 $\pm$ 0.045	0.588 $\pm$ 0.025
STOCK (milliQ)		257.6 $\pm$ 8.3		
<b>Ag NM-300K (JRC)</b>				
DMEM	110.6 $\pm$ 6.9	108.4 $\pm$ 3.2	0.369 $\pm$ 0.031	0.374 $\pm$ 0.017
STOCK (milliQ)		79.8 $\pm$ 0.2		

#### 4.2.2 Impedance-based measurements using the xCELLigence system

The impedance-based xCELLigence system measured the cell index (CI) of A549-cells. The CI gives an indication of the proliferation and viability of the cells. Details regarding the CI, the CI normalization (NCI), and fold change (FC) calculation were given in *section 3.3.4*. Figure 10 shows the NCI for A549 cells exposed to the RR1-ENMs and Figure 11 shows the NCI for A549 cells exposed to RR2-ENMs. The

figures display the real-time proliferation or decrease of the NCI for each ENM, due to the real-time aspect it is possible to determine when or how quickly the NCI increases or decreases.

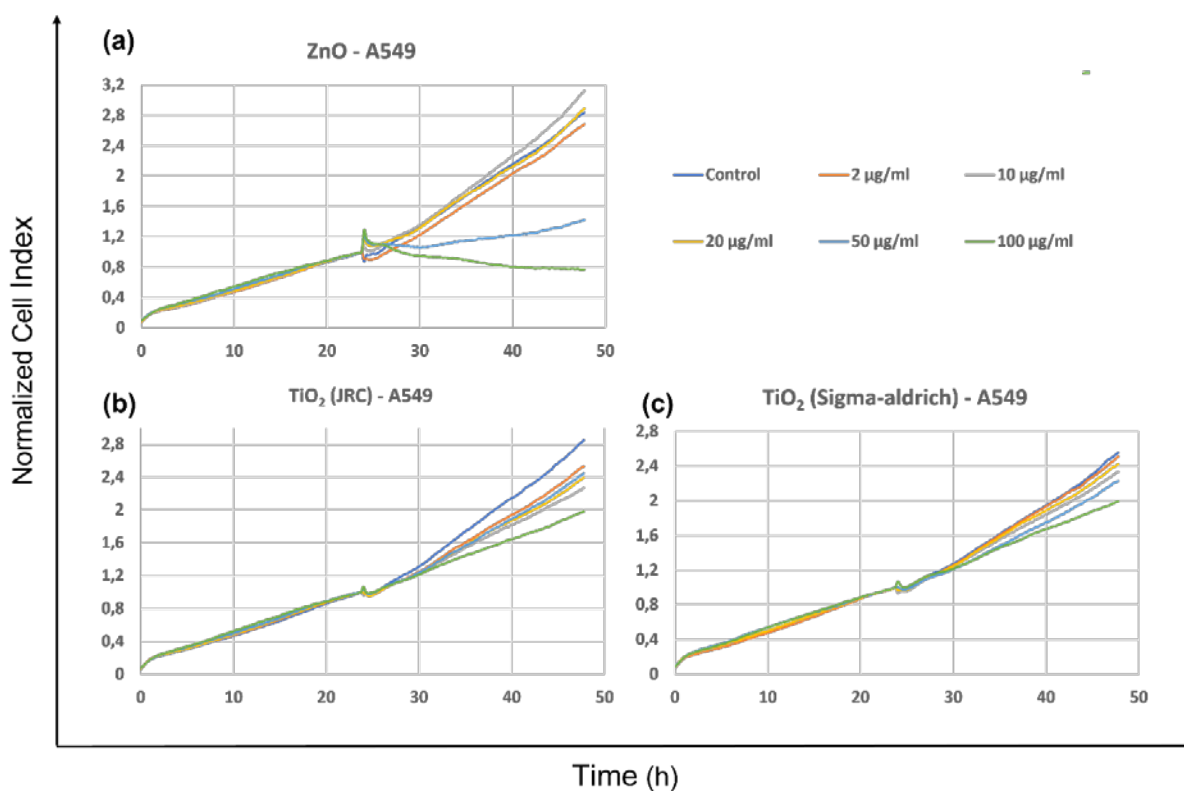


Fig. 10: Normalized Cell Index (NCI) of A549-cells grown in DMEM medium in xCelligence E-plates exposed to RR1-ENMs (UiB): (a) ZnO, (b) TiO<sub>2</sub>(JRC) and (c) TiO<sub>2</sub>(Sigma). Cells were seeded at 5 000 cells/well (25 000 cells/cm<sup>2</sup>). After 24 h the cells were exposed to 5 different concentrations of ENMs. Each of the experiments were done in triplicates and in three individual experimental repetitions. The curves represent the mean of three individual experimental repetitions.



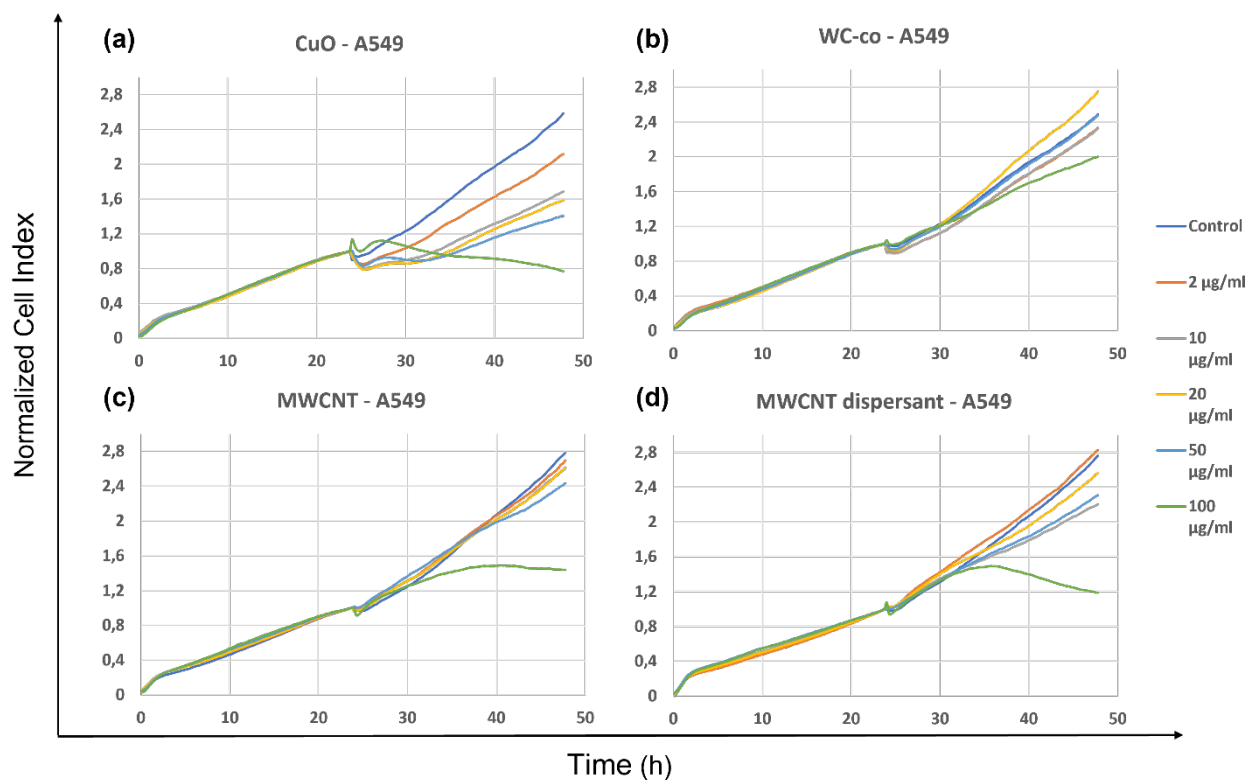


Fig. 11: Normalized Cell Index (NCI) of A549-cells grown in DMEM medium in xCelligence E-plates exposed to RR2-ENMs (UiB): (a) CuO, (b) WC-co, (c) MWCNT and (d) MWCNT-dispersant. Cells were seeded at 5 000 cells/well (25 000 cells/cm<sup>2</sup>). After 24 h the cells were exposed to 5 different concentrations of ENMs. Each of the experiments were done in triplicates and in three individual experimental repetitions. The curves represent the mean of three individual experimental repetitions.

The FC data for the RR1-NMs exposed to A549-cells are presented in Figure 12. The cells exposed to the ZnO have a low FC at higher concentrations, with statistical significance at 50 and 100 µg/mL. Both TiO<sub>2</sub> ENMs have similar trends, the only statistical significance difference from control is at the highest concentration 100 µg/mL.

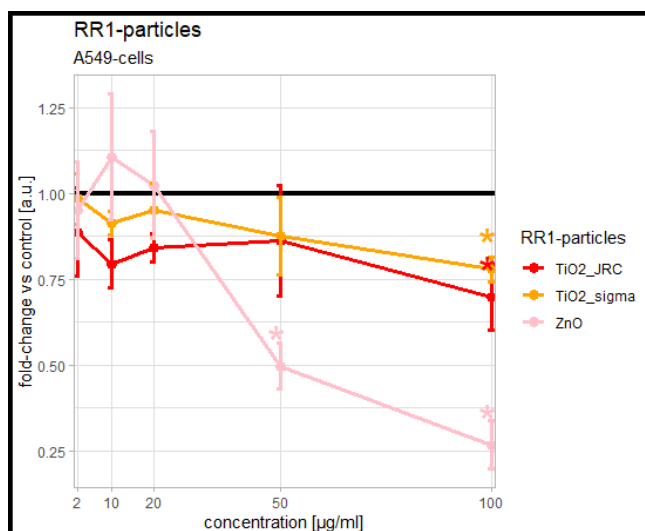


Fig. 12: The fold change (FC) of the impedance measurements for A549-cells exposed to RR1-ENMs (UiB): ZnO (Sigma) (pink), TiO<sub>2</sub> (JRC) (red) and TiO<sub>2</sub> (Sigma) (orange) 24 h after exposure to 2, 10, 20, 50 and 100 µg/mL. The figure shows the mean of the three independent repetitions. The control (unexposed cells) is marked as the black line at FC = 1. “\*” marked statistical significance in respect to control, p<0.05.

The results for the A549 cells exposed to RR2-NMs are presented in Figure 13. The CuO has a low value of FC for every concentration with statistical significance at cells exposed to 10, 20, 50 and 100 µg/mL. The WC-co shows proliferation at 20 µg/mL, and lower value for 100 µg/mL which is the only concentration with statistical significance. The MWCNT and MWCNT dispersant are similar, however there are lower values indicating higher toxicity for the MWCNT dispersant.

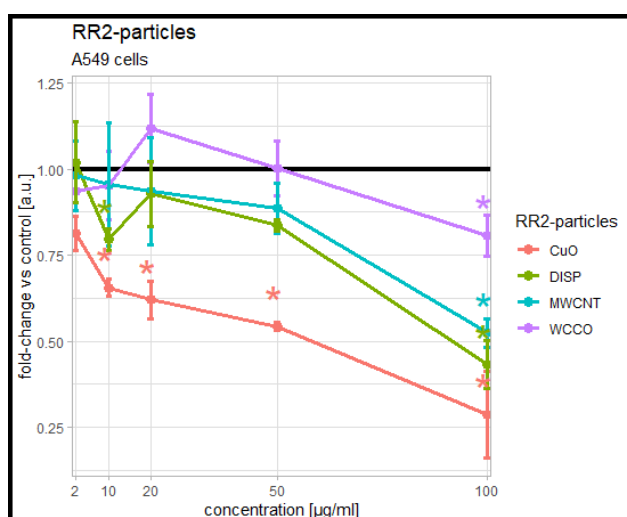


Fig. 13: The fold change (FC) of the impedance measurements for A549-cells exposed to RR1-ENMs (UiB): CuO (red), WC-co (purple), MWCNT (blue) and the dispersant from MWCNT (green) 24 h after exposure to 2, 10, 20, 50 and 100 µg/mL. The figure shows the mean of the three independent repetitions. The control (unexposed cells) is marked as the black line at FC = 1. “\*” marked statistical significance in respect to control, p<0.05.

The results for ZnO NM-110, ZnO NM-111, NM-200, NM300K, were obtained in the FP7 NANoREG project by UiB and are presented below in Figure 14. The RiskGone project had the inclusion of data from previous projects as one of its objectives. The results obtained by NILU in Task 5.2 are shown in Figure 15.

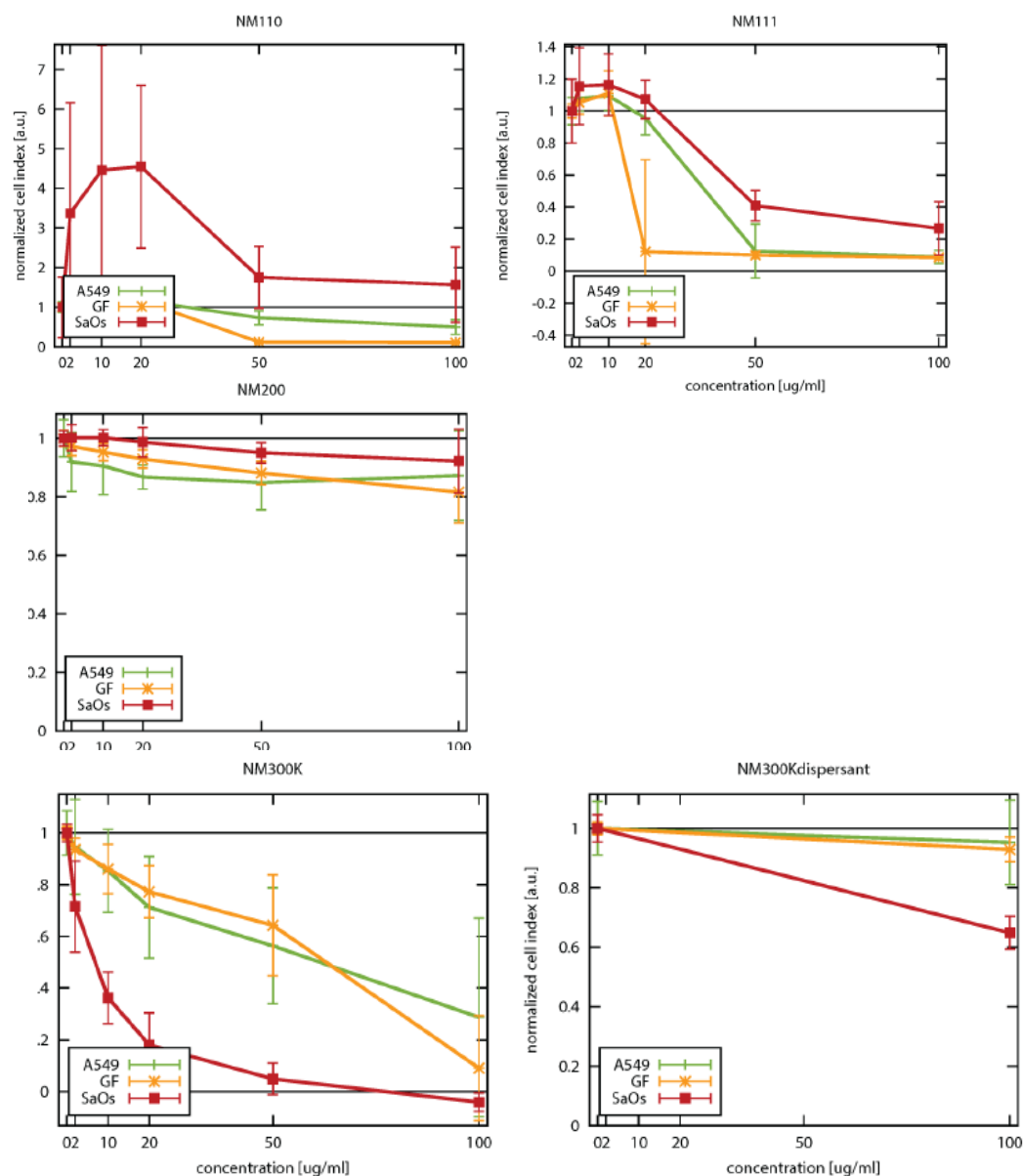


Fig. 14. Real-time impedance results (xCELLigence system) obtained in the FP7 NANoREG project by (UiB). Assessment of cell viability and proliferation. Only results on A549 (green line) were included in Task 5.2. A549 cells exposed to NM-110, NM-111, NM-200, and NM-300k and NM-300K dispersant at 2, 10, 20, 50, 100  $\mu\text{g}/\text{mL}$  (i.e., 1, 5, 10, 25, 50  $\mu\text{g}/\text{cm}^2$ ) for 24 h. Increased proliferation can be correlated to values over 1 and cell death to values below 1.

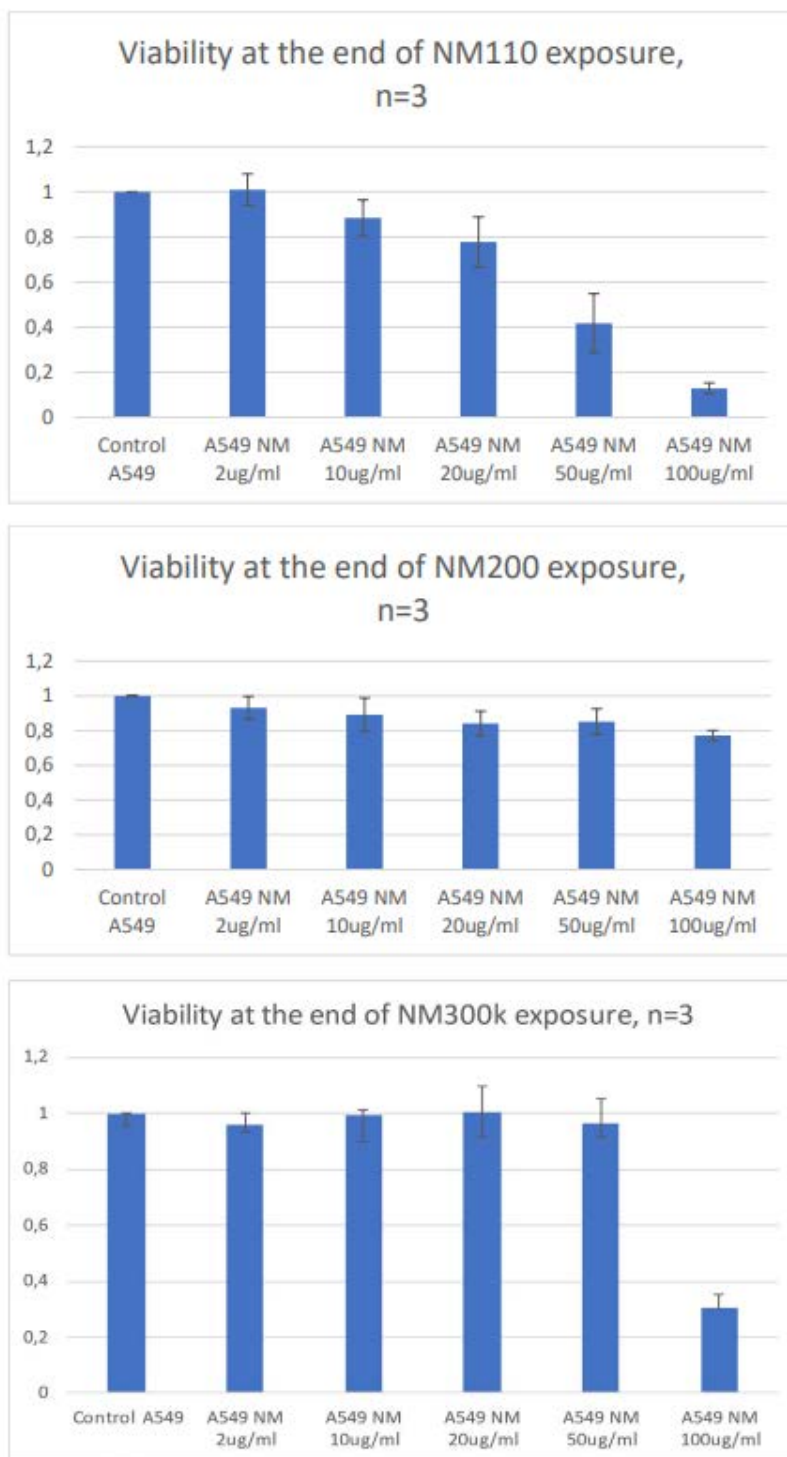


Fig. 15. Real-time impedance results (xCELLigence system) (NILU). Assessment of cell viability and proliferation. A549 cells exposed to NM-110, NM-111, NM-200, and NM-300k and NM-300K dispersant at 2, 10, 20, 50, 100 µg/mL (i.e., 1, 5, 10, 25, 50 µg/cm<sup>2</sup>) for 24 h.

### 4.3 Cell viability assessed by Impedance-based Flow Cytometry (UiB)

The IFC has been tested and further developed in T5.2, having in mind its possible use for regulatory testing. Due to the limitations caused by the Covid-19, the time devoted to this method was reduced. All experiments were done on U937 cells in triplicates and in three independent experimental repetitions. The cells were seeded in 6-well plate with a seeding density of 100 000 cells/mL. The ENMs that with the highest cytotoxic effect, according to the xCELLigence data were ZnO, CuO and MWCNT. Therefore, these ENMs were chosen for testing by IFC. However, due to chip clogging by MWCNT, only ZnO and CuO were tested in the end. The cells were exposed to ENMs at five different concentrations (2, 10, 20, 50, 100 µg/mL).

#### 4.3.1 IFC of U937-cells exposed to nano-CuO (Plasmachem)

A representative dot-plot of U937-cells exposed to CuO at 10, 50 and 100 µg/mL, including negative and positive controls, is shown in Fig. 16. The gating is done with reference to the negative control. All the cells to the right of the gating (black vertical line) are alive, while the cells on the left of the gating are either dead or in the process of dying. It is possible to see a shift to the left (dead cells) in the population cells exposed to nano-CuO compared to the control. For the cells exposed to 10 and 50 µg/mL there is a small shift towards the left side of the gating, while the cells exposed to the 100 µg/mL have a bigger shift, which overlaps with the population of death cells from the positive control.

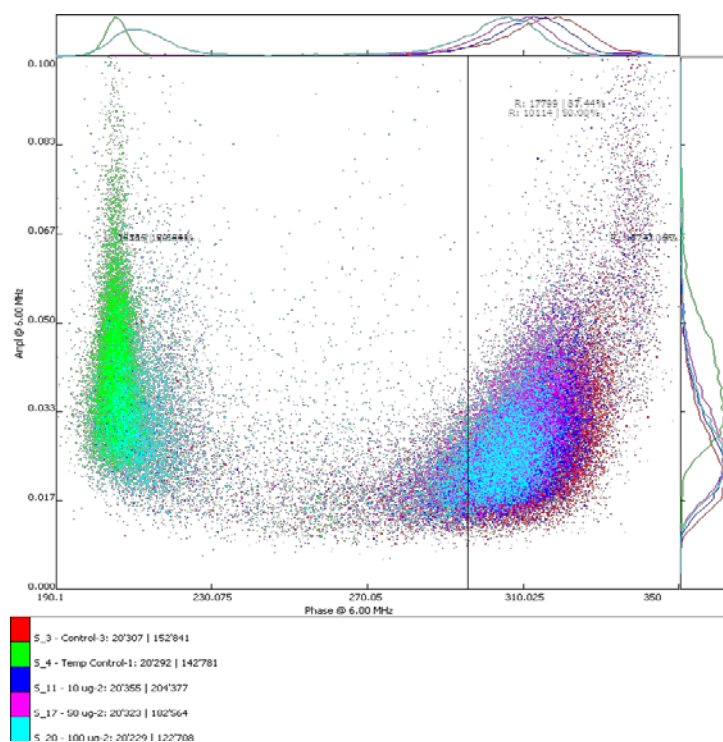


Fig. 16: Dot-plot of U937-cells exposed to nano-CuO (Plasmachem). Each dot represents a measurement. Viable cells are at the right of the vertical line. Red = Negative control, Green = Positive control, blue = 10 µg/ml, purple = 50 µg/ml, teal = 100 µg/ml.

The effect of nano-CuO on the viability of U937 cells is shown in Figure 17.

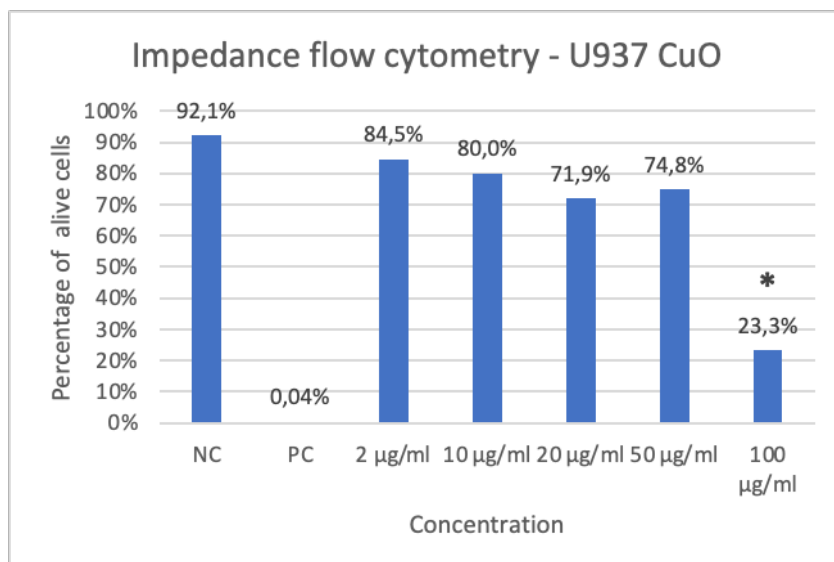


Fig. 17: Percentage of viable U937 cells following exposure for 24 h to nano-CuO (Plasmachem) (2, 10, 20, 50 and 100 µg/mL). NC = negative control, PC = Positive control. “\*” marked statistical significance compared to the control,  $p < 0.05$ .

#### 4.3.2 IFC of U937-cells exposed to nano-ZnO (Sigma)

The amplitude and phase shift of U937 cells exposed to nano-ZnO (Sigma) for 24 h can be seen in Figure 18. The gating is done with reference to the negative control. All the cells to the right of the gating (black vertical line) are alive, while the cells on the left of the gating are either dead or in the process of dying. A shift to the left can be observed for cells exposed to 10, 50 and 100 µg/mL compared to the negative control. This shift is particularly large at the highest exposure concentration.

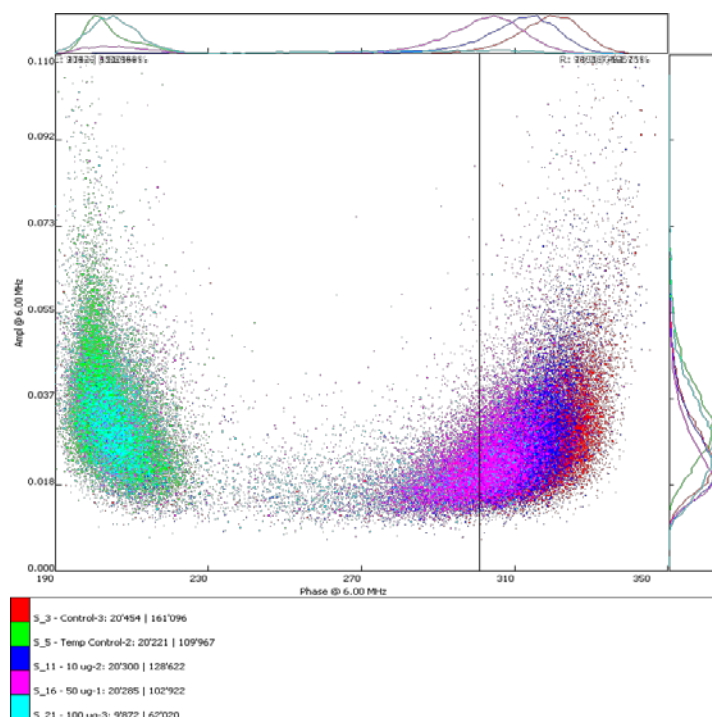


Fig. 18: Dot-plot of U937-cells exposed to nano-ZnO (Sigma). Viable cells are at the right of the vertical line. Red = Negative control, Green = Positive control, blue = 10 ug/ml, purple = 50 ug/ml, teal = 100 ug/ml.

The effects of nano-ZnO (Sigma) on the viability of U937 are summarized in Figure 19. The viability decreased with the increasing concentration of the ENM. The decrease in viability percentage for each concentration indicates a harmful effect of nano-ZnO.

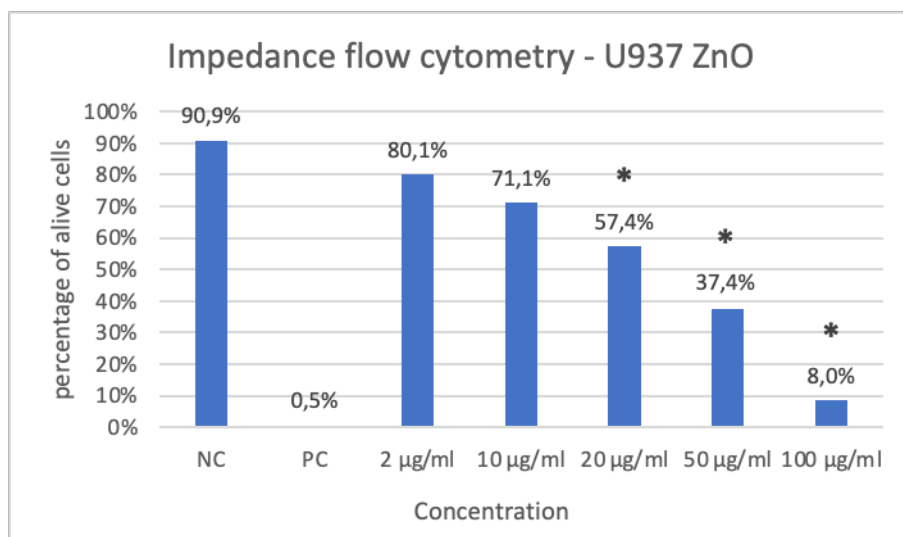


Fig. 19: Percentage of viable U937 cells following exposure for 24 h to nano-ZnO (Sigma) (2, 10, 20, 50 and 100 µg/mL). NC = negative control, PC = Positive control. “\*” marked statistical significance compared to the control, p<0.05.

The results shown above were not included in the interlaboratory comparison due to the limited number of ENMs that could be tested.

#### 4.4 Microfluidic system (UiB)

To better mimic real-life exposure, a microfluidic testing system offering a dynamic environment, i.e., constant perfusion of nutrients and homogenous ENM dispersions, has been developed by UiB (I. Rios-Mondragon). With the intention of developing a dynamic environment to mimic the *in vivo* microvascular channels, a microfluidic system was developed.

##### 4.4.1 Fabrication of the microfluidic chip

A hard mold (SI-master) was manufactured utilizing photolithography, which made it possible to cast PDMS inside a Teflon base polycarbonate lid. The casted PDMS chip was thereafter mounted to a glass cover slip, thus resulting in the assembled chip. Co-cultures of HULEC-5a with fibroblasts embedded in fibrin gel were seeded into the middle channel – diamond-shaped chambers - and incubated with media perfused from reservoirs (Figure 20). These media reservoirs were filled with different height of medium to create a pressure difference, thereby creating interstitial flow through the microchannel containing cells. Medium exchange was performed once a day to maintain the constant perfusion. This was executed so the cells were exposed to shear stress and constant perfusion of nutrients, thus simulating the mechanical forces found in *in vivo* (Paszowski et al. 2003).

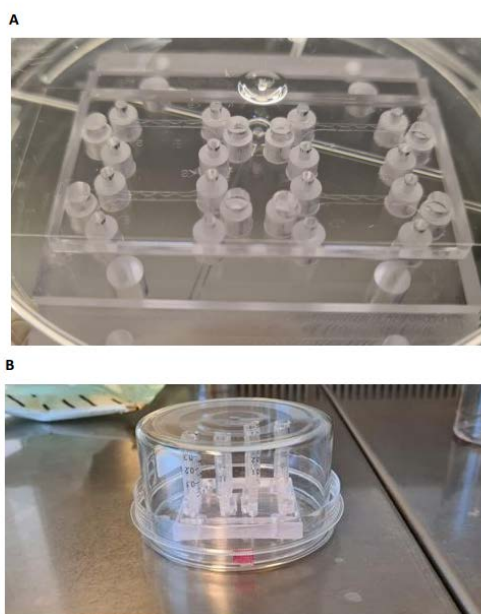


*Fig. 20:* A) A picture of an assembled PDMS microfluidic (microvasculature) chip. B) Mixture of HULEC-5a and Human pulmonary fibroblasts were seeded into the assembled chip and perfused with nutrients from media reservoirs. The chip with the seeded cells and media reservoirs was enclosed in a petri dish. Thereafter, it was placed in an incubator at 37°C and 5.0% CO<sub>2</sub> for cells to proliferate and form vascular network.

**4.4.2 Optimal cell ratio to co-culture HULEC-5a and Fibroblast.** A traditional well plate assay was utilized to optimise the ratio of fibroblast to HULEC-5a needed to attain a spontaneous vascular network



formation in vitro. The ratio that showed the ideal formation was seeded into the middle channel of the microfluidic chip. Two different cell ratios of HULEC-5a and Human pulmonary fibroblast were co-cultured to find the optimal ratio to use in the microfluidic chip. The cell ratios that were tested are 1:1 and 1:2 (fibroblasts to HULEC-5a), where each ratio was cultured in complete EGM-2 medium the first two days after cell seeding and then with EGM-2 without VEGF and FGF or complete MCDB131 medium with 10%FBS. The ratio samples were fixed and immunostained for VEcadherin, actin and nucleus. Samples were imaged using a fluorescence microscope (Leica TCS SP8 STED 3X). The results are presented in Figure 21.

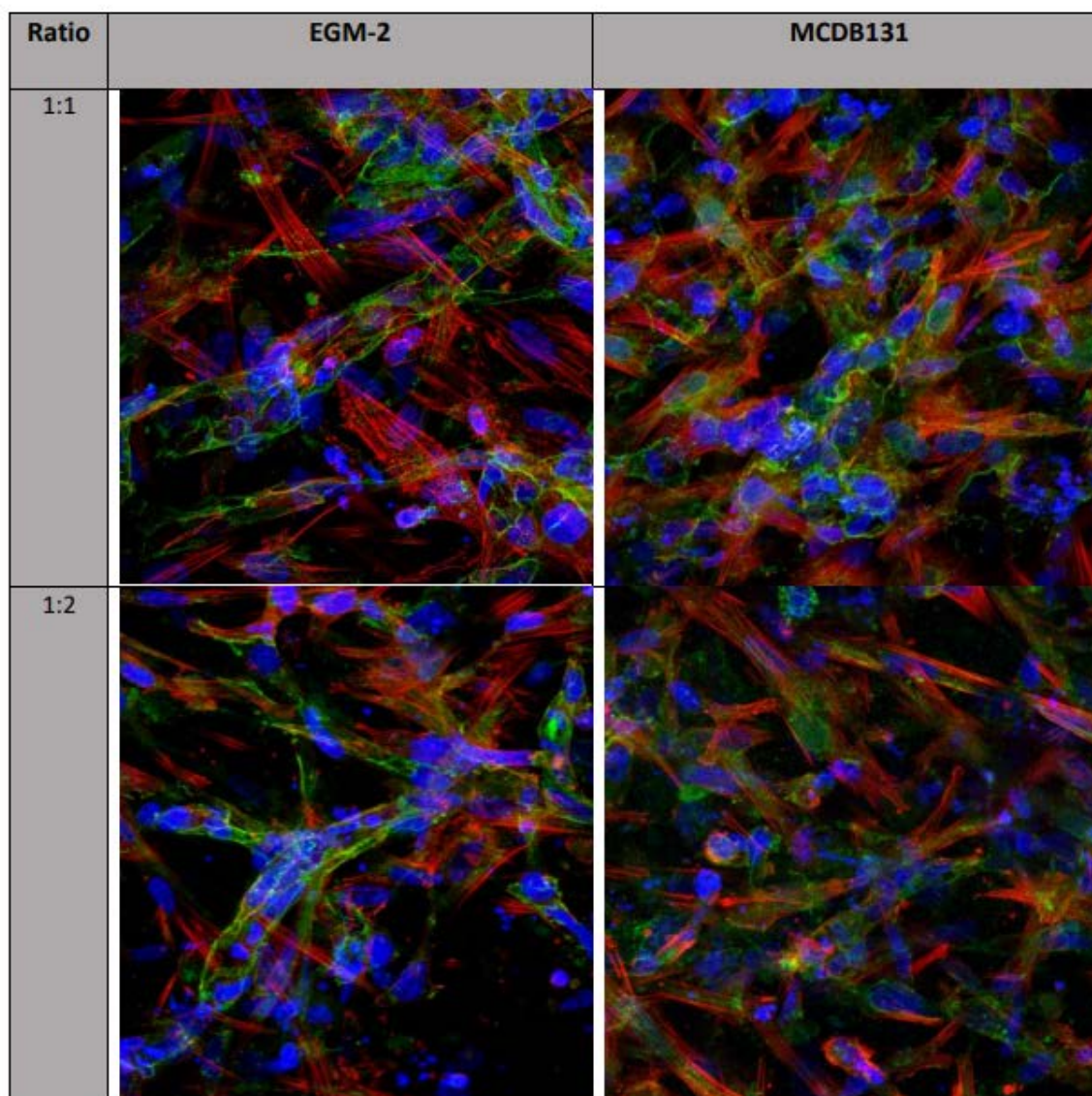


*Fig. 21: Images of Human pulmonary fibroblast cells co-cultured with HULEC-5a in fibrin gel. Two ratios were assessed: 1:1 and 1:2 (fibroblast: HULEC-5a) supplied with either EGM-2 medium the first 2 days after seeding and then with EGM-2 without VEGF and FGF (column 1), or MCDB131 complete medium (column 2). The cultures were stained for VE-cadherin (green), actin (red) and nuclei (blue).*

From the imaging, both cell ratios exhibited clustering of HULEC-5a to form the characteristic tube-like structure of vasculature. These structures showed VE-cadherin staining at cell-cell contacts, which is a known vascular endothelial cell markers (Sorrell et al. 2007). Co-cultures grown in EGM2 seemed to

form more tube-like structures and showed brighter VE-cadherin staining at cell-cell contacts compared to cells cultured in MCDB131. As VE-cadherin is an endothelial cell marker, actin filament staining was performed to mainly visualize the fibroblast cells. Actin (red) was present in both cell culture media and ratio conditions. Fibroblasts developed an elongated shape with long filamentous actin bundles across the cytoplasm in all ratios and media tested. In summary, both cell ratios in EGM-2 seemed to facilitate the formation of capillary networks with no noticeable difference. However, we observed more nuclear debris in the 1:1 than in 1:2 ratio. Thus, we chose the 1:2 ratio when co-culturing HULEC-5a and fibroblast in the microfluidic chip to prevent depletion of nutrients due to over-grow of fibroblasts. 84 Ratio EGM-2 MCDB131 1:1 1:2 Figure 4.23: Images of Human pulmonary fibroblast cells co-cultured with HULEC-5a in fibrin gel. Two ratios were assessed: 1:1 and 1:2 (fibroblast: HULEC-5a) supplied with either EGM-2 medium the first 2 days after seeding and then with EGM-2 without VEGF and FGF (column 1), or MCDB131 complete medium (column 2). The cultures were stained for VE-cadherin (green), actin (red) and nuclei (blue). Next, we seeded fibroblasts: HULEC-5a in fibrin gels into the middle channel of the full assembled chip (PDMS chip fused together with glass cover slip) and incubated it for 7 days. The cells were cultured in fibrin gel, where two different amount of thrombin was added to the fibrinogen cell solution to evaluate the influence that gel stiffness has on the vasculature formation. To note, higher amount of thrombin produces a firmer gel matrix for the cells (Narayanan 1999). The tested conditions were either 2.5 U/ml or 5.0 U/ml thrombin. A picture was taken of the cells 1, 2, 4 85 and 7 days after seeding. The co-cultured cells formed tube-like structures as early as 2 days after seeding for both thrombin concentrations. The system is currently being optimized.

## 4.5. Results from the colorimetric tests (NILU, KUL, INIC, ANSES)

### 4.5.1. Dispersion protocol

As described in **Deliverable 5.1**, the stock dispersions for each ENM tested were prepared following a harmonised SOP for the resuspension of ENMs in biological media and *in vitro* dosimetry (see deliverable D4.9 for details). The overview of the tested particle can be found in Table 4. The protocol was provided by WP4 (LIST). The DeLoid protocol was to be followed during RR1 for TiO<sub>2</sub> and ZnO ENMs, and for CuO and MWCNTs in RR2. The Tungsten and the last two ENMS; NM300K and NM111 were dispersed following NANOGENOTOX protocol.

**During RR1**, 5 mL of stock solution of TiO<sub>2</sub> and ZnO ENM at 5 mg/mL were prepared in MilliQ water and vortexed. Samples were sonicated using a probe sonicator which was previously calibrated by all partners as part of WP4 SOP harmonisation for ENMs dispersion, to be able to define the sonication energy that is really delivered to the solution. In the case of the TiO<sub>2</sub> and ZnO ENMs, the total energy to be used by all partners to disperse the particles was 322.32 J/mL.

**During RR2**, the CuO and MWCNT ENMs were prepared following the LIST protocol (see deliverable D4.9 for details). Specifically, for Nano Tungsten Carbide/Cobalt (NanoAmor) particles, partners followed the NANOGENOTOX protocol. The NANOGENOTOX protocol was chosen here in order to allow the comparison of the results with those from previous EU projects where the same type of particles was employed. Briefly, the stock was first diluted in filtered MilliQ water containing 0.05% Bovine serum albumin (BSA) to achieve a stock solution of 2.56 mg/mL. The sample was sonicated for a specific time to be able to deliver a total energy of 7056 +/- 103 Joule in total volume of 6ml. The sample was kept on ice during the process of sonication to avoid overheating.

Similarly, during **Task 5.2** the **NANOGENOTOX protocol** was followed to prepare the **NM300K and NM111** dispersion to allow comparison of the results with those from previous EU projects where same particles were tested (e.g., NanoREG, Nanoreg2).

The obtained dispersions, each ENM was further diluted in the cell culture medium to achieve the desired concentrations to be used in each test.

#### 4.5.2. Overview of colorimetric methods, cell lines and exposure conditions

The selected test methods to test the cytotoxic effect of each of the ENMs as well as the concentrations, exposure time and cell lines are listed below in Table 7.

**Table 7. Overview of the selected colorimetric methods for cytotoxicity testing, cell lines, exposure times, concentrations and controls used in RR1&RR2 (T5.1) and in T5.2.** AB, Alamar Blue, WST-1; TBA, trypan blue exclusion assay; MTT. NC, negative control; PC, positive control; PC1=CHL; chlorpromazine, PC2=MMS methylmethane sulfonate, PC3=Hydrogen peroxide H<sub>2</sub>O<sub>2</sub> or PC4= KBrO<sub>3</sub> potassium bromate.

	NMs-RR1	NMs-RR2	Task 5.2
ENMs tested	TiO <sub>2</sub> ZnO	CuO Tungsten MWCNT	NM300K & NM111
Colorimetric Assays	AB/WST/TBA/MTT	AB/WST	AB
Cell line	A549 TK6	A549 TK6	A549
Exposure time	3, 24h	3, 24h	3, 24h
Concentrations	1-100 µg/mL or 1- 25 µg/mL	1-100 µg/mL or 1- 25 µg/mL	1-100 µg/mL or 1- 25 µg/mL
Controls	NC (medium) PC1 CHL. PC2 MMS PC3 H <sub>2</sub> O <sub>2</sub> PC4 KBrO <sub>3</sub>	NC (medium) PC1 CHL. PC2 MMS PC3 H <sub>2</sub> O <sub>2</sub> PC4 KBrO <sub>3</sub>	NC (medium) PC1 CHL.
Partners involved	NILU (AB assay), INIC (AB assay), ANSES (TBA, MTT)	NILU (AB) & KuLeuven (WST)	NILU

Cytotoxicity can be measured by colouring of dead cells, such as the TBA assay (ANSES) which uses conjugation of (4-thiobutylamidine), or metabolic activity and conversion from non-fluorescent to fluorescent dye in metabolic active and viable cells, such as **AlamarBlue (AB) assay (NILU (RR1&RR2 and Task5.2) and INIC (RR1)), WST-1 assay (KU Leuven (RR2)) and MTT and TBA (ANSES, RR1)**. These assays for cytotoxicity were performed as part of the genotoxicity testing to distinguish between primary and secondary genotoxicity detected by measuring of DNA strand breaks and oxidised DNA lesions. The cells were exposed to each ENM for 3 and 24 hours, and 2-3 independent experiments

including at least 2 replicate wells for each treatment in each experiment were included. Testing for interference of ENMs with the test methods has been also conducted.

#### 4.5.3. RR1 and RR2 Summary of data (NILU, KU Leuven, INIC)

(see DELIVERABLE D5.1 for more info)

In RR1, both human lung epithelial cells A549 and human lymphoblastoid TK6 cells were exposed to ZnO and TiO<sub>2</sub> ENMs. Results from RR1 showed no cytotoxic effect of TiO<sub>2</sub> ENM after exposure of TK6 and A549 cells using the AB assay (NILU) or MTT assay (ANSES) for A549 cells or TBA assay (ANSES) for TK6 (see D5.1). The ZnO ENM was found to be highly toxic at both 3 and 24 h exposure (NILU) by the AB assay in both cell lines, while with the TBA assay cytotoxicity was only detected after 24h exposure of A549 cells (ANSES).

In RR2, human lung epithelial cells A549 and human lymphoblastoid TK6 cells were again used and exposed this time to Tungsten, CuO or MWCNTs for 3 or 24 h and cell viability measured by metabolic reduction and fluorescent signal of the dyes in living cells. Two different colorimetric assays were used – AB assay (NILU) and WST-1 assay (KU Leuven). In A549 cells, Tungsten was found not to be cytotoxic, while CuO and MWCNTs ENMs reduced cell viability in a concentration-dependent manner. The two assays gave rather consistent results, except after 3 h exposure for MWCNTs ENM, where increased fluorescence intensity was measured by AB assay, while decreased cell viability is reported by WST-1. No interference (INT) with the readouts of the assays were detected using both methods (D5.1). In TK6 cells, Tungsten did not induce cytotoxicity, in line with the results from A549 cells. CuO ENM reduced cell viability in a concentration-dependent manner after 24 h, and only a very slight reduction was measured only with the WST-1 assay after 3h. MWCNTs ENM reduced cell viability at the from 50 µg/mL, and the effect was most pronounced with the AB assay (D5.1). Also, in TK6 cells, the results were found to be rather consistent between the two assays.

NOTE. All Data from RR1: TiO<sub>2</sub> and ZnO ENMs (NILU & ANSES) and Data from RR2: CuO, Tungsten and MWCNT ENMs (NILU and KU Leuven) are available in TEAMS and were reported in Deliverable 5.1. Additional data from the INIC partner were also delivered on AB assay but not included in the D5.1.

#### 4.5.4. Comparison of the methods between partners (RR1 & RR2 data in Task 5.1)

The QSAR Lab conducted additional statistical analysis *for the experimental toxicity data (AB and WST-1 assays)* between partners. The aim is to determine if the obtained measurements between different labs (NILU & INIC or NILU % KU Leuven) are consistent. QSAR Lab performed the analysis on the data delivered and reported in D5.1 by task 5.1 during RR1 (NILU & INIC) and during RR2 (NILU & KUL).

##### 4.5.4.1. AB assay data comparison between partners (NILU & INIC) (RR1 T 5.1).

As previously described and reported in D5.1, the cytotoxicity was measured using the AB assay by NILU and INIC. Negative control and four different concentrations (0 – negative control, and 1-100 µg/mL) of the two ENMs (TiO<sub>2</sub> JRCNM01005a or ZnO (Sigma Aldrich 721077) were tested on A549 human lung epithelial cells for 3 or 24 hours. Additionally, the human lymphoblastoid cells (TK6) were also used by NILU lab and exposed similarly as A549 cells (data reported in D5.1).

At least two independent experiments with two replicates were conducted for each ENM. Relative cell viability was measured and calculated fold-change versus control set to 100%. The AB assay was conducted by NILU and INIC. Two independent experiments with three replicates were performed. A comparison of the results with their standard deviations (SD) is shown in Figure 22.

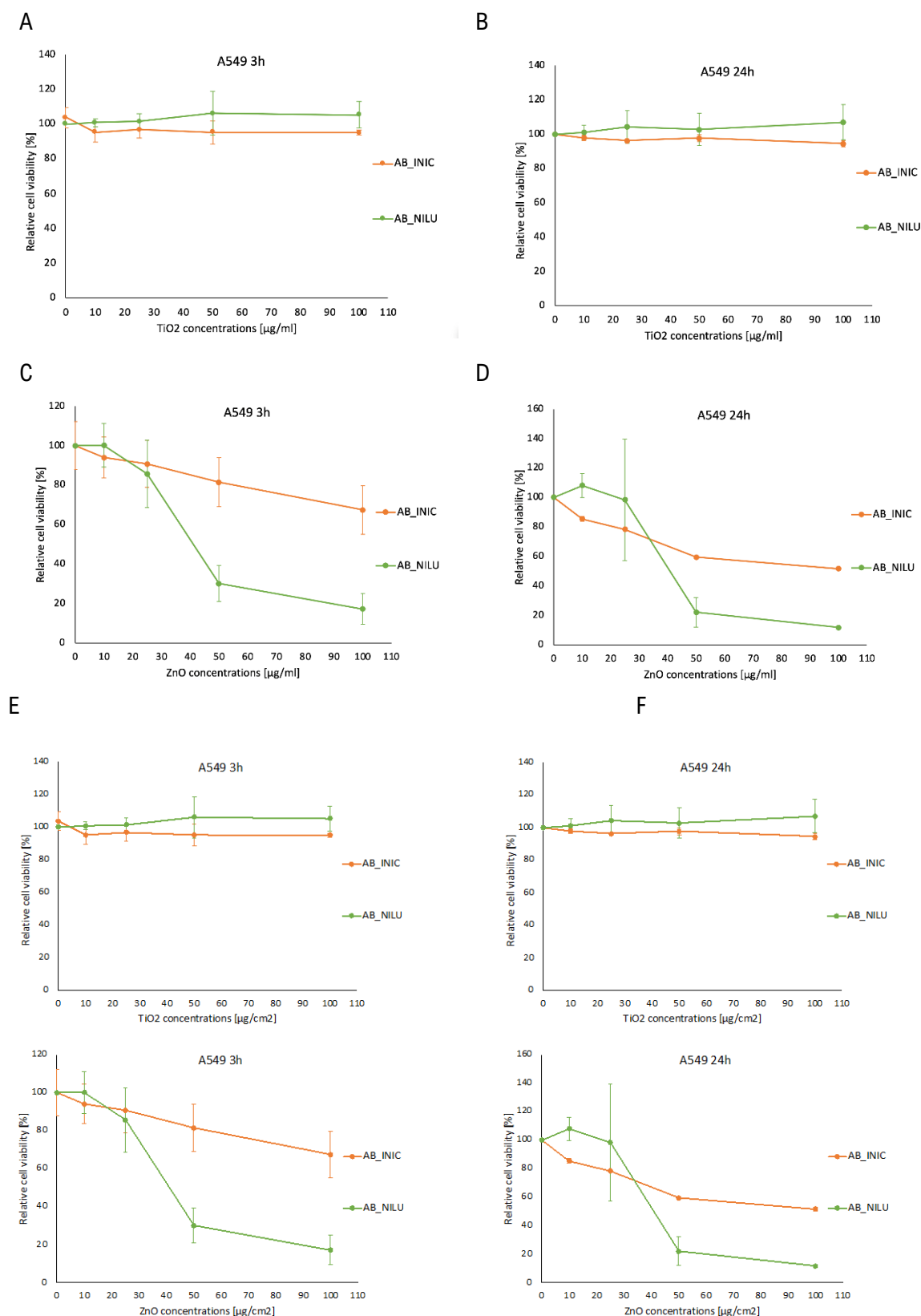


Fig. 22. Relative cell viability [%] after exposure of A549 cells for 3h or 24h to TiO<sub>2</sub> (A, B respectively), and ZnO Sigma Aldrich 721077 (C, D respectively). Data are shown as relative to the negative control (set to 100 %). Data are presented as mean +/-SD from at least 2 independent experiments for each partner, (INIC) – orange, (NILU) – green. h, hours. (DATA from D5.1).

According to this analysis, the TiO<sub>2</sub> (JRCNM01005a) was not found to be cytotoxic by both laboratories at both time points (Figure 22 A, B). Moreover, the results obtained for each of the measurements are characterized by a low SD value.

In the case of ZnO (**Sigma Aldrich 721077**), no cytotoxic effect was observed at the lower concentrations (10, 25 µg/ml) at both time points 3 and 24h (Figure 22 C, D). At higher concentrations (50, 100 µg/ml), a decrease in cell viability was observed by both labs NILU and INIC after 3 and 24h (Figure 22 C&D). The decrease pattern is different between both laboratories. The ZnO didn't induce more than 20% decrease in cell viability after 3h (INIC) compared to 60% decrease in cell viability after 3 h (NILU). After 24 h, a significant decrease in cell viability was detected by both laboratories. For more information on this comparison, EC50 values were calculated for both labs on both ENMs tested (Table 8).

#### *4.5.4.2. AB assay data and WST-1 assay data comparison (NILU & KuLeuven) (RR2).*

The three ENMs (MWCNT, CuO, Tungsten Carbide) were tested on A549 human lung epithelial cells, and human lymphoblastoid TK6 cells for 3 or 24 hours. Cell viability was measured AB assay (NILU) and WST-1 (KUL). The concentration-dependent comparison could help to identify methods more prone to NM interferences.

The data from AB and WST-1 assays on A549 cells are presented below in Figure 23 and from TK6 on Figure 24.

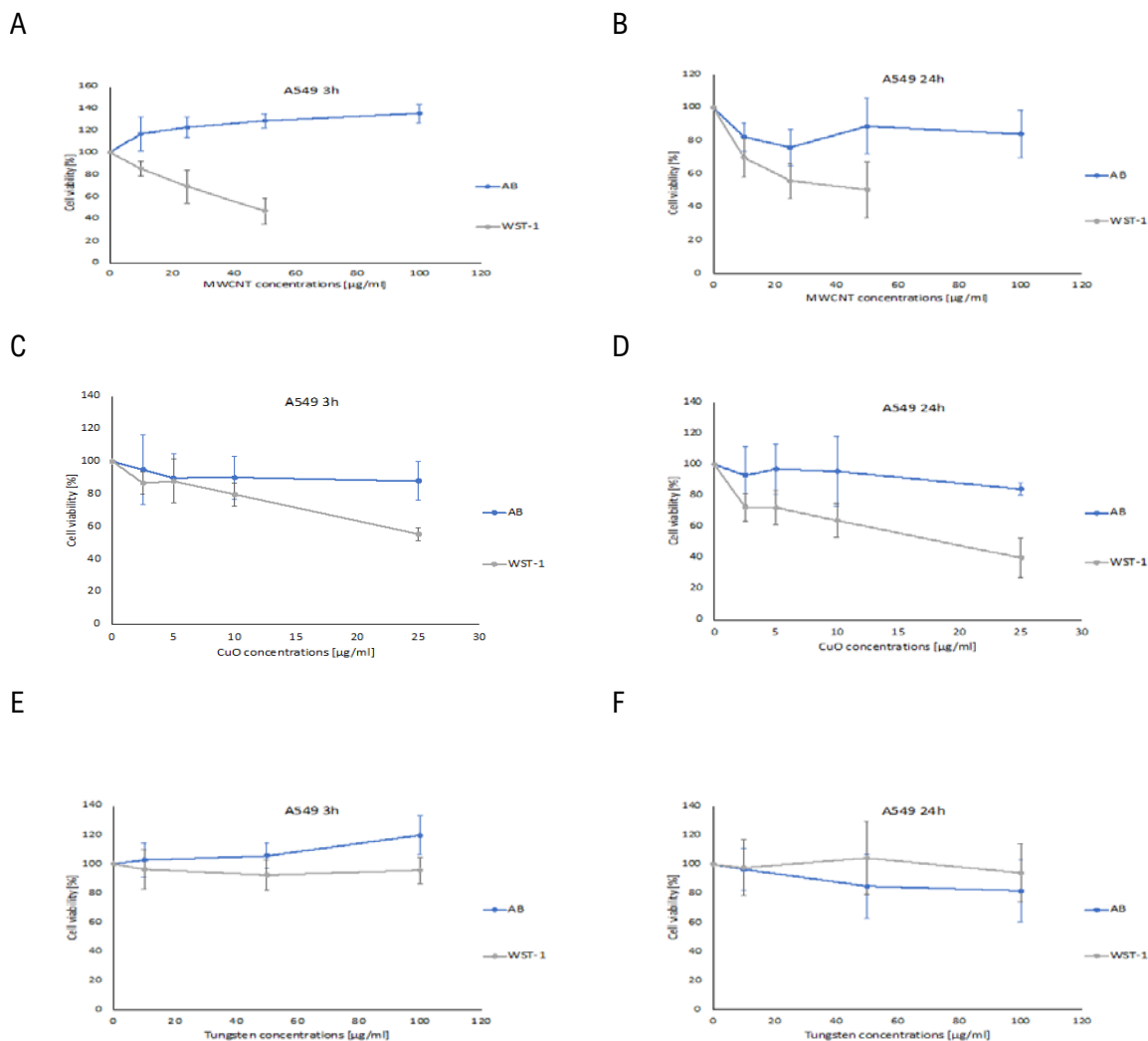


**Fig. 23. Cell viability [%] tested by AB and WST-1. A549** cells were treated for 3h or 24h with MWCNT (A, B respectively), CuO (C, D respectively), Tungsten (E, F respectively), and cell viability was measured. Cell viability is shown relative to the negative control (set to 100 %) as mean  $\pm$  SD from at least 2 independent experiments for each method, Alamar Blue (AB) – blue, WST-1 – grey. (DATA reported in D5.1).

### A549. CuO 40NM

For CuO, the results of measurements for 3h and 24h (Figure 23C and 23D) are very close to each other in all concentrations (2.5, 5, 10, 25 µg/ml) by NILU. There is a slight to no decrease in cell viability after exposure to CuO using AB assay. However, the use of WST-1 revealed a decrease of 40% of cell viability at 25 µg/ml after 3h exposure, while the decrease was more pronounced (60%) after 24h at the same concentration. Based on this comparison there is a difference between both AB and WST-1 assay to detect the cytotoxic effect of the CuO especially after 24h.

### **A549. Tungsten Carbide (WC)**

Tungsten carbide in this study did not induce any significant decrease of cell viability using both AB and WST-1 assays at both time points 3h (Figure 23E) and 24 h (Figure 23F). Tungsten is therefore categorized as non-cytotoxic by both methods.

### **A549. MWCNT 3WT% AQUACYL 0303-NC7000**

In the case of A549 cells treated with MWCNT for 3 hours (Figure 23A), we observed a significant difference in the effect obtained by either AB or WST-1. For the AB assay, no cytotoxic effect of MWCNT was observed rather the cell viability % increases with an increase in ENMs concentration, while using the WST-1 method, the MWCNT did reduce the cell viability with an increase in MWCNT concentrations. After 24-hour exposure and below 50 µg/ml (Figure 23B), the cell viability decreased in concentration-effect manner detected by both AB and WST-1 assays. However, at 50 µg/ml and above, the trend shifted and there is again an increase in % cell viability measured by AB while the decrease of cell viability continues as detected by WST-1.

For more comparison between the two methods, the EC50 values were calculated for each ENMs tested (Table 8).



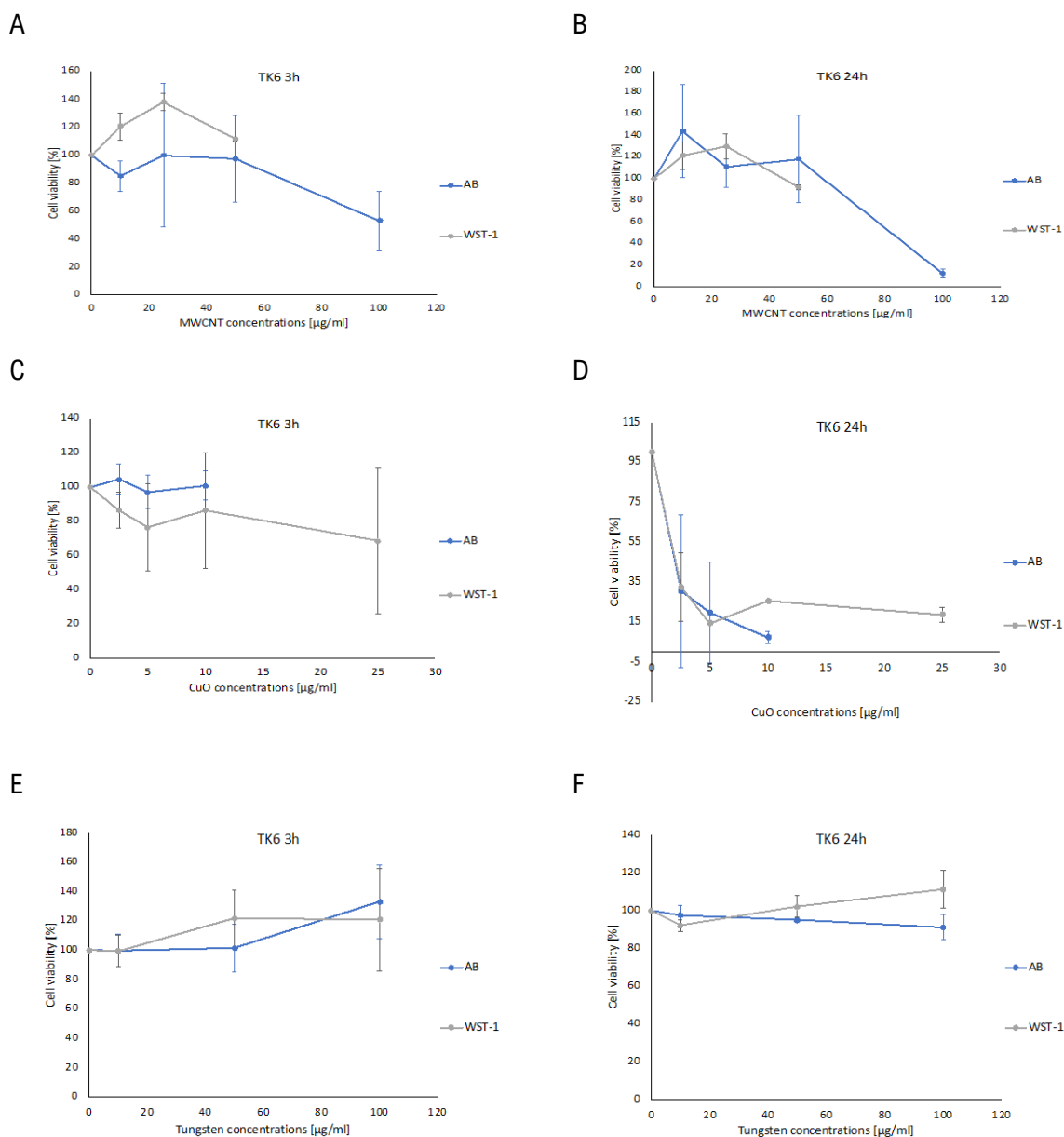


**Fig. 24. Cell viability [%] of TK6 cells tested by AB and WST-1. TK6 cells** were treated for 3h or 24h with MWCNT (A, B respectively), CuO (C, D respectively), Tungsten (E, F respectively), and cell viability was measured. Cell viability is shown relative to the negative control (set to 100 %) as mean  $\pm$  SD from at least 2 independent experiments for each method, Alamar Blue (AB) – blue, WST-1 – grey. (DATA reported in D5.1).

### TK6-CuO 40NM

After 3 h exposure (Figure 24C), there is a slight decrease in cell viability by CuO detected using WST-1 method but not AB method which is relatively similar to what we observed using A549 cells. After 24 h (Figure 24D), a significant decrease in cell viability was detected by both AB and WST-1. Compared to A549 cells, we can conclude that TK6 cells are more sensitive or prone to cytotoxic effect by CuO after 24h.

### **TK6-Tungsten Carbide (WC)**

The WC showed no significant decrease of cell viability using both methods AB and WST-1 after 3h exposure (Figure 24E) nor 24h (Figure 24F). This is in accordance to what was observed using A549 cells. It is also interesting to mention, that both methods detected a slight increase in % cell viability at the higher concentrations (50 µg/ml) either after 3 or 24 h exposure by both AB and WST-1. It is also worth mentioning that measurements for concentrations of 50 µg/ml and 100 µg/ml are characterized by relatively high SD values (15-29%). This may be a clear indication of an interference issue that has happened at higher concentration which is similar to what was observed when testing MWCNT on A549 cells.

### **TK6-MWCNT 3WT% AQUACYL 0303-NC7000**

After 3h (Figure 24B), MWCNT didn't show any cytotoxic effect at the concentrations tested by both laboratories up to 50 µg/ml. Similarly, to what we observed in other cases, WST-1 detected an increase in % Cell viability. Basically, MWCNT didn't induce cytotoxic effect after 3h measured by WST-1 at the tested concentrations up to 50 µg/ml and effect was rather consistent between both methods. After 24h (Figure 24B), both methods detected a similar effect in cell viability up to 50 µg/ml. The effect was rather consistent between both methods.

NILU also included a higher concentration of 100 µg/ml at which we can observe a decrease in cell viability in both time points (3h and 24h) of the experiment. In general, the trend of results between the two methods used is similar and the observed effects were rather consistent between both methods. For more comparison, the EC50 values were calculated for both labs (Table 8).

Based on these data comparisons, issues related to interference of ENMs with the methods used were observed. It is also worth mentioning that in the approach of WST-1, a washing step of the cells in suspension after exposure. This approach may help reduce the effect of interference observed during the reading using plate reader. The other issue is the concentrations to be tested. There are several criteria to choose the top concentration to be tested one of them, pH changes and turbidity. At higher concentrations, those criteria may not be respected. In the method paper published by NILU team, this has been addressed and discussed (El Yamani et al., 2022). It is therefore necessary to choose carefully the top concentration of ENMs to be tested, check for any interference issues and mitigation action as described in the method paper by Longhin et al. 2022.

#### **4.5.5. Summary of data obtained with colorimetric methods in Task 5.2**

Within Task 5.2, following the same SOPs for AB assay from NILU and as published by Longhin et al., 2022 (Figure 25), and the testing conditions agreed.

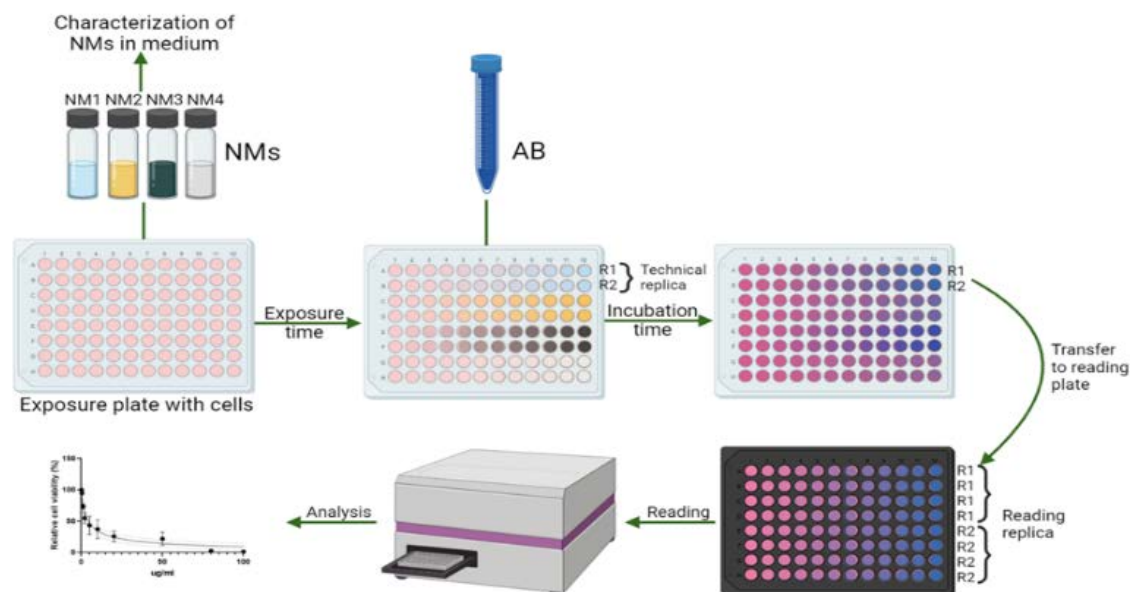


Fig. 25. Different steps of the AB assay. Caption from (Longhin et al., 2022). Frontier Special issue.

The ZnO NM111 (JRC) and Ag NM300K (Fraunhofer) were tested using one cell line. The A549 and two-time points exposure 3 and 24h were used. Basically, the same testing strategy used in RR2 was applied here to test these two ENMs. The results are presented in Figure 26.

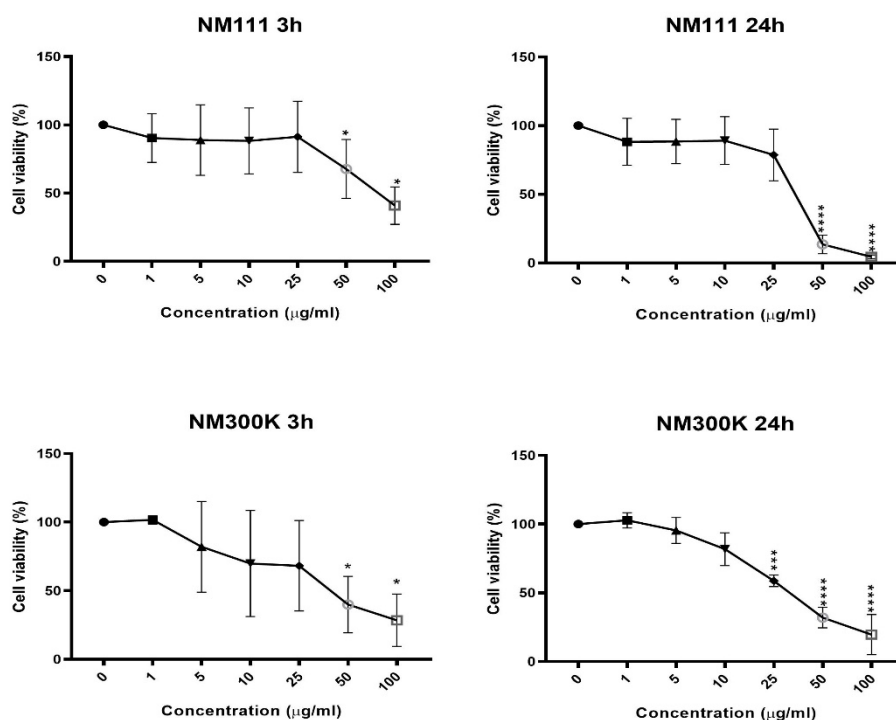


Fig. 26. Cell viability after exposure of A549 for 3 or 24 hours to NM111 (ZnO ENMs) and NM300K (Ag) measured by the AB assay after 3 and 24h exposure. The data are presented as mean of 3 independent experiments +/- SD. SC, solvent control (only medium) was also tested and no decrease on cell viability was observed (data not shown in figure but will be reported as Annex); h, hours. Possible interference of ENMs with the AB test was assessed by mixing ENMs suspensions with medium + 10 % AB (no cells).

No interference was seen at the highest concentration (100 µg/mL) (Data not shown in this figure but will be reported under test for interference section).

#### 4.5.6. Comparison of the data obtained with each method and compilation of all RRs data including task 5.2 data

For the comparison between each of the test methods, EC<sub>50</sub> values will be calculated after 3 and 24 h (Tables 8 and 9).

**Table 8. Calculated EC<sub>50</sub> values (mean ± SEM) for the cytotoxic effects of all the ENMs tested by each partner, NILU (AB assay), INIC (AB assay) and KuLeuven (WST-1) after exposure of A549 cells for 3 or 24 h.** The results are mean values calculated from three independent experiments and concentrations given as µg/ml +/- SEM. SEM, standard error of mean; h, hours. NA not available.

ENMs		EC <sub>50</sub> (µg/ml +/- SEM) 3 hours			EC <sub>50</sub> (µg/ml +/- SEM) 24 hours		
		NILU (AB)	INIC (AB)	KuLeuven (WST-1)	NILU (AB)	INIC(AB)	KuLeuven (WST-1)
RR1	ZnO	35.33	Not cytotoxic		36.9	99.87	
	TiO <sub>2</sub>	Not cytotoxic	Not cytotoxic		Not cytotoxic	Not cytotoxic	
RR2	CuO	Not cytotoxic		30.96	98.2		12.7
	Tungsten	Not cytotoxic		Not cytotoxic	Not cytotoxic		Not cytotoxic
	Aquacyl	Not cytotoxic		50.6	Not cytotoxic		48.41
T5.2	NM-300K	36.95+/-12.07			31.54+/-2.65		
	NM111	82.05+/-19.48			33.31+/-2.92		

**Table 9. Calculated EC<sub>50</sub> values (mean ± SEM) for the cytotoxic effects of the ENMs measured by each partner, NILU (AB assay), KuLeuven (WST-1) after exposure of TK6 cells for 3 or 24 h.** The results are mean values calculated from three independent experiments and concentrations given as µg/ml +/- SEM. SEM, standard error of mean; h, hours. NA not available.

ENMs		EC <sub>50</sub> (µg/ml +/- SEM) 3 hours		EC <sub>50</sub> (µg/ml +/- SEM) 24 hours	
		NILU (AB)	KuLeuven (WST-1)	NILU (AB)	KuLeuven (WST-1)
RR1	ZnO	12.84		9.58	
	TiO <sub>2</sub>	Not cytotoxic	Not cytotoxic	Not cytotoxic	Not cytotoxic
RR2	CuO	Not cytotoxic	Not cytotoxic	<b>1.39</b>	<b>1.28</b>
	Tungsten	Not cytotoxic	Not cytotoxic	Not cytotoxic	
	Aquacyl	>117.522 Not cytotoxic	Not cytotoxic	>89.27 Not cytotoxic	Not cytotoxic

#### 4.5.7. Test for possible ENM-induced interferences

For cytotoxicity testing of ENMs, interference is an important challenge especially in relation to colorimetric and fluorescent test methods. ENMs can in general interfere with toxicological tests at different levels, from the assay's chemical reactions to the test readout (Guadagnini et al., 2015). As an example, spectroscopic analyses have highlighted interactions (indicated by reduction of absorption/fluorescent emission) of single walled carbon nanotubes (SWCNT) with several dyes used for cytotoxicity investigations, including Neutral Red, MTT, WST-1, and also AB, which was found to be the most sensitive and reproducible method (Davoren et al., 2007). Interference of ENMs with the testing methods is of major concern. Interference issues might account for the inconsistency sometimes found

in the responses obtained with the different cytotoxicity methods; therefore, the verification of the results by using at least two methods is recommended (Dusinska et al., 2015). Repeated washing steps should be performed after exposure to remove as many particles as possible. However, internalized particles or particles adhering to the cell surface will not be removed after washing (Davoren et al., 2007). To properly address this issue, appropriate controls to check for interference should always be included in the experiments (Longhin et al., 2022).

The hazard testing of ENMs has been described to face issues attributed to various interferences due to their specific physicochemical characteristics, thus the potential interference of the ENM with the test assays has been carefully checked and controlled during the performance of AB assay. A simple approach consists of ENMs in cell culture medium in wells without cells (only medium with ENMs). The highest concentration tested for the ENMs should be included as a minimum condition, however other test concentrations could be added in an optimal situation. These controls will be incubated for the same time as the exposed cell samples.

Interference control samples for ENMs (10% AB in medium + ENMs without cells) should be compared with the blank control samples (10% AB in medium without cells). This can be done at the level of FU, i.e., no significant difference between FU of interference control samples and FU of blank samples. Alternatively, the interference controls can be analysed as the other samples, i.e., the relative fluorescence intensity can be calculated. In this case the relative fluorescence intensity value obtained for the interference control sample is expected to be around 0 %. This last approach has been used for the results to be reported. How interference controls have to be interpreted has been also described by Longhin et al. (2022). Briefly, if the FU value of the interference samples significantly deviates from that of the blank sample (or the relative fluorescence intensity deviates from 0 %), it means that the ENMs interfere with the AB assay and the results obtained are not reliable. Also in this case, the criteria for determining if an interference is present can depend on the application field, and on the criteria applied to determine the cytotoxicity of the test compound. A statistically significant difference between the interference control and the blank could be a sufficient indication of interference.

This interference testing strategy allows us to assess the potential of ENMs to interfere with the reagents before reading the fluorescence either by increasing or hindering the signal. However, they may be also other mechanisms involved in the interference of ENMs with the testing system. ENMs in presence of cells and during their uptake or metabolism may have induced some other mechanisms and thus interfered with other metabolites. Therefore, this test for interference is in some ways limited since it does only assess the potential of ENMs present in the cell culture media without looking into what happened when cells are present.

#### 4.5.8. Advantages and disadvantages of colorimetric tests

For colorimetric/fluorometric assays, there are some clear advantages and also some limitations. If we take for instance AB assay with respect to the MTT assay as example. There is evidence that AB assay is more reliable when it comes to ENMs testing i) first, being water-soluble resorufin of the AB is released in the cell culture medium, which can be directly used for measurement. In contrast, the insoluble formazan crystals produced by the conversion of the tetrazolium salt in MTT need to be dissolved by a solubilization step before reading the test. ii) Additionally, the cells used for MTT will thus be destroyed during the solubilization step, while the cells used for AB can be employed for other uses. iii) The previous point also relates to the fact that AB is non-toxic, while MTT has been reported to be cytotoxic itself (Ghasemi et al., 2021). Another advantage is that colorimetric assays can be used in a high throughput set up, allowing screening the toxicity of a large number of compounds at the same time (Hamid et al., 2004; OECD, 2018), 2018). To increase the robustness of the results, it is also possible

to go up to 8 reading replicas should be prepared from each sample. For example, if 96 well plates are used for exposure, transfer 40 µl of staining solution (medium) per 4 times into 4 different wells of flat bottom 96 wells black polystyrene microplates.

When it comes to disadvantages of the colorimetric assay, such as the AB assay, this has been described as well as the mitigation actions to control them (NILU method paper in Frontier). As an example, the clogging or precipitates of AB can be sometimes observed. Clogging in the staining solution will affect the results, making them unreliable. It is important to always check that the staining solution is free of precipitates. These can be removed by filtering the AB solution or the staining solution (AB and medium) before mixing it with the medium (syringe-filter through a 0.2 or 0.45 µm pores filter) (Longhin et al., 2022).

#### 4.5.9. Recommendations regarding colorimetric methods used in T 5.1 and T 5.2

Based on the data generated by partners, some of the ENMS didn't interfere with reading of fluorescence such as TiO<sub>2</sub>. However, the MWCNT may have increased the signal at some of the concentrations, even though we did not observe any increase of the reading signal following our approach to check for interference. Depending on what ENMs we are testing, several approaches for interference testing might be required.

It is highly recommended to build up a historical control database, with both negative as well as positive controls for each cell type and time point investigated. This allows the laboratory to demonstrate the ability to perform the assay consistently, and to show that the cells are capable of picking up positive effects and have reasonably low variability in responses. When reporting the results, it is advisable to show the average and minimum-maximum values of negative/positive historical controls from the last 10-20 experiments performed in the laboratory (Longhin et al., 2022).

In this context, the use of multiple assays (at least two cytotoxicity tests) is recommended to reduce false negative/positive results (Dusinska et al., 2015). A next step towards standardization should include a validation of the procedure through interlaboratory testing of specific settings (e.g., selected cell lines and test materials) to demonstrate the robustness of the method, i.e. the repeatability of the responses to standard ENMs.

#### 4.5.10 Conclusion on the results from the colorimetric tests

In conclusion, the AB assay and WST-1 have shown to be a reliable test to evaluate the cytotoxicity/proliferation/metabolic response of cells exposed to ENMs. Being high throughput makes them an ideal tool to be used on a large scale and in parallel or in combination with other assays, e.g., the comet assay for genotoxicity (Azqueta et al., 2022). However, washing steps after exposure and proper controls for possible interference of the ENMs with the test need to be always included. The coupling of this metabolism-based test with another class of cytotoxicity methods based for example on membrane integrity or cell number might be also a major recommendation to help strengthening the results.

## 4.6. High Content Analysis (HCA) of cell count, nuclear size, nuclear intensity, caspase-3 intensity, and DNA double strand breaks

### 4.6.1. Results from HCA analysis in A549 cells: Negative and positive controls

#### 4.6.1.1. Cell counts

Staurosporine induced a 73 % reduction in cell counts compared to control cells, while MMS induced only a slight decrease in cell counts (Figure 27).

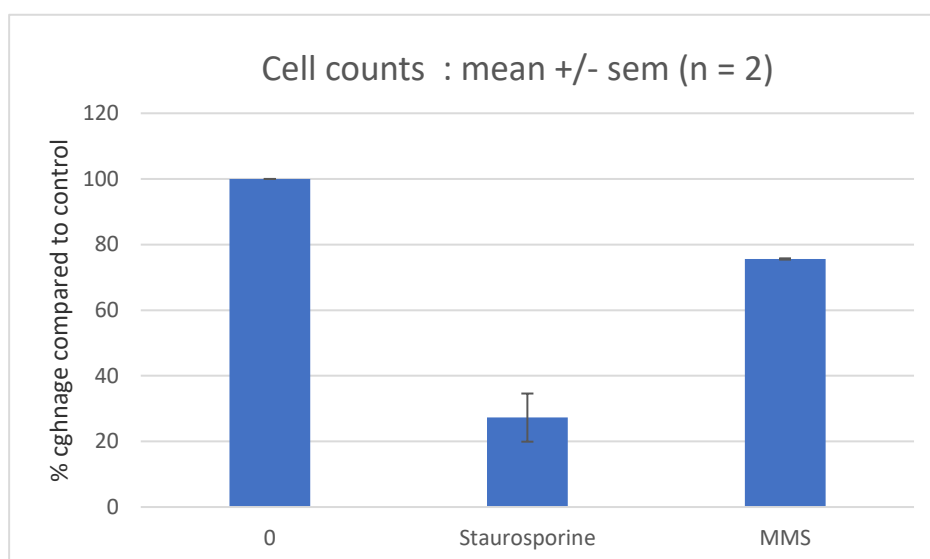


Fig. 27: Effect of positive controls on A549 cell counts.

#### 4.6.1.2. Nuclear size

No differences were observed following quantification of nuclear size between untreated cells and cells treated with positive controls, although a small increase was observed with MMS treatment (Figure 28). Early stages of apoptosis are associated with chromatin condensation, (Cummings and Schnellmann 2021), and Staurosporine has been shown to reduce nuclear size in a previous study in an immortalized retinal pigment epithelial cell line (ARPE-19) (Eidet et al. 2014). However, no effect on nuclear size in response to Staurosporine treatment was observed in our experiments, which may be related to the experimental parameters chosen.

Since MMS is known to induce cell cycle delay in S- phase and an arrest in G2/M phase (Morris et al. 1991), and since nuclear size is known to increase upon G2/M cell cycle arrest (Landry et al. 2022), the small increase in nuclear size observed upon MMS treatment could be due to its effect on cell cycle.

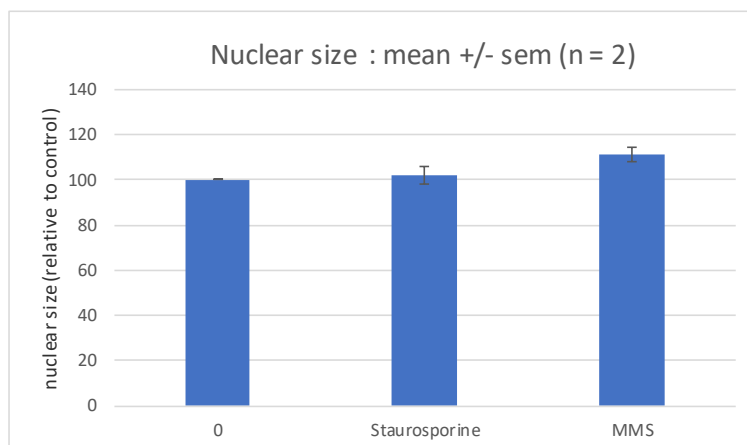


Fig. 28. Effect of positive controls on nuclear size.

#### 4.6.1.3. Average nuclear intensity

Staurosporine induced a small increase in nuclear intensity whereas MMS induced a small decrease (Figure 29). During the early stages of apoptosis, nuclei tend to appear brighter during chromatin condensation (Cummings and Schnellmann 2021). In our experiments, an increase in nuclear intensity was observed in A549 cells following staurosporine treatment, which is a known inducer apoptosis, but remained rather weak, which may be due to experimental conditions.

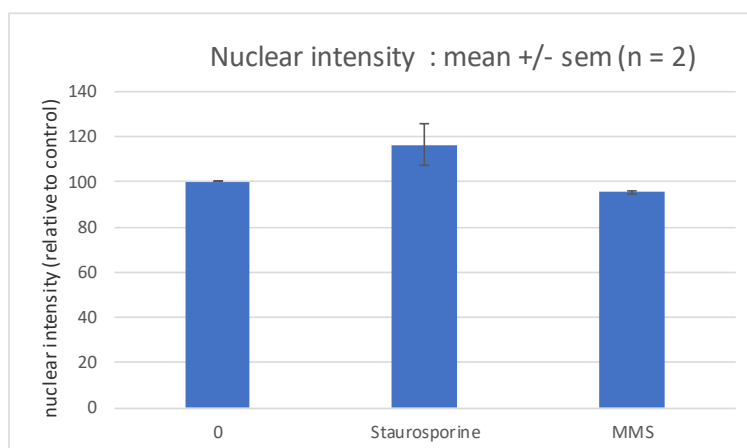


Fig. 29: Effect of positive controls on nuclear intensity.

#### 4.6.1.4. Active caspase-3 intensity

No interference was observed with the positive controls upon incubation when tested with the various controls for interference (Figure 30).

In order to assess potential induction of apoptosis in A549 cells, the level of active caspase-3 was quantified. In control cells, the average active caspase-3 intensity was low, as expected. Although staurosporine was used as a positive control for apoptosis, no difference in active caspase-3 levels were observed in staurosporine-treated A549 cells compared to control cells. In addition, after correction for interference, the levels of active caspase-3 were not different from the control. However, although strong staining for active caspase-3 could be observed by HCA, due to advanced cell death there was no



concomitant DAPI staining in these cells and therefore could not be quantified. This result suggests that the concentration of staurosporine used was not optimal and that further dilutions of the chemical should be tested. No significant change in active caspase-3 intensity could be observed in MMS treated cells.

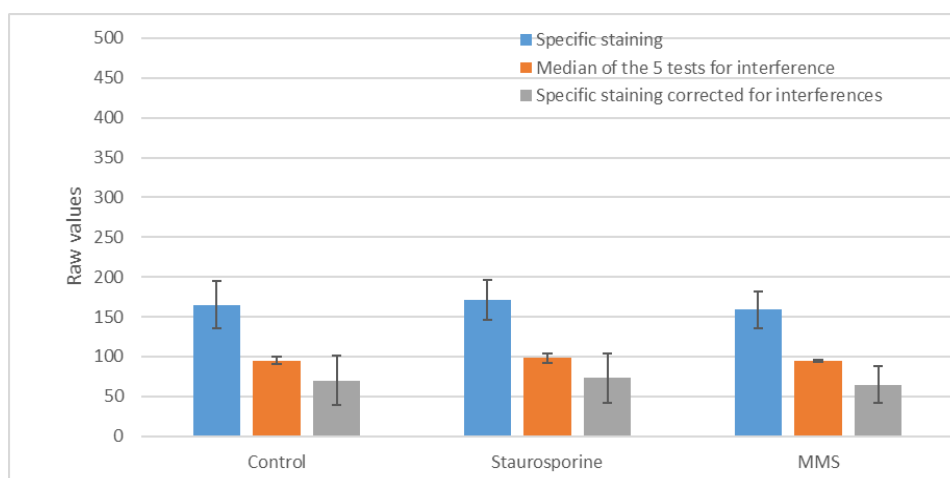


Fig. 30. Effect of positive controls on active caspase-3 intensity.

#### 4.6.1.5. $\gamma$ H2AX intensity

No fluorescence interference could be detected with MMS or staurosporine (Figure 31). The  $\gamma$ H2AX intensity was low in control cells, as expected. An increase in  $\gamma$ H2AX intensity was observed in cells treated with staurosporine (two-fold increase) (Figure 30). This increase in  $\gamma$ H2AX levels could be the consequence of DNA fragmentation, which is known to occur during the apoptotic process. Indeed, it has been shown in various cell types that staurosporine induces H2AX phosphorylation during apoptosis (Mukherjee et al. 2006). MMS was chosen as a positive control for  $\gamma$ H2AX staining since it has been previously reported to increase  $\gamma$ H2AX levels (Watters et al. 2009, Nikolova et al. 2014). However, when A549 cells were treated with MMS no significant change in  $\gamma$ H2AX intensity could be observed (Figure 30). This could be due to the concentration used (0.2 mM) that was not optimal for the assay. Moreover, it has been reported that 2 cell cycles are required for MMS to induce double strand breaks (Sánchez-Flores et al. 2015). However, in our experiments, cells were treated with MMS for 24 hours, which is only one cell cycle for A549 cells, and therefore could explain the absence of  $\gamma$ H2AX labelling. Upon correction for basal interference, only staurosporine increased  $\gamma$ H2AX staining compared to control (Figure 30).

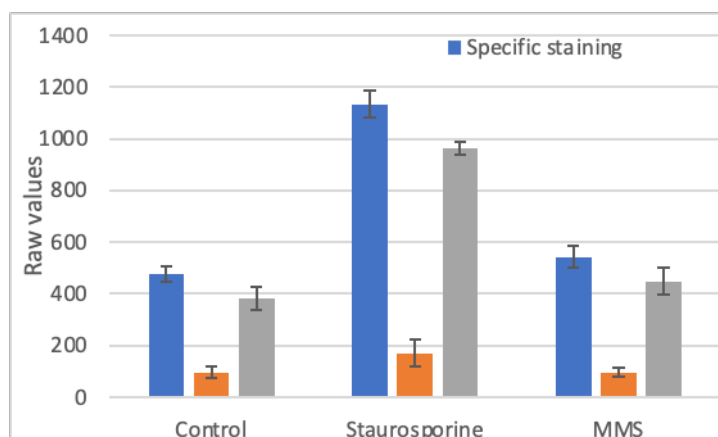


Fig. 31: Effect of positive controls on  $\gamma$ H2AX intensity.

**Table 10: Summarized results obtained with the positive controls on the various markers**

Treatment/parameter	Cell counts	Nuclear size	Nuclear Intensity	Active caspase-3 Intensity	$\gamma$ H2AX Intensity
Staurosporine	↓	-	↑	-	↑
MMS	↓	↑	↓	-	-

The cellular data from A549 cells treated with the positive controls (staurosporine and MMS) (Table 10) demonstrated that staurosporine induced a decrease in cell counts while MMS induced only a small reduction in cell counts. Staurosporine is a pro-apoptotic agent which could explain this decrease in cell count. As an inducer of apoptosis, staurosporine also induced an increase in nuclear intensity although a concomitant decrease in nuclear size was not observed. MMS had only minor effects on nuclear size and nuclear intensity. Staurosporine did not modify active caspase-3 intensity. The weak response with the positive controls for apoptotic markers could be due to the concentration used, or the time point chosen for the analysis with cells already being in an advanced state of apoptosis in our experimental conditions. MMS had no effects on active caspase-3 levels. Staurosporine induced an increase in  $\gamma$ H2AX intensity, which may be related to its induction of apoptosis. By contrast, the genotoxic agent MMS did not modify  $\gamma$ H2AX levels, which may be due to the choice of the experimental conditions, such as the concentration tested, or the time point chosen for analysis.

#### 4.6.2. CuO: Results from HCA analysis in A549 cells

##### 4.6.2.1. Cell counts, nuclear size, nuclear intensity

Upon treatment with CuO ENMs, a concentration dependent decrease in cell counts was observed (approximately 60 %) (Figure 32). In addition, CuO induced changes in nuclear size compared to control cells at 10 and 50  $\mu$ g/mL, but this decreased to control levels at 100  $\mu$ g/mL, probably due to cytotoxicity (Figure 33). Treatment with CuO ENMs induced a small increase in nuclear intensity compared to control (Figure 34). An increase in nuclear intensity and nuclear size has been previously described in the literature to be associated with oxidative stress or cell cycle arrest (Landry et al. 2022). Indeed, induction

of oxidative stress following treatment with CuO ENMs has already been reported in human bronchial epithelial BEAS-2B cells (Strauch et al. 2017).

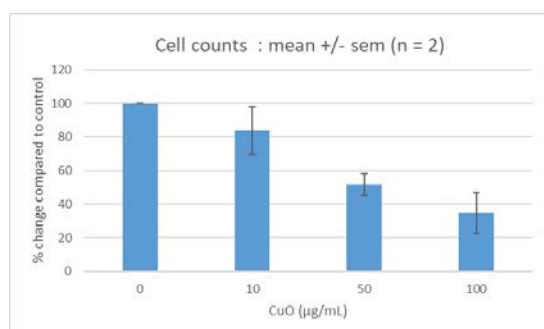


Fig. 32: Effect of CuO ENMs on cell counts.

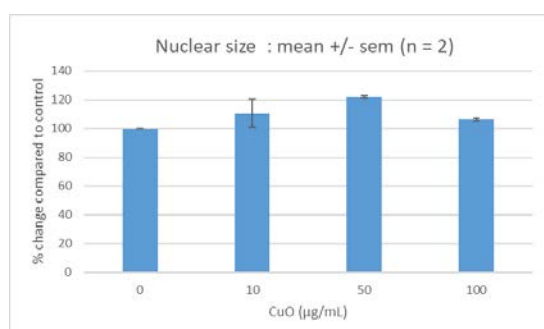


Fig. 33: Effect of CuO ENMs on nuclear size.

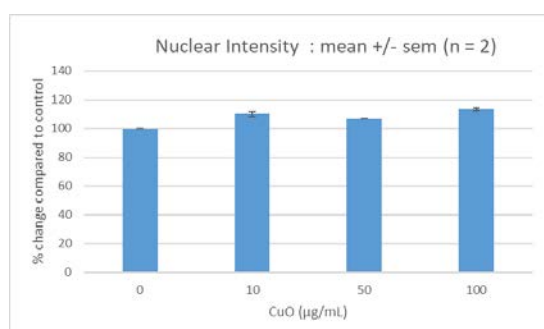


Figure 34: Effect of CuO ENMs on nuclear intensity.

#### 4.6.2.2. Active caspase-3 Intensity

No interference in fluorescence signals was observed with CuO ENMs in the wavelength used for active caspase-3 labelling (647 nm).

CuO induced a concentration-dependent increase in active caspase-3 intensity, at 50 and 100 µg/mL. Upon correction for interference, this concentration-dependent increase in active caspase-3 intensity upon CuO treatment was still observed (Figure 35).

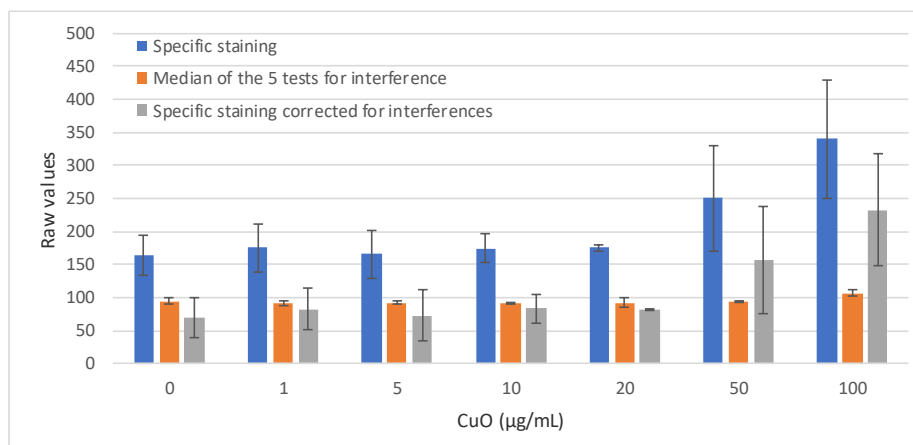


Fig. 35: Effect of CuO ENMs on active caspase-3 intensity.

#### 4.6.2.3. $\gamma$ H2AX intensity

In tests for interference, a concentration-dependent increase in fluorescence intensities in the channel used for  $\gamma$ H2AX quantification (480 nm) was observed. This suggests that the presence of CuO may interfere with quantification of  $\gamma$ H2AX intensity.

CuO treatment induced a concentration-dependent increase in  $\gamma$ H2AX intensity, even after taking into account interference (Figure 36).

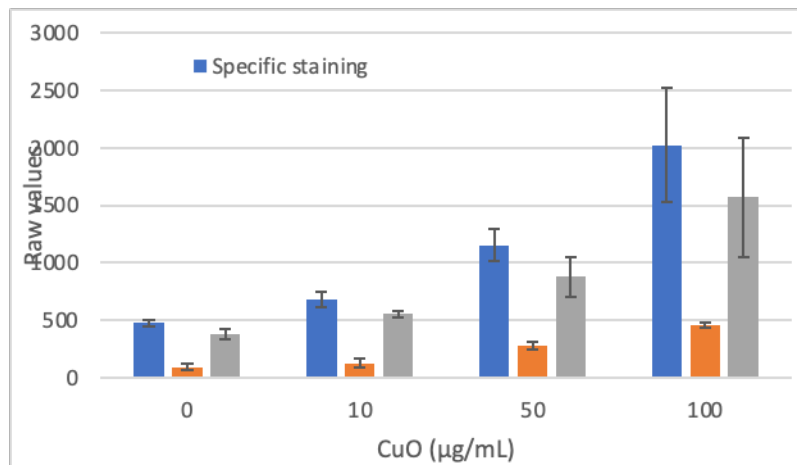


Fig. 36: Effect of CuO ENMs on  $\gamma$ H2AX intensity.

Table 11: Summary of results obtained with CuO ENMs on the various markers

Treatment/parameter	Cell counts	Nuclear size	Nuclear Intensity	Active caspase-3 Intensity	$\gamma$ H2AX Intensity
CuO NM	↓	↑	↑	↑	↑

Altogether, the data (Table 11) suggest that CuO ENMs have a cytotoxic effect on A549 cells, which could be associated with apoptosis. Cytotoxicity of CuO ENMs has previously been reported in the literature in A549 cells as well as immortalised human lung bronchial epithelial BEAS-2B cells (Sun et al. 2012, Semisch et al. 2014, Strauch et al. 2017, Kalaiarasi et al. 2018, Fahmy et al. 2020). However, the induction of apoptosis in A549 cells in response to treatment with CuO ENMs has not always been observed. Indeed, Sun et al. did observe cell death in A549 cells treated with CuO ENMs but they could not show apoptosis by TUNEL analysis and quantification of activate caspase-3 levels (Sun et al. 2012). By contrast, apoptosis was detected by Semisch et al. where they observed the translocation of the apoptosis inducing factor (AIF) into the cell nucleus and the accumulation of subdiploid DNA. However, the authors did not observe any effect on active caspase-3 activity in A549 cells upon incubation with CuO ENMs (Semisch et al. 2014). By contrast, clear activation of the caspase pathway (including caspase-3) was shown in A549 treated with CuO ENMs, at both the RNA and protein level (Kalaiarasi et al. 2018).

In our study, treatment of A549 cells with CuO ENMs increased  $\gamma$ H2AX levels. Importantly, since active caspase-3 was increased upon treatment with CuO ENMs, it could be hypothesised that the underlying apoptotic process triggered H2AX phosphorylation. Interestingly, a study performed in human umbilical vein endothelial cells (HUVECs) showed that CuO ENMs induced cell death as well as DNA damage, as assessed by increased  $\gamma$ H2AX foci formation (immunofluorescence) and increased phosphorylation of  $\gamma$ H2AX (Western Blot) (He et al. 2020) Finally, although several studies have previously demonstrated a genotoxic effect of CuO ENMs in A549 cells (Semisch et al. 2014, Fahmy et al. 2020), our results do not allow a confirmation of such an effect simply through  $\gamma$ H2AX induction, but rather to an apoptotic effect.

#### 4.6.3. WC/Co: Results from HCA analysis in A549 cells

##### 4.6.3.1. Cell counts, nuclear size, nuclear intensity

WC/Co induced a very small increase in cell counts at the highest concentration tested (Figure 37). Nuclear size was unchanged upon WC/Co treatment after 24h incubation (Figure 38). Moreover, treatment with WC/Co did not have an effect on the nuclear intensity (Figure 39).

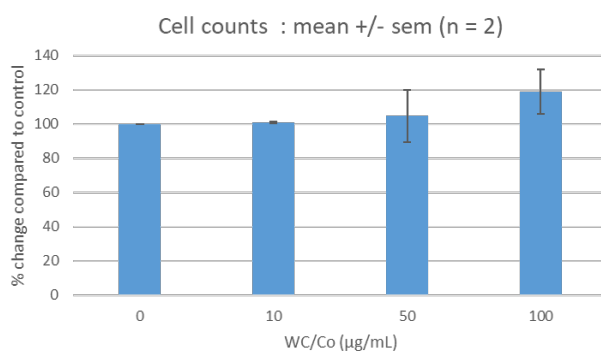


Figure 37: Effect of WC/Co ENMs on cell counts.

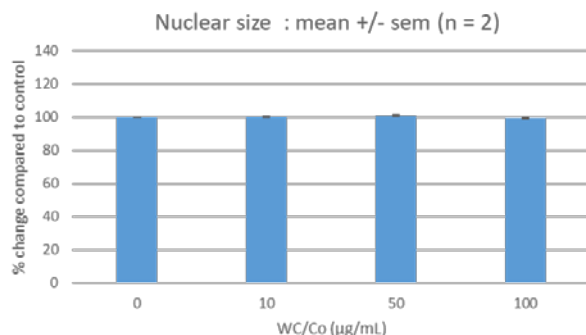


Figure 38: Effect of WC/Co ENMs on nuclear size.

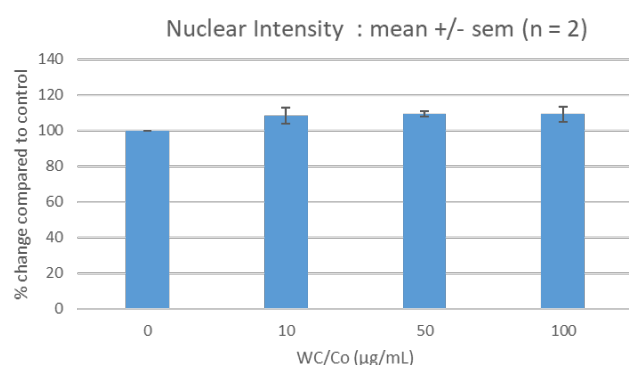


Fig. 39: Effect of WC/Co ENMs on nuclear intensity.

#### 4.6.3.2. Active caspase-3 intensity

No significant interference compared to control was observed in presence of WC/Co ENMs. Treatment of A549 cells with WC/Co ENMs induced a small increase in active caspase-3 intensity. In agreement with raw results on active caspase-3 intensity, after correction for interference, a small concentration-dependent increase in active caspase-3 intensity was observed (Figure 40).

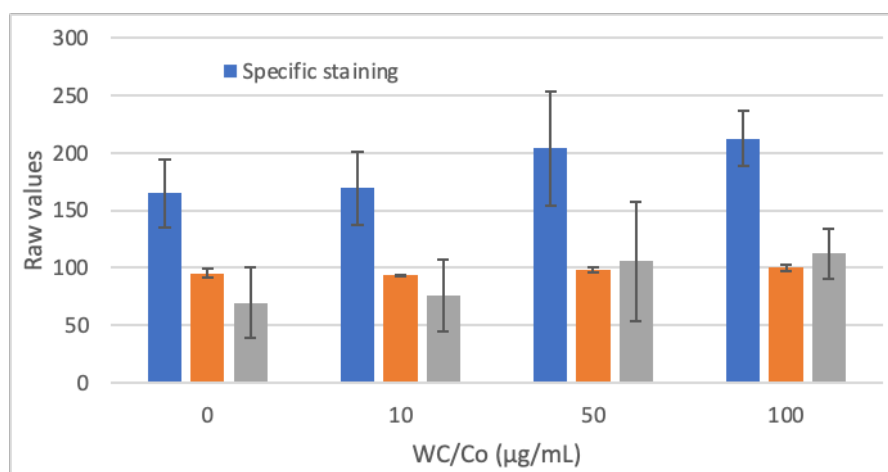


Fig. 40: Effect of WC/Co ENMs on active caspase-3 intensity.

#### 4.6.3.3. $\gamma$ H2AX intensity

WC/Co ENMs had no effect on  $\gamma$ H2AX intensity compared to control (Figure 41).

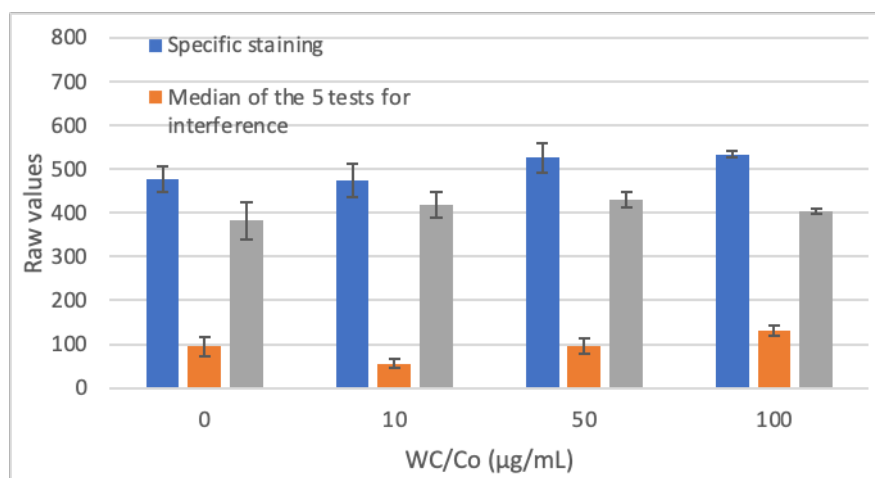


Fig. 41. Effect of WC/Co ENMs on  $\gamma$ H2AX intensity.

**Table 12. Summarized results obtained with WC/Co ENMs on the various markers**

Treatment/parameter	Cell counts	Nuclear size	Nuclear Intensity	Active caspase-3 Intensity	$\gamma$ H2AX Intensity
WC/Co NM	↑	-	-	↑	-

Our results (Table 12) showed that WC/Co ENMs did not induce major cytotoxic effects in A549 cells, although a small increase in active caspase-3 signal was observed. These results are in agreement with a study by Paget et al. where no substantial cytotoxicity with WC/Co ENMs was observed in A549 cells (Paget et al. 2015). In our study using an HCA approach, no effect on  $\gamma$ H2AX was observed in A549 cells treated with WC/Co ENMs. However, no studies investigating such effects of WC/Co on A549 cells are available in the literature. Importantly, WC/Co has been shown to be a genotoxic nanomaterial in several assays (Micronucleus assay and comet assay) (Moche et al. 2014, Moche et al. 2015). In particular, WC/Co increased  $\gamma$ H2AX foci in two different cell lines (Hep3B cells (liver), and Caki-1 cells (kidney)), although it was not tested in A549 cells for genotoxicity because this cell line was less responsive in terms of cytotoxicity and ROS production (Paget et al. 2015). Still in the lung, but using lung epithelial BEAS-2B cells, it was shown that nano-sized WC/Co was more cytotoxic than micro-sized material, and although cytotoxicity was reported from 1  $\mu$ g/mL, it was following a 48h incubation. Moreover, apoptosis and ROS production was shown to be impacted by WC/Co ENMs only at very high concentration (1000  $\mu$ g/mL) (Armstead 2014). Additionally, in A549 cells it was reported that WC/Co treatment (at 33  $\mu$ g/mL) induced cytotoxicity following 3 days of treatment (Bastian et al. 2009). Importantly, when tested in human keratinocytes (HaCaT), WC/Co ENMs did not induce significant toxicity nor DNA damage as assessed by the Micronucleus assay (Kühnel et al. 2012). For a review of the studies performed with WC/Co NM and additional toxicological endpoints, please refer to (Armstead and Li 2016).

#### 4.6.4. NM-300K and its diluent: Results from HCA analysis in A549 cells

##### 4.6.4.1. Cell counts, nuclear size, nuclear intensity

NM-300K treatment induced a strong and concentration-dependent decrease in cell counts from 10 to 100  $\mu\text{g/mL}$  (Figure 42). Very few cells remained following the treatment of A549 cells with 100  $\mu\text{g/mL}$  NM-300K, and for this reason, HCA results at this concentration must be interpreted with caution. The effect of the diluent alone was also analysed. A slight decrease in cell counts was observed at the highest concentration of the diluent (Figure 43) (one experimental repeat had to be excluded due to suspected seeding problem).

NM-300K treatment induced an increase in the nuclear size at 10 and 50  $\mu\text{g/mL}$ , with a subsequent decrease at the highest concentration of 100  $\mu\text{g/mL}$ . This decrease at the highest concentration could be due to an advanced state of cell death, or due to the very low number of cells analysed (Figure 44). The diluent had no effect on the nuclear size (Figure 45). NM-300K treatment did not have an effect on nuclear intensity, (Figure 46), as well, the NM-300K diluent had no effect on nuclear intensity (Figure 47).

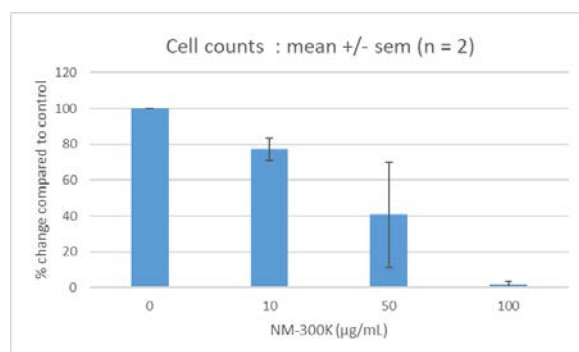


Fig. 42: Effect of NM-300K on cell counts.

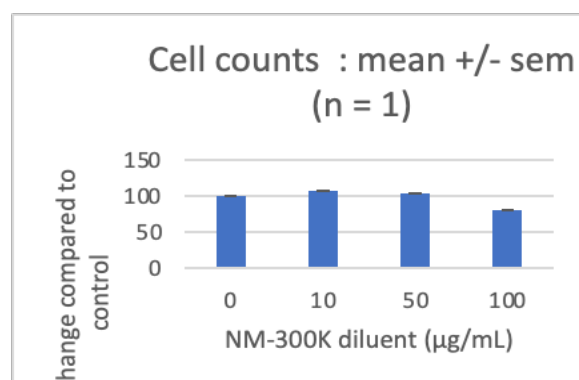


Fig. 43: Effect of NM-300K diluent on cell counts (equivalent concentration).



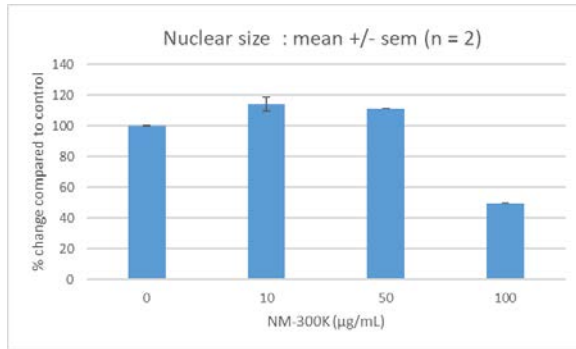


Fig. 44: Effect of NM-300K on nuclear size.

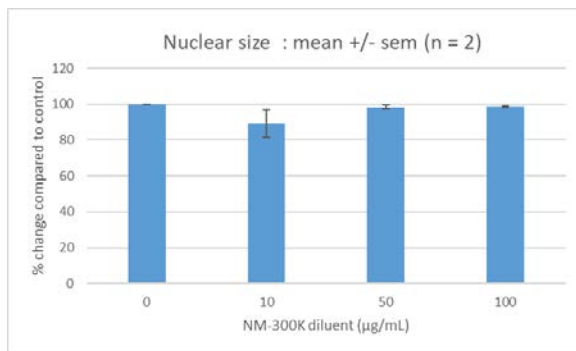


Fig. 45: Effect of NM-300K diluent on nuclear size (equivalent concentration).

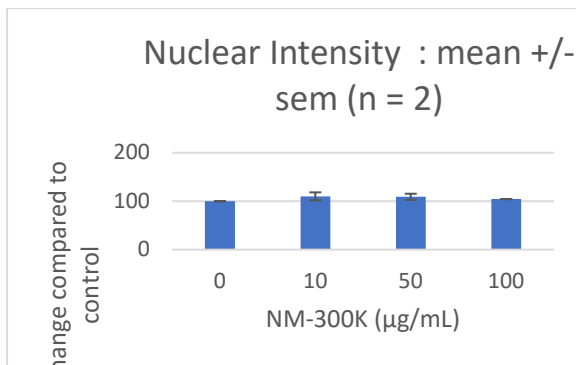


Fig. 46: Effect of NM-300K on nuclear intensity.

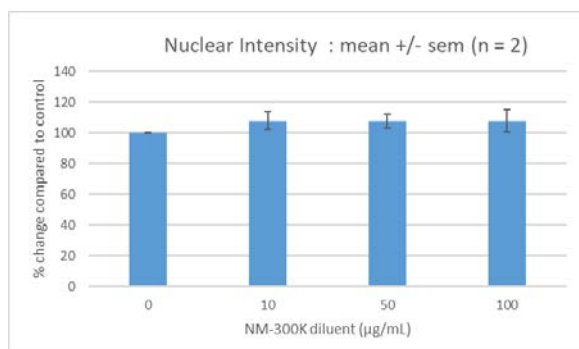


Fig. 47: Effect of NM-300K diluent on nuclear intensity (equivalent concentration).

#### 4.6.4.2. Active caspase-3 intensity

No significant interference with the nanomaterial or its diluent could be observed compared to control, except a small increase in interference with NM-300K at the highest concentration tested.

No clear effect on active caspase-3 intensity was observed from 10 to 50 µg/mL NM-300K. A decrease in active caspase-3 was observed at 100 µg/mL. However, at this concentration, very few cells remained and this result should be taken with caution (Figure 48). No effect on active caspase-3 was observed for the (Figure 49).

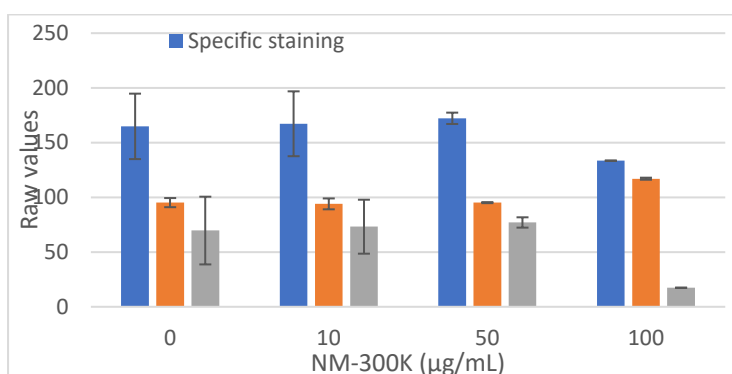


Fig. 48: Effect of NM-300K on active caspase-3 intensity.

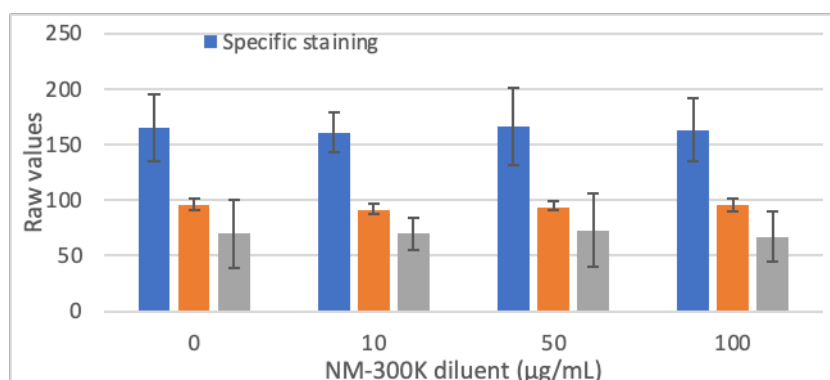


Fig. 49: Effect of NM-300K diluent on active caspase-3 intensity (equivalent concentration).

#### 4.6.4.3. $\gamma$ H2AX intensity

NM-300K induced a small concentration-dependent increase in interference signal at 480 nm, whereas the diluent alone had no effect on fluorescence intensities.

A strong concentration-dependent increase in  $\gamma$ H2AX intensity was observed upon treatment with NM-300K at concentrations from 10 to 100  $\mu$ g/mL (Figure 50). Upon correction for interference, a dose dependent increase in specific  $\gamma$ H2AX staining was still observed at 10 and 50  $\mu$ g/mL (reaching 262% of control value at 50  $\mu$ g/mL).

Results obtained with the diluent only showed an increase in  $\gamma$ H2AX intensity at 50  $\mu$ g/mL but with large experimental variations (Figure 51). Overall, the diluent slightly increased  $\gamma$ H2AX intensity. Upon correction for interference, there was an increase in  $\gamma$ H2AX specific staining for all 3 concentrations. The NM-300K diluent induced increases in  $\gamma$ H2AX reaching 213% compared to control values at the equivalent dose of 50  $\mu$ g/mL, although large experimental variations were observed.

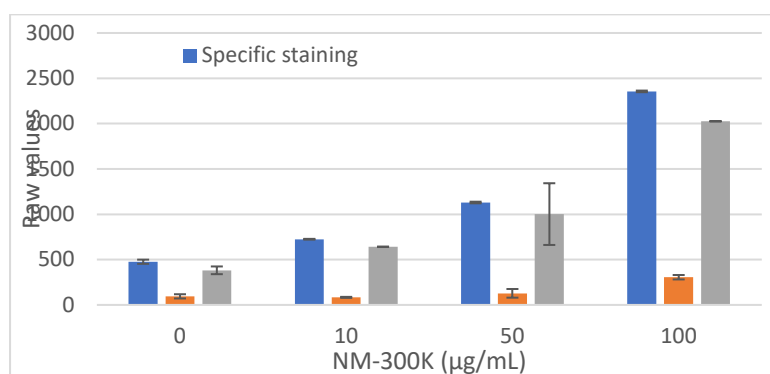


Fig. 50: Effect of NM-300K on  $\gamma$ H2AX intensity.

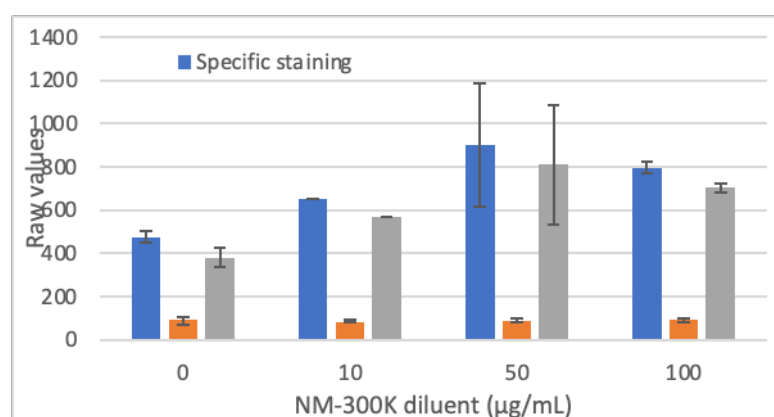


Fig. 51: Effect of NM-300K diluent on  $\gamma$ H2AX intensity (equivalent concentration).

**Table 13: Summary of results obtained with NM-300K and its diluent on the various markers**

Treatment/parameter	Cell counts	Nuclear size	Nuclear Intensity	Active caspase-3 Intensity	$\gamma$ H2AX Intensity
NM-300K	↓	- ↓	-	- ↓	↑
NM-300K diluent	↓	-	-	-	↑

In our study, NM-300K induced a strong cytotoxic effect in A549 cells, while its diluent on its own had very little effect. These results are in accordance with previous cytotoxicity study on A549 cells which also reported a strong cytotoxic effect of NM-300K although they had not tested its diluent (Zhao et al. 2016, Hansjosten et al. 2018, Laure 2021). Information regarding NM-300K diluent from its supplier indicate it is an aqueous solution containing stabilizing agents 4% Polyoxyethylene Glycerol Trioleate (Triolein) and 4% Tween20. The  $IC_{50}$  for Tween 20 in A549 has been reported to be 0.04% (Vol/Vol) (Eskandani et al. 2013). In our experimental set-up, the diluent at the highest dose tested is diluted by 1176 fold and therefore the concentration of Triolein and Tween 20 is 0.003 %. Therefore, Tween 20 as part of the diluent should not induce cytotoxicity. An increase in nuclear size and nuclear intensity were observed at 10 and 50  $\mu$ g/mL NM-300K, while a decrease in nuclear size was observed at the highest concentration of NM-300K tested, but these latter observations should be taken with caution due to the very few cells analysed. These results are in agreement with the results of the NANOREG project report, which also demonstrated a small increase in nuclear size and intensity in A549 treated with 50  $\mu$ g/mL NM-300K (Dusinska, Cimpan et al. 2016). Importantly, no major change in nuclear size nor intensity were reported in A549 cells upon NM-300K diluent treatment.

Our data also showed a very small increase in active caspase-3 intensity from 10 to 50  $\mu$ g/mL followed by a decrease at the highest concentration tested. Nevertheless, quantification at this highest concentration should be taken with caution due to the very low number of cells remaining for analysis. Importantly, no effect in active caspase-3 was observed with the diluent on its own. Our results are in agreement with those of Hansjosten et al. who found a significant and dose dependent increase in the number of A549 cells in necrotic and late apoptotic state upon treatment with NM-300K (Hansjosten, et al. 2018). NANOREG data could not demonstrate any change in active caspase-3 in A549 cells (Dusinska, Cimpan et al. 2016).

Our results also showed a concentration dependent increase in  $\gamma$ H2AX intensity in cells treated with NM-300K. This increased signal for  $\gamma$ H2AX may be linked whether to apoptosis or to the genotoxic process induced by NM-300K. It has been already shown that silver ENMs could induce  $\gamma$ H2AX in A549 cells, while having only slight effect on cell survival in this reported study, suggesting a genotoxic effect of silver ENMs (Zhao et al. 2016). Importantly, the diluent alone also resulted in an increase in  $\gamma$ H2AX intensity, but to a lower extent. Therefore, no conclusion can be driven on the effect of NM-300K particles on their own on  $\gamma$ H2AX. Indeed, it has been previously reported that Tween 20 could induce  $\gamma$ H2AX from 0.03% in cancer cells (human breast adenocarcinoma, MCF-7) (Zhao et al. 2015). However, the level of Tween 20 in our system are considerably lower, even at the highest concentration of diluent tested. Regarding Triolein, no genotoxicity has been reported in various in vitro systems. Therefore, it cannot be excluded that the effect of the diluent alone could contribute in part to the effect of NM-300K on  $\gamma$ H2AX in A549 cells. Moreover, some genotoxic effects of the NM-300K diluent has already been reported in the comet assay using several cell lines including A549 cells (Thongkam et al. 2016).

#### 4.6.5. TiO<sub>2</sub> (JRC): Results from HCA analysis in A549 cells

##### 4.6.5.1 Cell count, nuclear size, nuclear intensity

Treatment of A549 cells with TiO<sub>2</sub> ENMs induced a concentration dependent increase in cell counts from 10 µg/mL (Figure 52). TiO<sub>2</sub> ENMs induced a small, concentration dependent increase in nuclear size, which reached 120 % at 100 µg/mL (Figure 53). However, this effect is most likely artefactual due to the perinuclear accumulation of TiO<sub>2</sub> particles and potential interaction with DAPI and/or autofluorescence. TiO<sub>2</sub> ENMs induced a concentration-dependent increase in nuclear intensity from 10 µg/mL reaching nearly 50 % above control at the highest dose tested (Figure 54). However, this increase is due to interference with at the wavelength used for identification of nuclei (386 nm) (Figure 55) and results from problems of nuclear identification and segmentation.

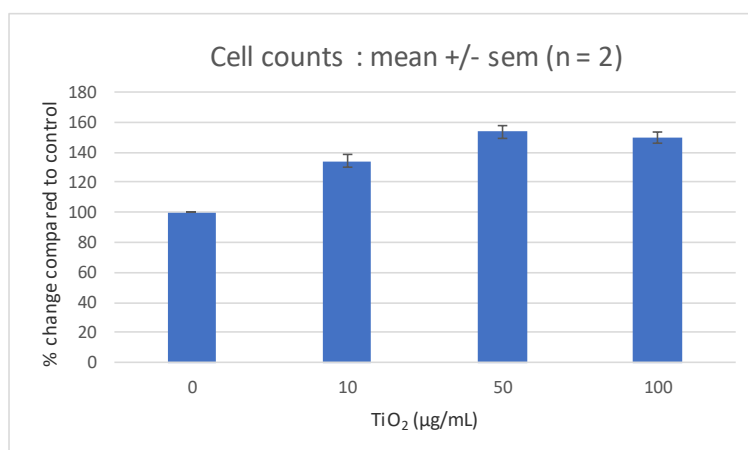


Fig. 52: Effect of TiO<sub>2</sub> ENMs on cell counts.

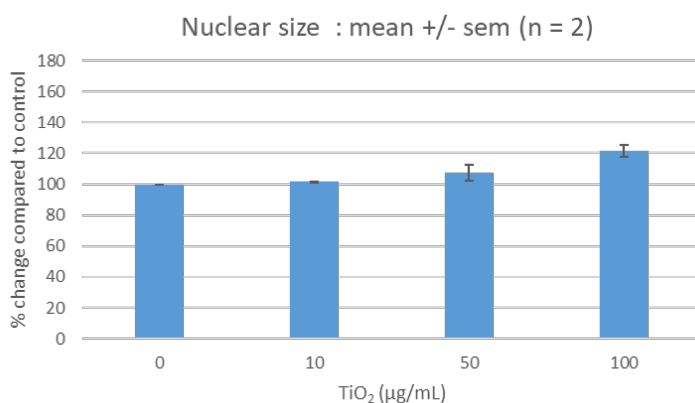


Fig. 53: Effect of TiO<sub>2</sub> ENMs on nuclear size.

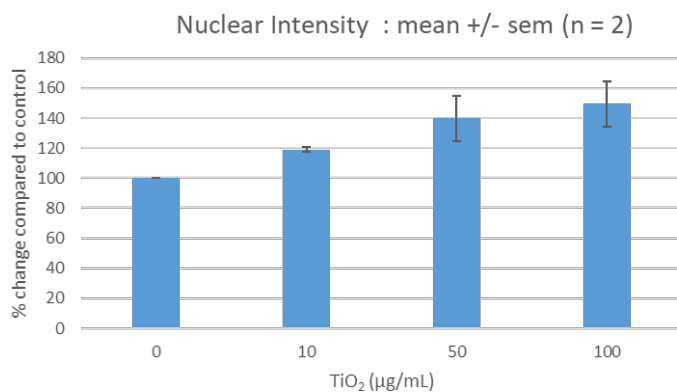


Fig. 54: Effect of TiO<sub>2</sub> ENMs on nuclear intensity.

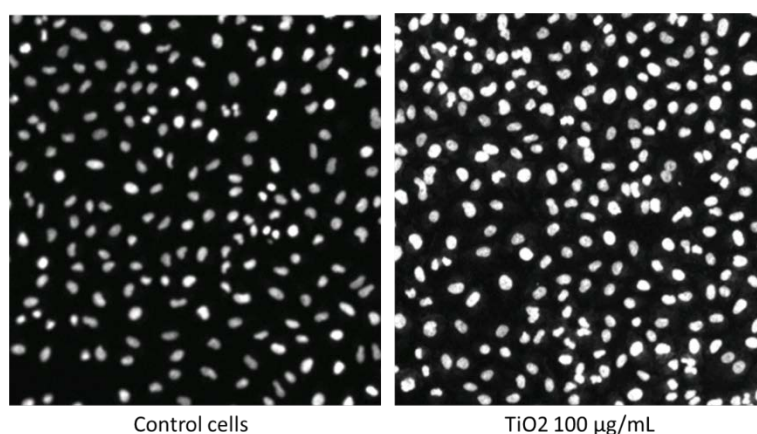


Fig. 55: DAPI staining of control cells, and A549 cells treated with 100 µg/mL TiO<sub>2</sub> ENMs. A perinuclear accumulation of ENMs is associated with fluorescence interference at 386 nm wavelength. This interference generates problems for the correct identification of the nuclear border and correct identification of cells. This leads to artificially elevated values for nuclear size and nuclear intensity.

#### 4.6.5.2. Active caspase-3 intensity

No significant interference with TiO<sub>2</sub> ENMs could be detected at the wavelength used for active caspase-3 quantification (647 nm).

TiO<sub>2</sub> ENMs induced a concentration-dependent increase in active caspase-3 intensity, reaching 329 % above control at the highest concentration tested (Figure 56). Interestingly, no decrease in cell counts was observed with this increase in active caspase-3 intensity.

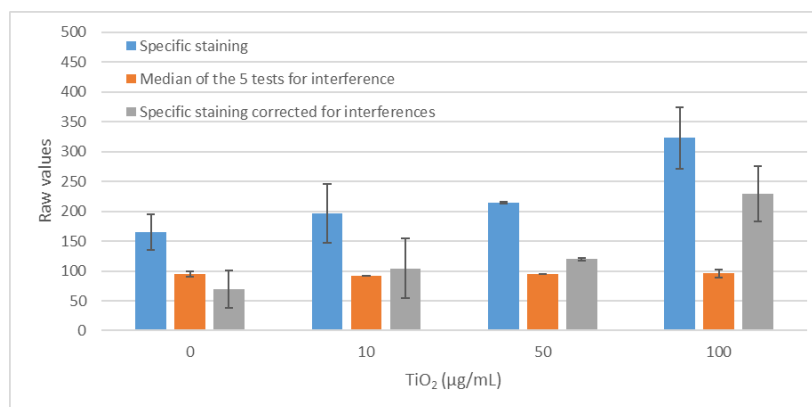


Fig. 56: Effect of TiO<sub>2</sub> ENMs on active caspase-3 intensity.

#### 4.6.5.3. γH2AX intensity

No interference was observed with TiO<sub>2</sub> ENMs in the wavelength used for γH2AX quantification (480 nm) (Figure 57).

Significant concentration-dependent increases in γH2AX intensity were observed upon treatment with TiO<sub>2</sub> ENMs for 50 and 100 µg/mL. After correction for interference, this concentration-dependent increase in specific γH2AX staining was still apparent for TiO<sub>2</sub> concentrations from 50 µg/mL, reaching 154 % of control value at 100 µg/mL.

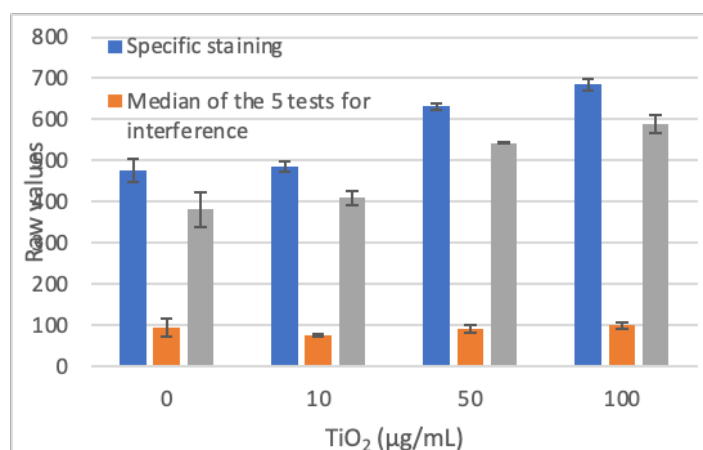


Fig. 57: Effect of TiO<sub>2</sub> ENMs on γH2AX intensity.

**Table 14: Summarized results obtained with TiO<sub>2</sub> ENMs on the various markers**

Treatment/parameter	Cell counts	Nuclear size	Nuclear Intensity	Active caspase-3 Intensity	γH2AX Intensity
TiO <sub>2</sub> NM	↑	(↑)	(↑)	↑	↑

In our experiments, treatment of A549 cells with TiO<sub>2</sub> ENMs slightly increased cell counts, according to HCA analysis. We observed a small increase in nuclear size and nuclear intensity, which would be

suggestive of an apoptotic process, at the highest dose tested. However, it has been shown that TiO<sub>2</sub> ENMs could be found in the perinuclear area of the cells (Stearns et al. 2001). Hence, we hypothesised that the increased nuclear size and intensity following treatment of A549 cells with TiO<sub>2</sub> ENMs could result of fluorescence interference. This interference is associated with problems in the accurate delimitation of cell nuclei in the HCA workflow, and therefore generates aberrant data on nuclear size and nuclear intensity.

Active caspase-3 intensity was increased upon incubation with TiO<sub>2</sub> ENMs. This increase in active-caspase-3 staining without any effect on cell counts was unexpected. However, using another type of TiO<sub>2</sub> ENMs, it was shown that TiO<sub>2</sub> ENMs could induce apoptosis in A549 cells upon 48h incubation (Kansara et al. 2015). Our results could therefore represent the onset of apoptosis, and longer incubations with TiO<sub>2</sub> ENMs would therefore be required to observe decreases in cell counts. In addition, our results showed that TiO<sub>2</sub> ENMs increased  $\gamma$ H2AX intensity. These data are in accordance with a study showing that TiO<sub>2</sub> ENMs could induce  $\gamma$ H2AX levels in A549 cells (Toyooka et al. 2012).

#### 4.6.6. ZnO (Sigma): Results from HCA analysis in A549 cells

ZnO ENMs (Sigma) induced an increase in cell counts at 10  $\mu$ g/mL (up to nearly 152 %). At higher concentrations, ZnO ENMs induced a concentration- dependent decrease in cell counts (down to 80% at 100  $\mu$ g/mL) (Figure 58).

A concentration-dependent decrease in nuclear size was observed upon treatment with ZnO ENMs, with a 71 % decrease at 100  $\mu$ g/mL (Figure 59). As well, a concentration-dependent increase in nuclear intensity was observed following a 24h incubation with ZnO ENMs (Sigma), reaching 174% of control value at 100  $\mu$ g/mL (Figure 60).

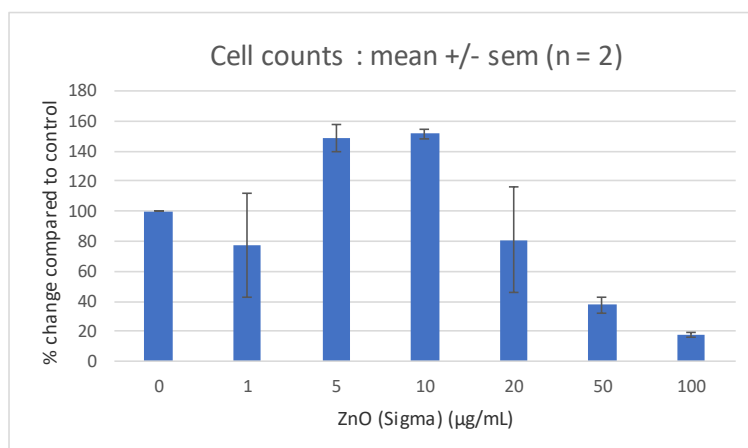


Fig. 58: Effect of ZnO ENMs (Sigma) on cell counts.



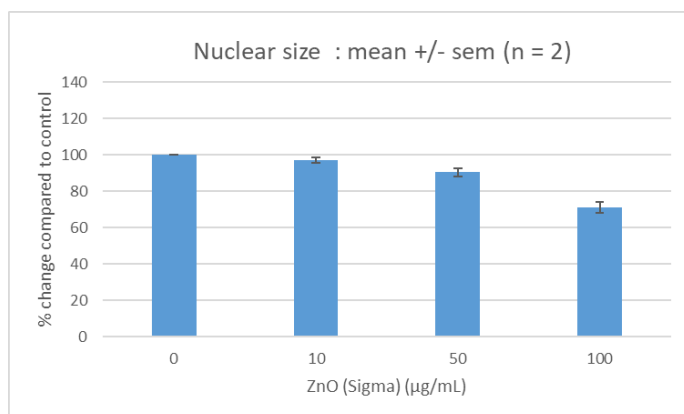


Fig. 59: Effect of ZnO ENMs (Sigma) on nuclear size.

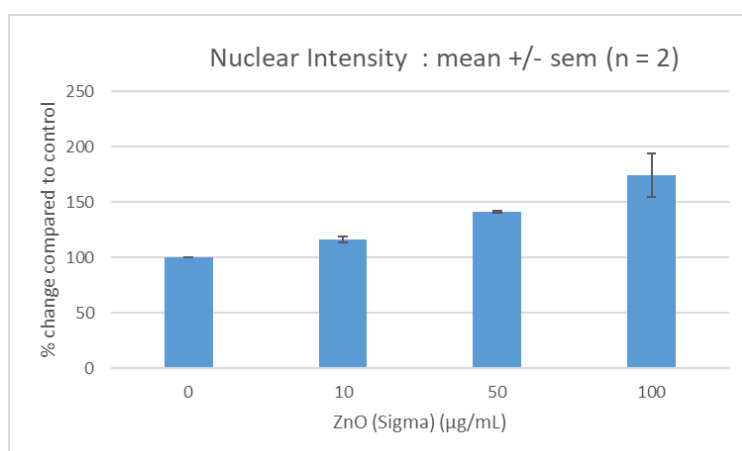


Fig. 60: Effect of ZnO ENMs (Sigma) on nuclear intensity.

#### 4.6.6.2. Active caspase-3 Intensity

Tests for interference showed a consistent concentration-dependent increase in signal in the channel used for quantification of active caspase-3 (647 nm).

Treatment of cells with ZnO ENMs (Sigma) induced a concentration-dependent increase in active caspase-3 intensity from 10 to 100 µg/mL, reaching 140% of control value at 100 µg/mL (Figure 61). Upon correction for interference, the concentration-dependent increase in active caspase-3 could be observed only at 10 and 50 µg/mL but no longer at the highest concentration tested due to material interference and/or to an advanced state of cell death.

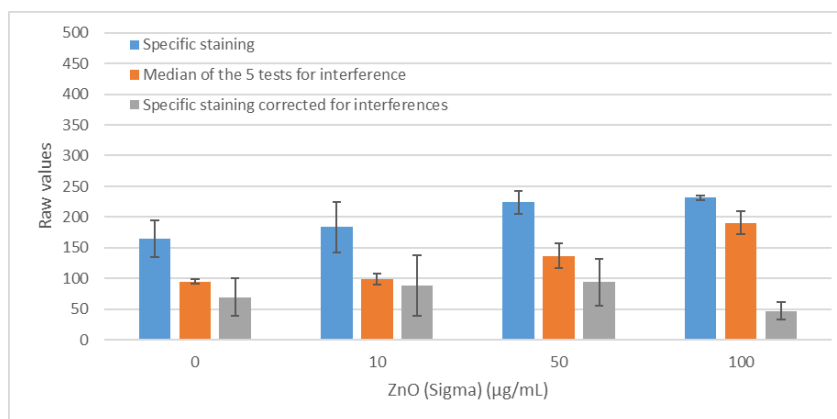


Fig. 61: Effect of ZnO ENMs (Sigma) on active caspase-3 intensity.

#### 4.6.6.3. $\gamma$ H2AX intensity

Tests for interference in the channel used for  $\gamma$ H2AX quantification also showed a concentration-dependent increase in signal from 50  $\mu$ g/mL, suggesting therefore that any increase in  $\gamma$ H2AX intensity observed at higher concentrations of ZnO materials may be partly artefactual. ZnO ENMs (Sigma) induced a concentration-dependent increase in  $\gamma$ H2AX intensity, reaching 680 % of control value at 100  $\mu$ g/mL (uncorrected data) (Figure 62). Upon correction for interference, ZnO still induced a concentration-dependent increase in  $\gamma$ H2AX specific staining, reaching 762 % of control value at the highest concentration tested.

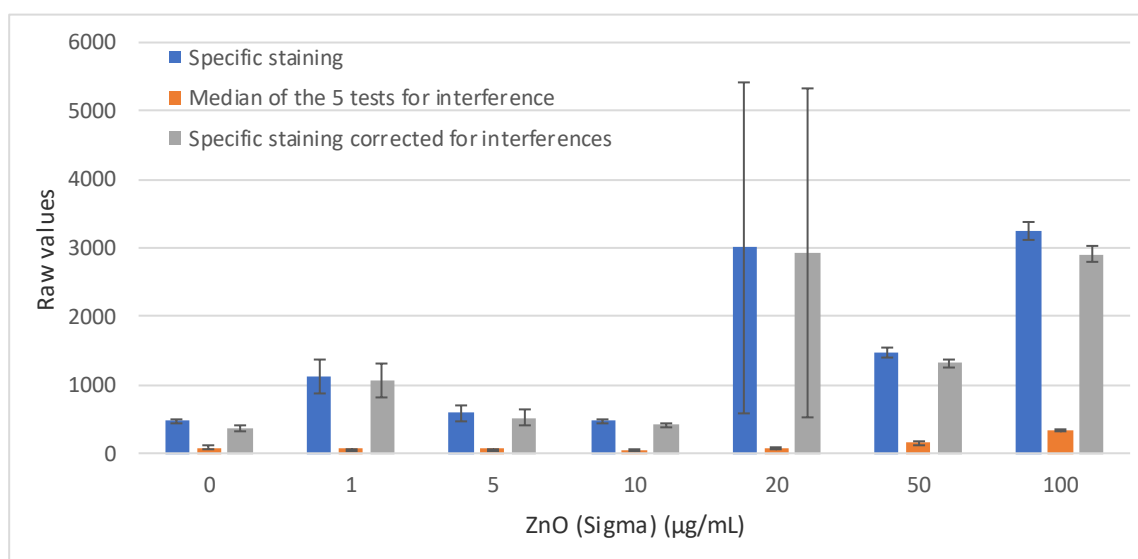


Fig. 62: Effect of ZnO ENMs (Sigma) on  $\gamma$ H2AX intensity.

Table 15: Summary of results obtained with ZnO ENMs (Sigma) on the various markers

Treatment/parameter	Cell counts	Nuclear size	Nuclear Intensity	Active caspase-3 Intensity	$\gamma$ H2AX Intensity
ZnO NM	↓	↓	↑	↑ -	↑

#### 4.6.7. ZnO NM-111 (JRC): Results from HCA analysis in A549 cells

##### 4.6.7.1. Cell count, nuclear size, nuclear intensity.

NM-111 treatment induced a concentration-dependent decrease in cell counts, with an 80% decrease at the highest concentration tested (Figure 63). NM-111 treatment decreased nuclear size at 50 and 100 µg/mL by around 33 % compared to control cells (Figure 64). An increase in nuclear intensity was observed following NM-111 treatment at 50 and 100 µg/mL (Figure 65).

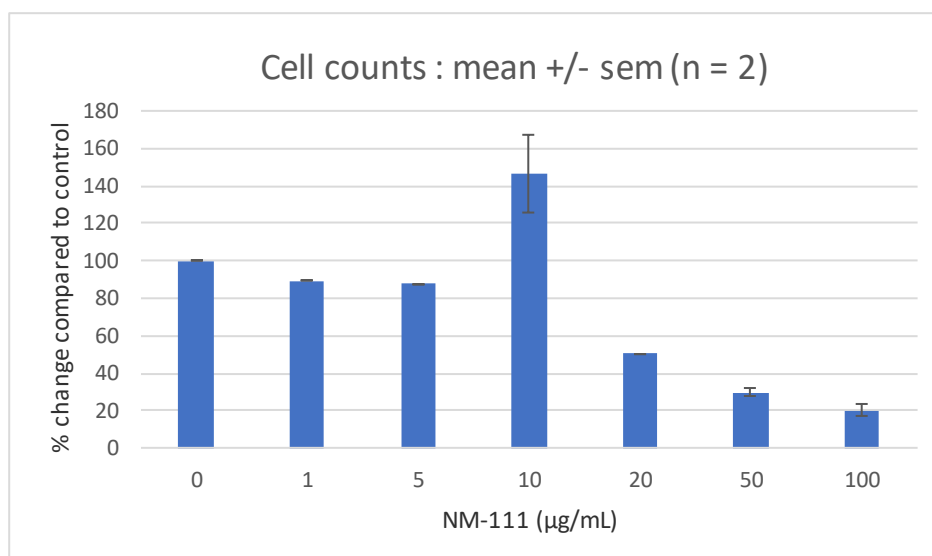


Figure 63: Effect of NM-111 on cell counts.

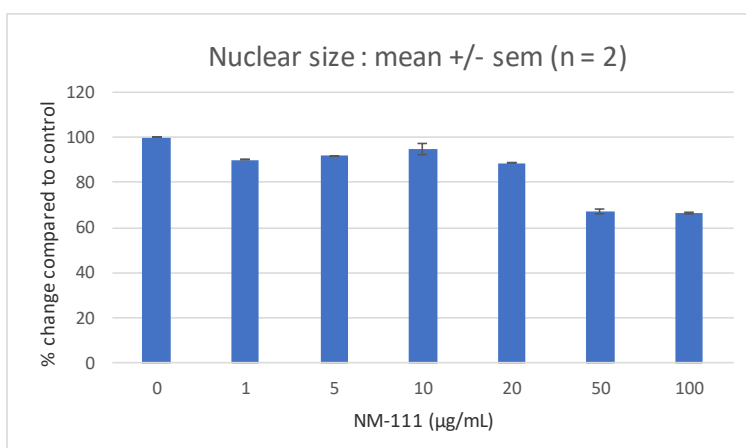


Fig. 64: Effect of NM-111 on nuclear size.

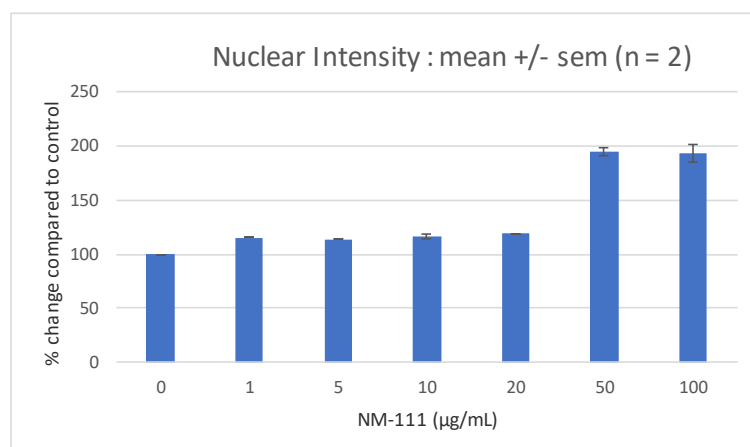


Fig. 65: Effect of NM-111 on nuclear intensity.

#### 4.6.7.2. Active caspase-3 intensity

NM-111 treatment induced an increase in active caspase-3 intensity at 100 µg/mL reaching 228 % of control value (uncorrected data). However, NM-111 induced a concentration-dependent increase in interference signal in the channel used for active-caspase-3 quantification (Figure 66). Upon correction for interference, a 126 % increase in active caspase-3 intensity was observed relative to control cells at 100 µg/mL.

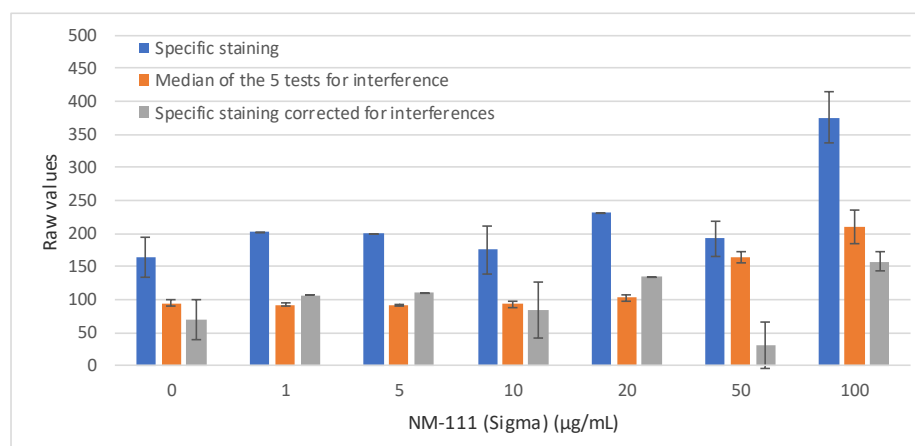


Fig. 66: Effect of NM-111 on active caspase-3 intensity.

#### 4.6.7.3 $\gamma$ H2AX intensity

An increase in  $\gamma$ H2AX intensity was observed (reaching around 700 % of control value) following treatment with NM-111 at concentrations of 50 and 100 µg/mL (before correction for interference) (Fig. 67). Controls for interference showed a concentration-dependent increase in signal from 50 µg/mL suggesting a contribution of fluorescence interference to the total  $\gamma$ H2AX intensity signal. Upon correction for interference, a concentration-dependent increase in  $\gamma$ H2AX intensity was observed in A549 cells treated with NM-111 (705 % of control at 100 µg/mL).

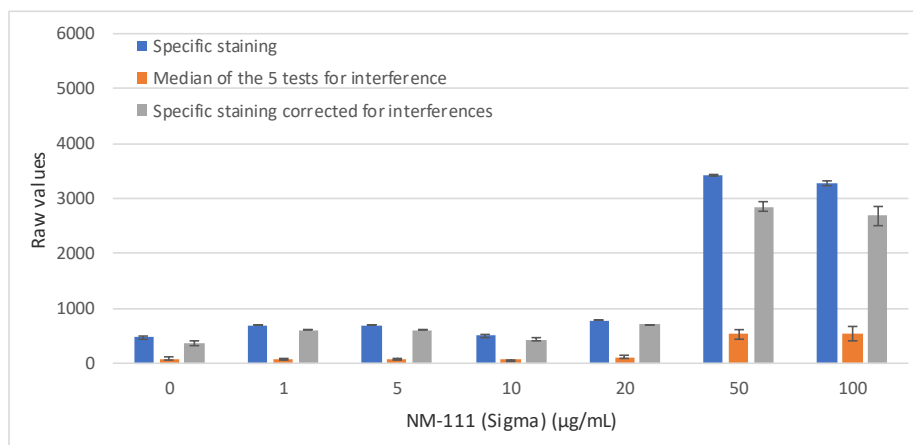


Fig. 67: Effect of NM-111 on  $\gamma$ H2AX intensity.

**Table 16: Summary of results obtained with NM-111 on the various markers**

Treatment/parameter	Cell counts	Nuclear size	Nuclear Intensity	Active caspase-3 Intensity	$\gamma$ H2AX Intensity
NM-111	↓	↓	↑	↑	↑

Our data showed that NM-111 generated a concentration-dependent decrease in cell counts, which is in agreement with published work (Hansjosten et al. 2018). In the same study, the authors also suggested that the hydrophobic coating of NM-111 rendered it more toxic than its non-coated form NM-110. However, in our study, the uncoated ZnO (Sigma) we tested showed a similar toxicity to the coated NM-111. Both ZnO ENMs reduced nuclear size and increased nuclear intensity, suggesting an apoptotic process. This was further supported by an increase of active caspase-3 levels, although this effect was reduced at the highest concentration of ZnO ENMs that could be likely due to cells already in an advanced state of apoptosis. Less experimental data for ZnO (Sigma) is available in the literature compared to NM-111. However, in A549 cells, it has previously been shown that NM-111 can induce apoptosis in a concentration-dependent manner, as well as necrosis at high concentrations (Hansjosten et al. 2018). Still in A549 cells, decreased viability and increased level of cells in sub-G1 phase of the cell cycle have been also reported upon treatment with ZnO NM (Rahimi et al. 2021) Finally, our data also showed a concentration-dependent increase in  $\gamma$ H2AX signal with both ZnO ENMs. Similar intensity of  $\gamma$ H2AX staining was observed for both ZnO ENMs. This effect on  $\gamma$ H2AX might be due to an underlying oxidative stress and eventually the apoptotic process due to ZnO treatment (Vandebriel and De Jong 2012). Indeed, oxidative stress is known to induce  $\gamma$ H2AX (Mah et al. 2010). From the literature, very little information is available concerning the effect of ZnO ENMs on  $\gamma$ H2AX. A study in the CHO-K1 cell line showed that ZnO particles could induce  $\gamma$ H2AX at 24h, although levels decreased below control level over-time (Liu et al. 2017). It was also shown that ZnO ENMs induce  $\gamma$ H2AX in human colon carcinoma cells, in the absence of serum (Condello et al. 2016).

#### 4.6.8. Nanocyl 7000 and its diluent: Results from HCA analysis in A549 cells

##### 4.6.8.1. Cell count, nuclear size, nuclear intensity

Treatments of A549 cells with Nanocyl 7000 induced an increase in cell counts at 50 and 100  $\mu\text{g/mL}$  reaching 135 % compared of control values (Figure 68). A similar increase in cell counts compared to control was observed with the diluent (Figure 69). Importantly, observation of cells under an optical microscope was difficult because of the presence of large amount of materials. However, previous data from Alamar Blue and WST-1 from other RiskGONE partners showed decreased cell viability at 100  $\mu\text{g/mL}$  Nanocyl 7000.

Nanocyl 7000 induced a small but significant reduction of nuclear size, reaching 89 % of control value at 100  $\mu\text{g/mL}$  (Figure 70). A small reduction in nuclear size (9 %) was also observed with the diluent on its own (Figure 71). Since the diluent and the nanomaterials had similar effects, it is difficult to determine a nanomaterial specific effect.

Nanocyl 7000 induced an increase in nuclear intensity by 20 % compared to control at all the concentrations tested (Figure 72). A slight increase in nuclear intensity was also observed with the diluent alone (Figure 73). Since the diluent and the nanomaterials had similar effects, it is difficult to attribute these changes to a nanomaterial specific effect.

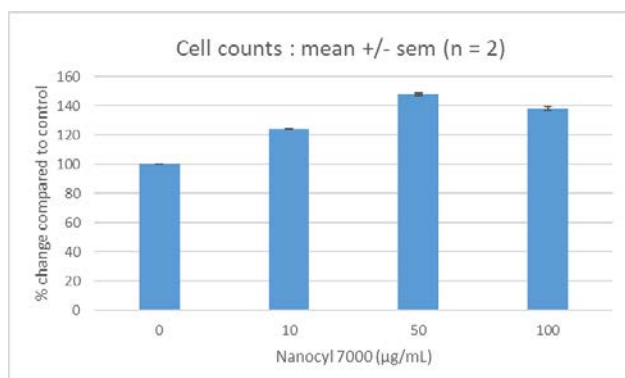


Fig. 68: Effect of Nanocyl 7000 on cell counts.

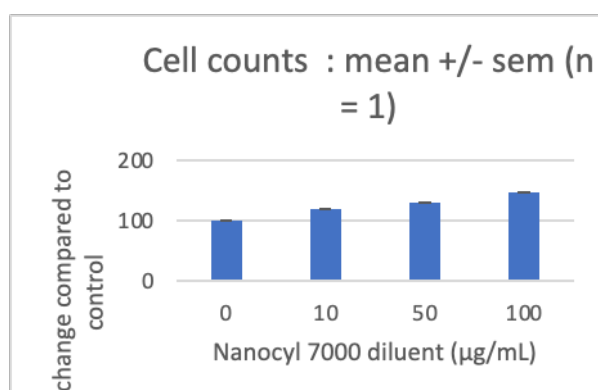


Fig. 69: Effect of Nanocyl 7000 diluent on cell counts (equivalent concentration).

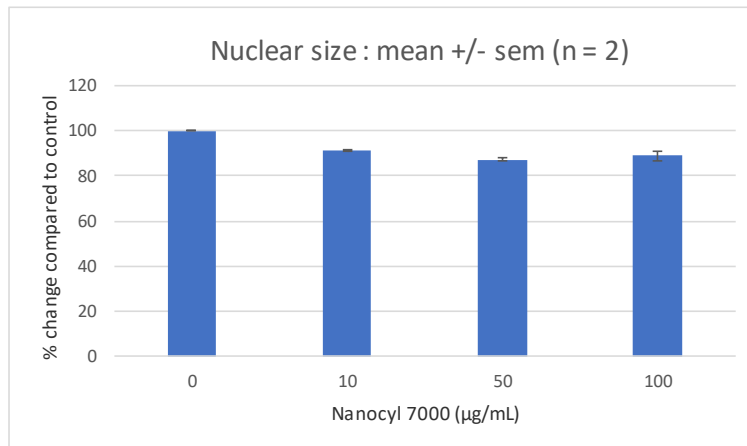


Fig. 70: Effect of Nanocyl 7000 on nuclear size.

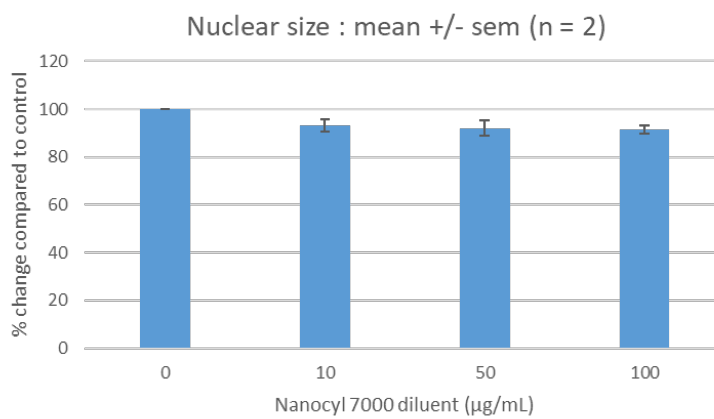


Fig. 71: Effect of Nanocyl 7000 diluent on nuclear size (equivalent concentration).

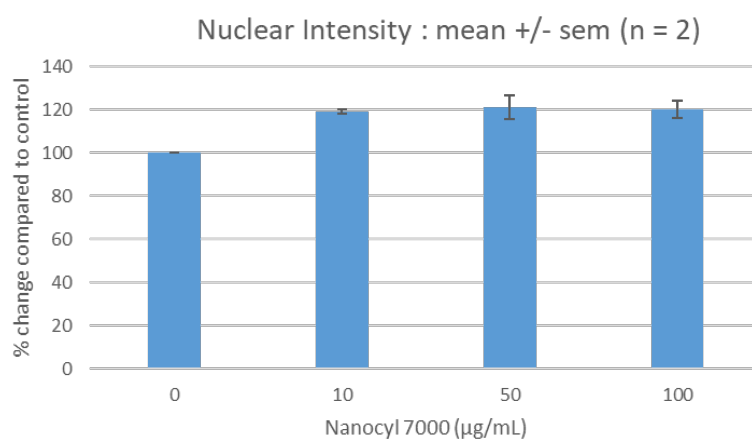


Figure 72: Effect of Nanocyl 7000 on nuclear intensity.

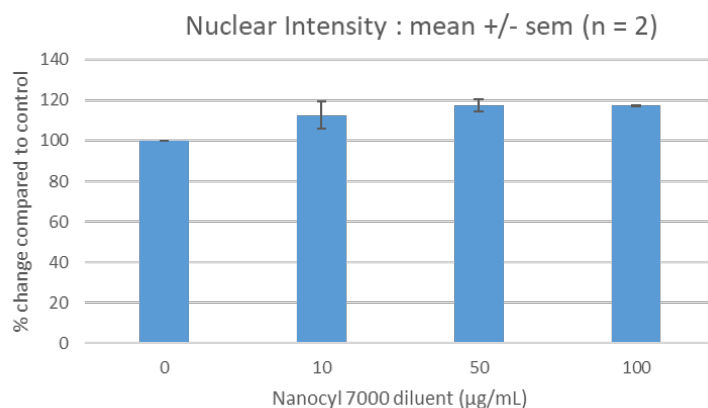


Figure 73: Effect of Nanocyl 7000 diluent on nuclear intensity (equivalent concentration).

#### 4.6.8.2 Active caspase-3 intensity

No interference could be detected for the diluent on its own, but a small dose dependent increase in non-specific signal could be detected with Nanocyl 7000 from 10 µg/mL, suggesting that the presence of ENMs may interfere with fluorescence measurements.

Nanocyl 7000 induced a concentration-dependent increase in active caspase-3 intensity, reaching 58 % increase at 100 µg/mL (Figure 74). On its own, the diluent only slightly increased the active caspase-3 intensity measured compared to control (Figure 74). Upon correction for interference, Nanocyl 7000 induced a concentration-dependent increase in active caspase-3 specific staining, which reached 206 % of control values at 100 µg/mL while the diluent on its own reached 124 % of control values. These results suggest that Nanocyl 7000 has an apoptotic effect in A549 cells.

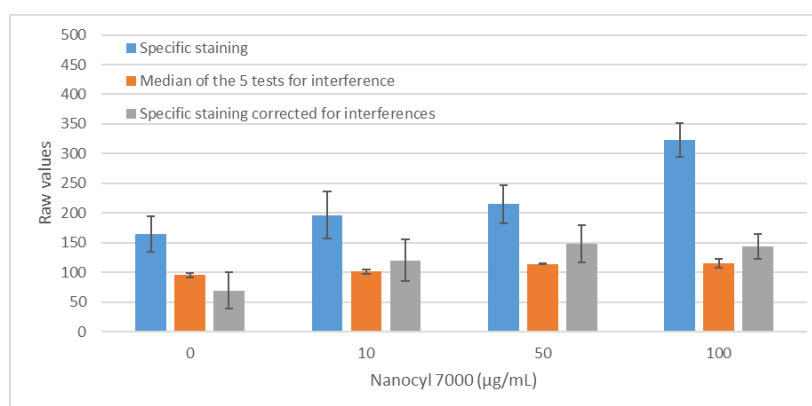


Fig. 74: Effect of Nanocyl 7000 on active caspase-3 intensity.



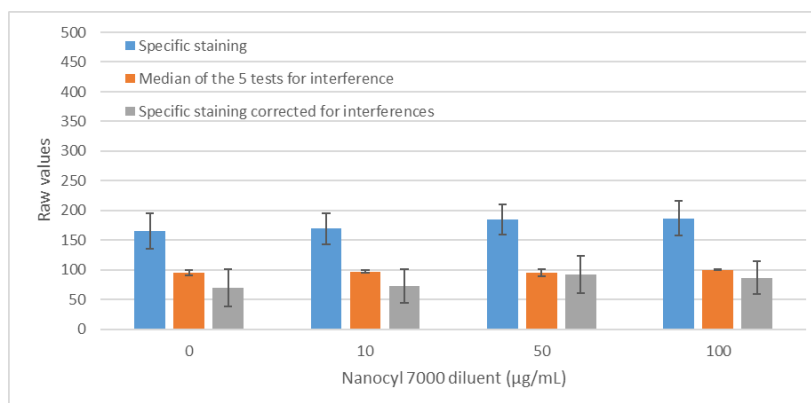


Fig. 75: Effect of Nanocyl 7000 diluent on active caspase-3 intensity (equivalent concentration).

#### 4.6.8.3 $\gamma$ H2AX intensity

No particular interference could be detected with Nanocyl 7000 or the diluent in the channel used for  $\gamma$ H2AX quantification (480 nm).

Before correction for interference, treatment of A549 cells with Nanocyl 7000 induced a concentration-dependent increase in  $\gamma$ H2AX intensity, which reached around 140 % compared to control value at 50 and 100  $\mu$ g/mL (Figure 76). With the diluent on its own, an increase in  $\gamma$ H2AX intensity was also observed reaching 187% of control values at 100  $\mu$ g/mL (before correction for interference), but with large variations between experiments for the latter concentration (Figure 77). Importantly, the diluent on its own seemed to have more effect than the carbon nanotube suspension, with an increase in  $\gamma$ H2AX signal at the equivalent dose of 100  $\mu$ g/mL reaching 207% of control value for the diluent but only 151% for Nanocyl 7000, after correction for interference.

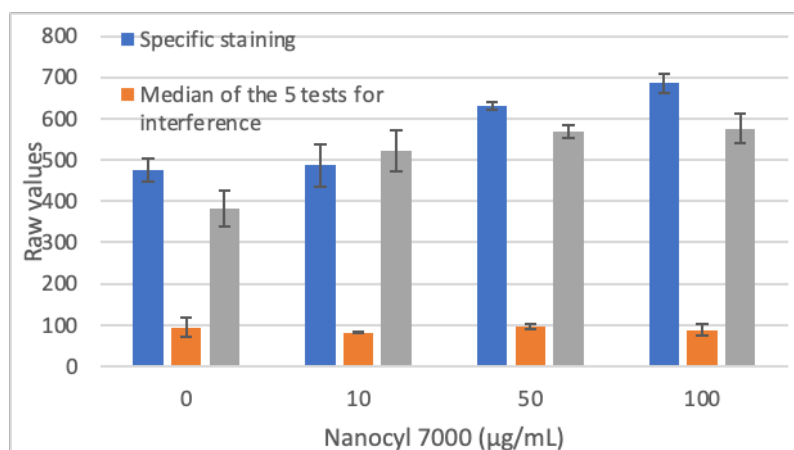


Fig. 76: Effect of Nanocyl 7000 on  $\gamma$ H2AX intensity.

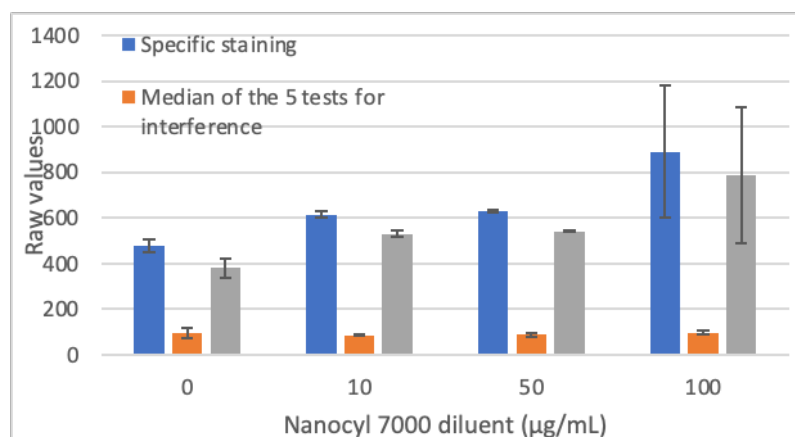


Fig. 77: Effect of Nanocyl 7000 diluent on  $\gamma$ H2AX intensity (equivalent concentration).

**Table 17: Summary of results obtained with Nanocyl 7000 and its diluent on the various markers**

Treatment/parameter	Cell counts	Nuclear size	Nuclear Intensity	Active caspase-3 Intensity	$\gamma$ H2AX Intensity
Nanocyl 7000	↑	↓	↑	↑	↑
Nanocyl 7000 diluent	↑	↓	↑	↑	↑

Our results showed an increase in cell counts following Nanocyl 7000 treatment (Table 17). It is unclear why we observed this increase since a very low cytotoxic effect has been shown using Alamar Blue and strong cytotoxicity was shown with the WST-1 assay, by other RiskGONE partners, in A549 cells, at 24h. These discrepancies may be further discussed in light with the impedance data, which are less likely to be subject of interference, and also indicated a decrease in impedance upon treatment with the CNT. However, in our study, Nanocyl 7000 decreased nuclear size and increased nuclear intensity suggestive of cytotoxic effects. In another study, no cytotoxic effects were observed with Nanocyl 7000 in A549 cells when tested at 20  $\mu\text{g/mL}$  (Savvina 2019). Importantly, the diluent on its own also had some effect on cell counts, and it also induced a reduction in nuclear size and an increase in nuclear intensity in A549 cells. Nanocyl 7000 increased active caspase-3 intensity. Importantly, the diluent on its own had also an effect on active caspase-3 levels in A549 cells. Regarding  $\gamma$ H2AX staining, both Nanocyl 7000 and its diluent increased the signal and it was difficult to determine the respective role of each component. Therefore, it is difficult to assess the specific contribution of the CNT compared to its diluent. A rapid literature search did not retrieve sufficient information regarding the effects of Nanocyl 7000 nor its diluent (proprietary) in vitro, on active caspase-3 and  $\gamma$ H2AX. From the literature, several studies have reported the induction of  $\gamma$ H2AX by multiwall carbon nanotubes in vitro and in vivo (Zhu et al. 2007, Cveticanin et al. 2010, Aimonen et al. 2019).

#### 4.6.9. Conclusion HCA Analysis

Table 18 summarizes the results obtained in testing the various ENMs on A549 cells and measuring different markers by HCA. In some cases, interference issues were raised that could give rise to inaccurate results with the methodology used if not taken into consideration. In some cases of ENM

interference, use of a different combination of antibodies to work at a different wavelength may be a potential mitigation measure useful to overcome such issues.

**Table 18: Heatmap representative of the results obtained in A549 cells after a 24h incubation, using HCA.**

Treatment/parameter	Cell counts	Nuclear size	Nuclear Intensity	Interferences at 647 nm ( $\lambda$ for active caspase-3)	Active caspase-3 Intensity (corrected for interferences)	Interferences at 480 nm ( $\lambda$ for $\gamma$ H2AX)	$\gamma$ H2AX Intensity (corrected for interferences)
Staurosporine	↓	-	↑		-		↑
MMS	↓	↑	↓		-		-
CuO NM	↓	↑	↑		↑		↑
WC/Co NM	↑	-	-		↑		-
NM-300K	↓	-	↓		-	↓	↑
NM-300K diluent	↓	-	-		-	↑	↑
TiO <sub>2</sub> NM	↑	(↑)	(↑)		↑		↑
ZnO NM (Sigma)	↓	↓	↑		↑		↑
NM-111	↓	↓	↑		↑		↑
Nanocyl 7000	↑	↓	↑	↑	↑		↑
Nanocyl 7000 diluent	↑	↓	↑		↑		↑

	no or very small effect (less than 20 %)
	small effect (20 to 39 %)
	strong effect (40 to 60%)
	very strong effect (more than 60 %)
( )	interferences

#### 4.7 Genotoxicity testing using the Comet assay (NILU)

The CA SOP was used. Human lymphoblastoid cells TK6 and the human lung epithelial cells A549 were exposed to the five ENMs used in RR1 and RR2, with 3 or 24 h exposure times. Each partner provided data for 2-3 independent experiments for each ENM, cell line and time point. An amended SOP was prepared and followed during RR2. One of the most important changes to the SOP based on the RR1 training, was the use the same source of Fpg (Norgenotech, Norway). During RR2, an amended SOP was distributed to all partners involved and data were completed and provided on CuO, Tungsten and MWCNT ENMs by NILU and KU Leuven. The comparison of the results showed that both partners obtained very close results during this round. For task 5.2, the testing of additional ENMS was agreed; Nm300K and NM111. The SOPs from RR2 were followed.

##### 4.7.1 In Vitro comet Assay data from RR1 and RR2 (DELIVERABLE D5.1) also included in T5.2

**Task 5.2 made use of data obtained in Task 5.1.** Task 5.1 aimed at developing robust assays to study the toxicity of nanomaterials and round-robins were organized amongst partners to evaluate the shared Standard Operating Procedure (SOPs). Partners were tasked to critically evaluate the SOP and to determine its suitability for ENMs hazard assessment and if there is a need for potential assay adaptations. The collected data for SBs (measured as % DNA in tail), SBs+Fpg and netFpg (calculated as the difference in %DNA in tails between samples with Fpg incubation and samples without Fpg incubation) for each cell line (**A549 & TK6**) and time point (3h and 24h) were reported by partner involved in RR1, RR2. The developed SOPs were further adapted for **Task 5.2**.

**NOTE. All Data from RR1: ZnO & TiO<sub>2</sub> ENMs (NILU, KU Leuven, ANSES) and Data from RR2: CuO, Tungsten, MWCNT ENMs (NILU and KU Leuven) were reported in deliverable 5.1. QSAR Lab statistical analysis for accuracy was also reported in D5.1.**

#### 4.7.2 In Vitro comet Assay data from Task 5.2 (NILU data)

During Task 5.2, NILU followed the SOP from RR2. The 2 ENMS were tested on A549 cells for 3 and 24h. data are shown in figure 78. None of the tested ENMS induced an increase of DNA Sbs neither DNA oxidised bases. The testing for interference did not show any interference issue following our set up.

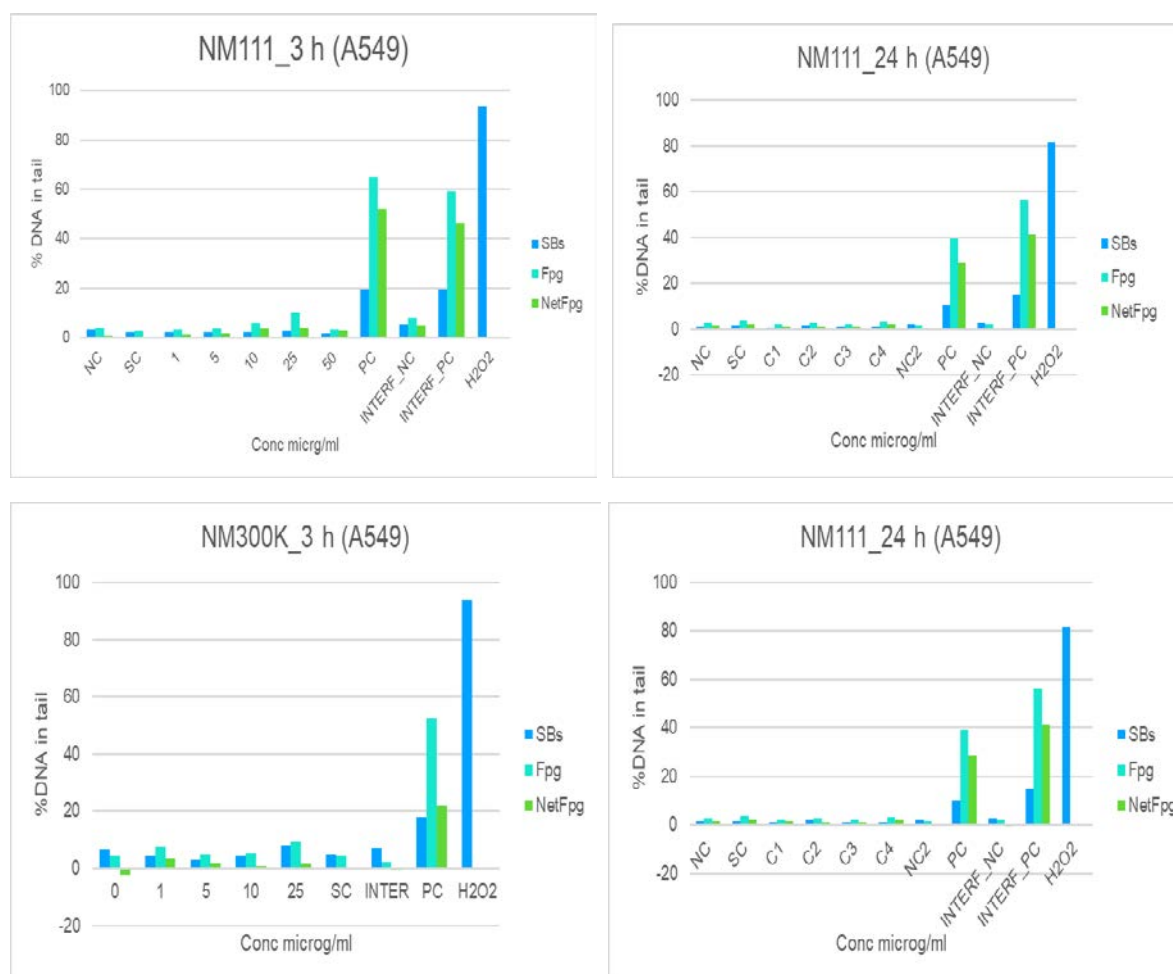


**Fig. 78. Summary data from NILU on DNA damage measured as tail intensity induced by NM111 and NM300K in A549 cells after 3- or 24-hours exposure.** 2-3 independent experiments were performed with duplicate wells for each exposure within each experiment. The results are shown as mean of the median of duplicate wells,  $\pm$  SD. SC, solvent control (MilliQ sterile water equivalent to the water content in the highest ENM concentration, here: 3% for 150  $\mu$ g/mL and 0.5 % for 25  $\mu$ g/mL of ENM). Interference control (INT, NC cells mixed with ENMs at the highest exposure concentration used (25 or 150  $\mu$ g/mL) just before embedding into agarose). PC: MMS (0.2 mM), H<sub>2</sub>O<sub>2</sub> (0.1 mM in jar for 5 min) and KBrO<sub>3</sub> (1mM).

#### 4.7.3. Categorization of the ENMs following the NanoREG2 approach

A scoring system was followed within the NanoREG2 project to assess cytotoxic and genotoxic effects. It is a cumulative system which in the case of the cytotoxicity endpoint takes into account the cytotoxicity value for the maximum concentration tested and the value of EC50 (NanoREG2 deliverable 1.6). For the scoring and categorization of ENMs genotoxicity and oxidative stress endpoints using the comet assay, the system including definition of acceptance criteria was followed as agreed within NanoREG2 project with some modifications (El Ymani et al. 2022). The genotoxic effect was subjected to statistical analysis and the criteria for positive response were a significant concentration- response relationship and at least one concentration significantly different from negative control, or at least two concentrations with a significantly increased frequency of strand breaks (SB) compared with negative control (Table 19).

**Table 19. Categorization scheme for genotoxicity of nanomaterials. NanoREG2 D1.7, (Naouale El Yamani et al., 2022).**

Categories	Criteria	Category number
Negative	Background level of damage, none of the criteria for positive are met. No significant effect	1
Equivocal	Significant linear trend OR one concentration significantly different from control	2
Positive	Significant linear trend AND at least one concentration significantly different from control; or at least two concentrations significantly higher from control	3

**Table 20. Categorization of the DNA damage for each ENMs tested by NILU on A549 cell line**

		NILU			
		DNA damage (SBs)		netFPG (DNA oxidised bases)	
		3h	24h	3h	24h
<b>T5.2</b>	<b>NM111</b>	1	1	1	1
	<b>NM300K</b>	1	1	1	1

#### 4.7.4 Test for interferences

The particular physicochemical properties of ENMs lead to potential interference with standard test methods including the comet assay; This has been well described by El Yamani et al. (2022). Certain ENMs, such as TiO<sub>2</sub>, and nanogold, are especially likely to cause interference. The possibility of interference with the comet assay by ENMs has been discussed previously (Magdolenova et al., 2012; Karlsson et al. 2015; Di Bucchianico et al. 2017). Interference may happen either directly or indirectly: i) direct/physical interference of the ENMs with the DNA (after lysis) creating additional breaks or

adducts; ii) possibilities for ENMs to interfere by reducing or blocking the DNA migration during electrophoresis; iii) inhibition/interaction with Fpg activity; iv) quenching /autofluorescence during quantification of signals/scoring; v) interference of photosensitive particles with direct light may cause changes in the particles (e.g., increase their reactivity or effect).

#### 4.7.5 Advantages and disadvantages

The in vitro comet assay is a versatile method to measure DNA damage and it has been used in several eukaryotic cells in different areas of research (Collins et al., 2022 in Nature protocols).

One of the biggest challenges and limitations of this method has been the scoring and analysis. Scoring and image analysis has been always a bottle neck, now with the availability of automatic scoring systems this seems to be solved. At NILU a validation has been performed. Validation of the advanced systems against manual scoring. To perform this validation, several slides with random samples, including samples untreated and treated with known and unknown substances will be analyzed with the semi-automatic Perceptives and with the Automatic system Metafer. In total 7 slides (12 gels per slide) were analyzed and data from both systems compiled and analyzed versus each other.

A correlation analysis was conducted, and we used the non-parametric Pearson analysis. Data points fall near the line of equality, suggesting there is a very good degree of agreement between the two methods. The correlation coefficient is 0.9911 ( $p < 0.0001$ ; 95% CI = 0.9848 to 0.9948) (Fig 79).

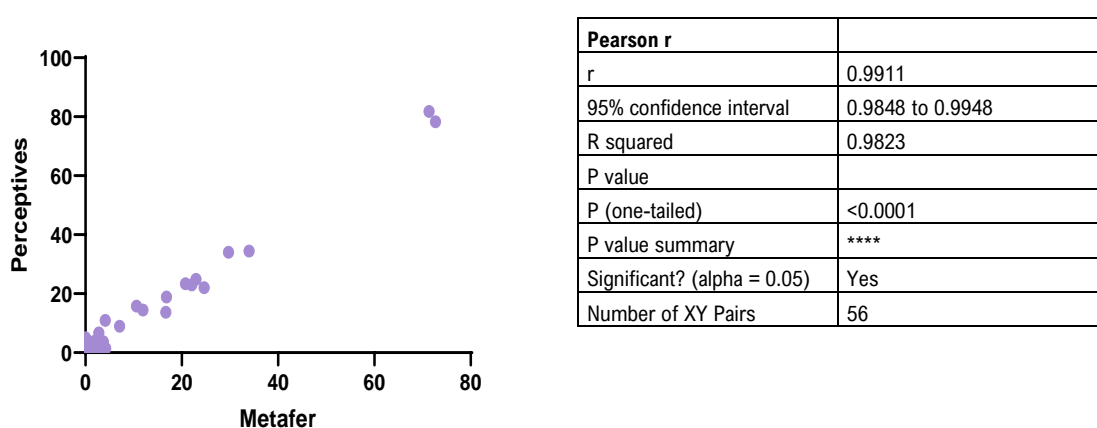


Fig. 79. Comparison between Perceptives and Metafer.

#### 4.7.6. Recommendations

In the method paper published by El Yamani et al. (2022), a list of recommendations as well as acceptance criteria and validity of the assay are listed.

The use of concurrent positive controls that allow statistically significant increase of DNA damage compared to negative control is important.

The use of positive controls will allow to normalize data between laboratories for better comparison.

As for any in vitro assay, it is highly recommended to build up an historical control database, with both negative as well as positive controls for each cell type and time point investigated. This allows the

laboratory to demonstrate the ability to perform the assay consistently, and to show that the cells are capable of picking up positive effects and have reasonably low variability in responses. When reporting the results, it is advisable to show the average and minimum-maximum values of negative/positive historical controls from the last 10-20 experiments performed in the laboratory (El Yamani et al. 2022) method paper.

Increasing the throughput of this method will allow reduced variability between samples. This method is highly sensitive.

Testing for interference following several approaches is also recommended as describe in the method paper.

#### 4.7.7. Statistical Analysis

Statistical differences between the treatment groups in the cytotoxicity and genotoxicity assays were calculated by one-way analysis of variance (ANOVA) followed by Dunnett's post-test to test for differences between ENMs concentrations and negative control. Calculations of half maximal effective concentration ( $EC_{50}$ ) values were performed by non-linear regression analysis using the four parameters Hill-equation. The difference in levels of DNA damage may often be small between treatment groups. A linear regression analysis of the genotoxic effects of the ENMs as a function of exposure concentration and effect was performed. To reduce skewness of the data the correlation analysis was therefore performed on log-transformed numbers (both concentration and effect). Statistics and regression analyses were computed in GraphPad Prism 9. Mathematical calculations were calculated in Excel 2013.

#### 4.7.8 Conclusion regarding the Comet Assay medium-throughput format

The CA is compatible with testing of genotoxicity of ENMs, but proper interference testing is needed for each ENM, as interference between the ENM and the assay can potentially occur at various stages as described in the method paper by El Yamani et al., 2022. It is further important to include cytotoxicity testing as part of the genotoxicity testing to avoid false positive results as DNA breaks occur also during apoptosis/necrosis. A cut-off for cytotoxic response and titration of concentrations of the ENM to be tested is needed. Based on the results from RR1, the importance of the Fpg enzyme source and harmonization became clear. The inclusion of several positive controls was also shown to be of importance, and  $H_2O_2$  was included by all partners as PC in RR2. The results for NILU and KU Leuven were largely consistent. The use of automatic scoring is a big advantage and at NILU a validation of Metafer system versus Perceptive has been conducted and good agreement between the two systems has been demonstrated. NILU is using the Metafer (automatic scoring) for the analysis of the comet assay and this has been an achievement to increase the performance of the assay and to save time which has been for many years a bottle neck for this assay. The 96-gel version of the comet assay is based on same principle as 12-gel system, this means that we can easily increase the throughput whenever this is necessary depending on the type of the study, the set-up of the study and the number and availability of the samples to be analysed.

### 4.8 Micronucleus Test – results obtained by ANSES

#### 4.8.1. Aim of task 5.2 regarding the micronucleus assay

Task 5.2 aimed at developing robust techniques to assess nanomaterial toxicity, designed in a high throughput format. Moreover, as already mentioned, it has been shown that nanomaterials could interfere with the micronucleus assay at several levels. By combining the common efforts from ANSES

and SU, using experience and work from task 5.1, it was commonly decided to develop a micronucleus assay using cytochalasin B on TK6 cells in a high throughput format. In between task 5.1 and task 5.2, ANSES acquired an automated microscope from MetaSystems, which allowed high throughput scoring of micronuclei. This system was already in place at SU. This automated scoring system increases the speed of scoring and the number of cells scored, which considerably improve the rate of analysis as well as the statistical power. This automated system also allows blind scoring when manual scoring may be biased by the presence of particle aggregates on the slides. Finally, as part of Task 5.2, it was decided to try to evaluate the robustness of the assay in terms of potential interference with the scoring.

#### 4.8.2. Development of an SOP for task 5.2: SOP for a micronucleus assay on TK6 cells using cytochalasin B in a 12-well plate format.

ANSES slightly changed the initial SOP of the micronucleus assay on TK6 cells in a 12-well plate format, to accommodate a step with cytochalasin B. The SOP was discussed with SU and adopted for further analysis. Due to cost and time constraints, the workload was equally distributed between partners and a minimum of 1 experiment was required with the 3 nanomaterials for each team. The nanomaterials chosen for task 5.2 were the same as those used for task 5.1 to compare results obtained in the various protocols set-up. Briefly, TK6 cells were seeded in 12-well plates and treated with control medium or positive control or nanomaterials. After 1.5 cell cycle incubation, cells were washed with PBS and incubated in cell culture medium in the presence of cytochalasin B. After another 1.5 cell cycle, cells were harvested, fixed and micronuclei in binucleated cells were assessed using an automated platform. Cells counts were also performed in order to insure cell multiplication occurred during treatment; hence parameters such as Cytokinesis-Block Proliferation Index (CBPI) and Replication Index (RI) were assessed according to the OECD test guideline 487. Additionally, testing for potential interference of nanomaterials with the detection of micronuclei was also performed. Methyl methanesulfonate and mitomycin C (MMC) were used as positive controls for the micronucleus assay. A preliminary dose response of cells to various concentrations of cytochalasin B had been performed so that an appropriate amount of binucleated cells could be analysed. Data gathered at ANSES indicated that 3  $\mu\text{g}/\text{mL}$  cytochalasin B yielded to less than 20 % binucleated cells, therefore the dose of 6  $\mu\text{g}/\text{mL}$  was chosen (minimum of 50 % binucleated cells). (Figures 80, 81, 82)

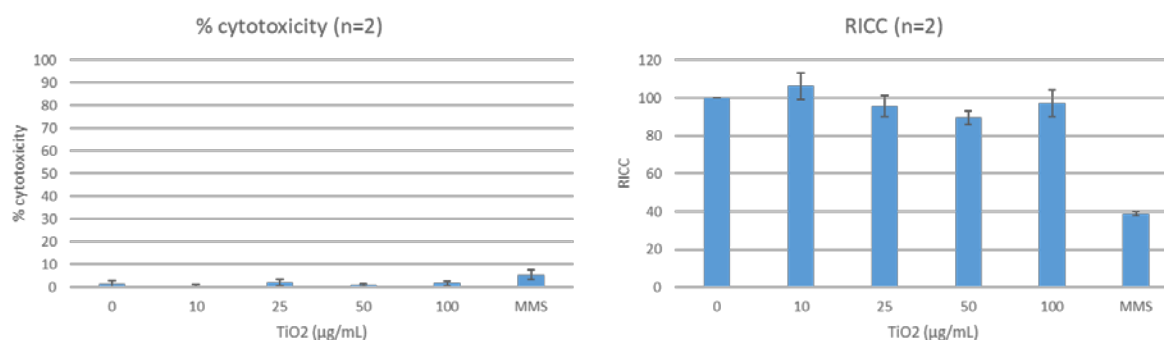


Fig. 80. Cytotoxicity and RICC analysis of TK6 untreated or treated with positive control Methyl methanesulfonate (MMS) 10  $\mu\text{g}/\text{mL}$  or TiO<sub>2</sub> particles (n=2). Data was considered statistically significant compared to control when  $p < 0.05$  (\*  $p < 0.05$ , \*\*  $p < 0.01$ , \*\*\*  $p < 0.001$ ).



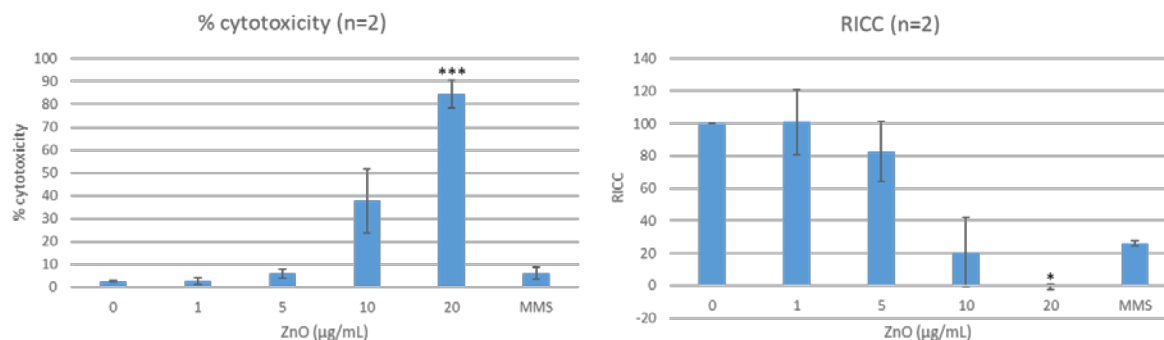


Fig. 81. Cytotoxicity and RICC analysis of TK6 untreated or treated with positive control Methyl methanesulfonate 10 µg/mL or ZnO particles (n=2). Data was considered statistically significant compared to control when  $p < 0.05$  (\*  $p < 0.05$ , \*\*  $p < 0.01$ , \*\*\*  $p < 0.001$ ).

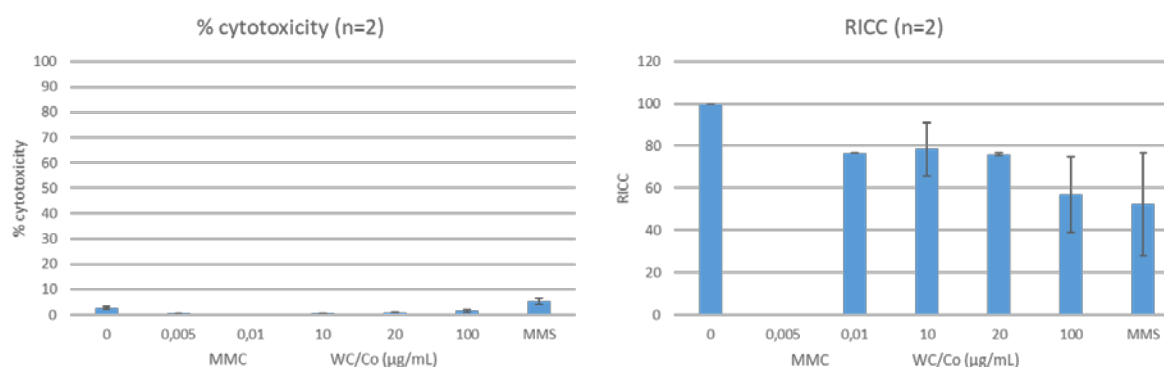


Fig. 82. Cytotoxicity and RICC analysis of TK6 untreated or treated with positive control Methyl methanesulfonate 10 µg/mL or WC/Co particles (n=2). Data was considered statistically significant compared to control when  $p < 0.05$  (\*  $p < 0.05$ , \*\*  $p < 0.01$ , \*\*\*  $p < 0.001$ ).

#### 4.8.3 Cytotoxicity, RICC and micronuclei analysis of TK6 cells

The presence of micronuclei was assessed by manual counting. TiO<sub>2</sub> treatment did not alter the frequency of micronuclei in cells (Figure 83). By contrast, a dose dependent increase in mononucleated cells containing micronuclei could be observed with ZnO, which was significant at 1 µg/mL but due to high toxicity no data could be gathered at 20 µg/mL (Figure 84). A dose dependent increase in the number of mononucleated cells containing micronuclei could be observed significantly from 10 µg/mL treatment with WC/Co (Figure 85).

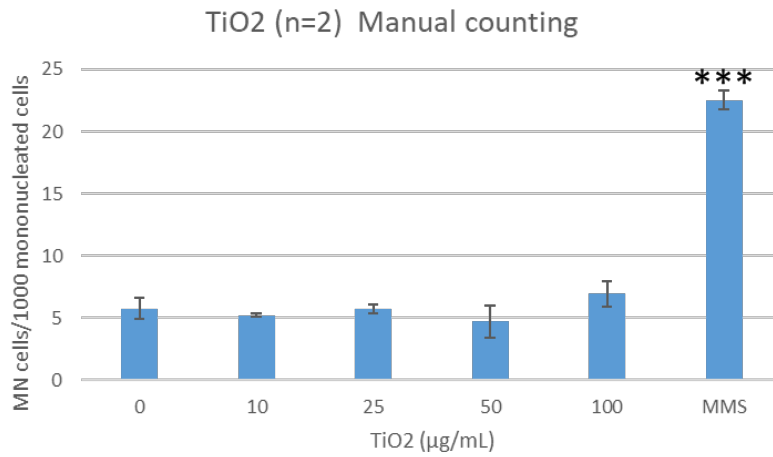


Fig. 83. Micronuclei analysis in mononucleated TK6 cells untreated or treated with TiO<sub>2</sub> (n=2). Data was considered statistically significant compared to control when p<0.05 (\*\* p<0.01, \*\*\* p<0.001).

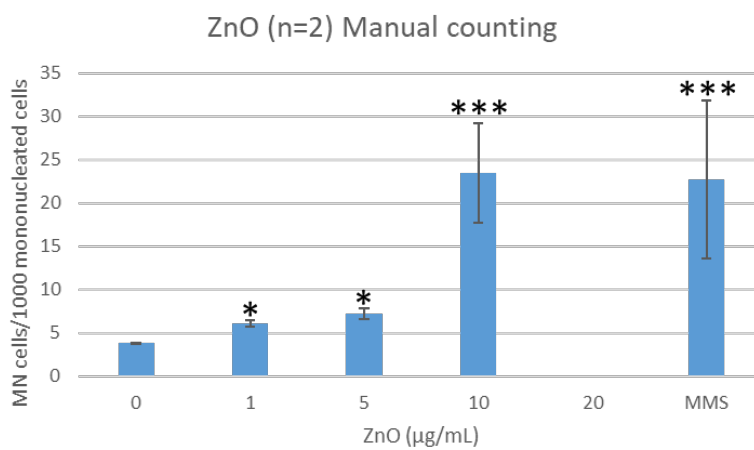


Fig. 84. Micronuclei analysis in mononucleated TK6 cells untreated or treated with ZnO (n=2). Data was considered statistically significant compared to control when p<0.05 (\*\* p<0.01, \*\*\* p<0.001).

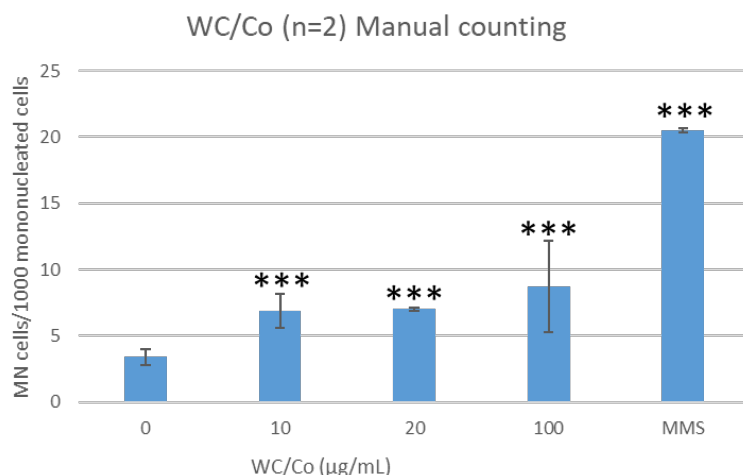


Fig. 85. Micronuclei analysis in mononucleated TK6 cells untreated or treated with WC/Co (n=2). Data was considered statistically significant compared to control when  $p < 0.05$  (\*\*\*)  $p < 0.001$ ).

#### 4.8.4. Comparison of micronucleus data gathered in the 12-well plate format in the absence of cytochalasin B, manual counting versus automated scoring.

As a starting point, ANSES compared data gathered by manual counting with those of the automated counting system Metafer, using control cells and cells treated with MMS, in the micronucleus assay without cytochalasin B. Table 21 and 22 present the data gathered from 6 experiments. Analysis was performed by manual counting (on a total of 35 000 control cells and 24 000 cells treated with MMS) and by automated Metafer analysis (on 157 000 control cells and 85 000 cells treated with MMS).

**Table 21: Percentage of micronuclei counted in control TK6 cells, using the micronucleus assay without cytochalasin B, following manual counting or Metafer analysis (n=6).**

	Frequency of mononucleated cells with micronuclei	
	mean	SEM
<b>control</b>		
Manual counting	0.43	0.05
Metafer	0.26	0.04

**Table 22: Fold increase in micronuclei frequency upon treatment with MMS, following manual counting or Metafer analysis (n=6).**

	Fold change in micronuclei frequency compared to control	
	mean	SEM
<b>MMS (10 µg/mL)</b>		
Manual counting	5.39	0.84
Metafer	4.36	1.25

These data indicate that Metafer analysis gave a lower basal level of micronuclei frequency than manual counting, in control cells. This suggests that Metafer is more stringent in detecting micronuclei than the operator for the manual counting. Upon treatment with MMS, manual counting gave a slightly higher mean fold increase in micronuclei frequency compared to Metafer analysis. This again may be due to the higher stringency of Metafer in detecting micronuclei. Importantly, to compare manual counting and Metafer analysis, slides stained with acridine orange for manual scoring were unstained for Metafer analysis. It could be hypothesised that some acridine orange may have remained onto slides and hindered slightly the detection of micronuclei. However, due to the higher number of cells analysed with Metafer compared to manual scoring, the statistical analysis of the data is improved with Metafer. Therefore, the Metafer analysis was considered sensitive and a reliable technique to count micronuclei in a high throughput way. Slides prepared during Task 5.1 by ANSES were used and analysed for micronuclei in mononucleated cells using Metafer and compared to data obtained from manual counting. As a mean 4 000 cells per condition per biological experiment were analysed by manual counting and around 26 000 cells with Metafer, for mononucleated cells analysis, in the micronucleus assay without cytochalasin B, in a 12-well plate format. Results with Metafer analysis indicated that TiO<sub>2</sub> did not change the frequency of micronuclei (Figure 86).

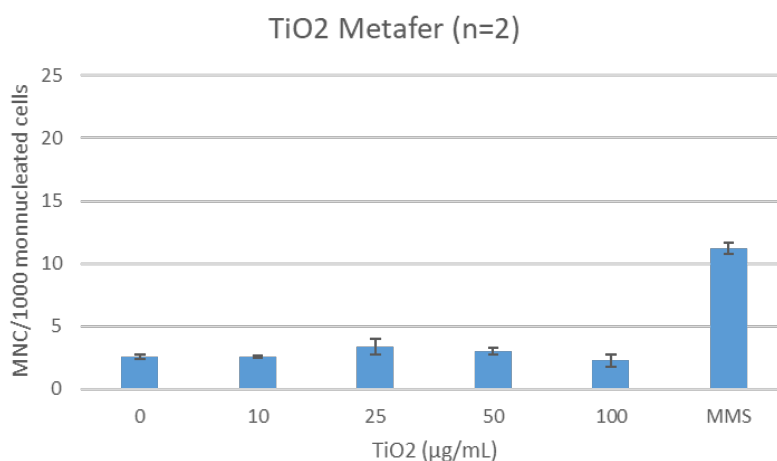


Fig. 86. Micronuclei analysis in mononucleated TK6 cells untreated or treated with TiO<sub>2</sub>, using Metafer (n=2). Data was considered statistically significant compared to control when p<0.05.

**Table 23: Fold change in micronuclei frequency in mononucleated cells, in the absence of cytochalasin B, upon treatment with positive control MMS (10 µg/mL) or TiO<sub>2</sub> NM.** Data was considered statistically significant compared to control when p<0.05 (\*\*\*) p<0.001) (n=2).

		Fold change in MN frequency compared to control	
		manual counting	Metafer
TiO <sub>2</sub> (µg/mL)	0		
	10	0.91	1.02
	25	1.00	1.32
	50	0.82	1.19
	100	1.21	0.90
	MMS	3.91 (***)	4.41 (***)

Metafer analysis of cells treated with ZnO indicated a dose dependent increase in micronuclei frequency, which was statistically significant from 1  $\mu\text{g}/\text{mL}$  (Figure 87). Similar data were obtained between the two methods of scoring, although the fold increase in micronuclei frequency seemed to be consistently higher with manual scoring than with the automated method (table 23). Again, results indicate that Metafer seems to be more stringent in micronuclei detection than the manual operator. At 1  $\mu\text{g}/\text{mL}$  ZnO, the results were statistically different from control ( $p < 0.05$  for manual counting and  $p < 0.001$  with Metafer) (table 24). Importantly, Metafer data analysis was performed on a higher number of cells than manual counting (8000 cells were analysed by manual counting while in average 26 000 cells were analysed by Metafer, per condition). Therefore, the statistical power of data gathered with Metafer was higher than those gathered by manual counting.

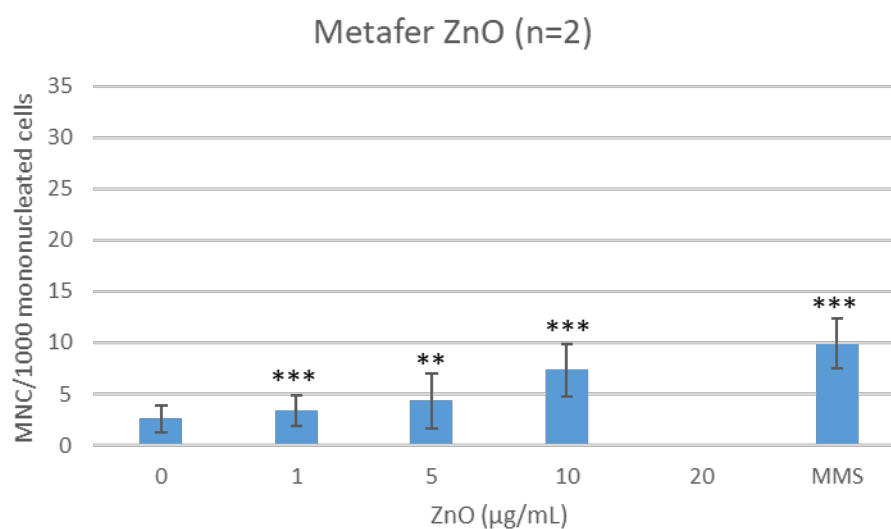


Fig. 87. Micronuclei analysis in mononucleated TK6 cells untreated or treated with ZnO, using Metafer (n=2). Data was considered statistically significant compared to control when  $p < 0.05$  (\*\*  $p < 0.01$ , \*\*\*  $p < 0.001$ ).

**Table 24: Fold change in micronuclei frequency in mononucleated cells, in the absence of cytochalasin B, upon treatment with positive control MMS (10  $\mu\text{g}/\text{mL}$ ) or ZnO NM.** Data was considered statistically significant compared to control when  $p < 0.05$  (\*\*  $p < 0.001$ ) (n=2).

		Fold change in MN frequency compared to control	
		manual counting	Metafer
ZnO ( $\mu\text{g}/\text{mL}$ )	0		
	1	1.6 (*)	1.31 (***)
	5	1.89 (*)	1.68 (**)
	10	6.13 (***)	2.84 (***)
	20		
	MMS	5.92 (***)	3.85 (***)

Regarding WC/Co, Metafer analysis showed a significant dose dependent increase in mononucleated cells containing micronuclei, from 20  $\mu\text{g/mL}$  (Figure 87). These results were slightly different from those obtained with manual counting, which were statistically significant from 10  $\mu\text{g/mL}$  (table 25). Again, this difference could be due to the increased stringency in analysis displayed by Metafer compared to the manual operator and/or to remaining traces of acridine orange.

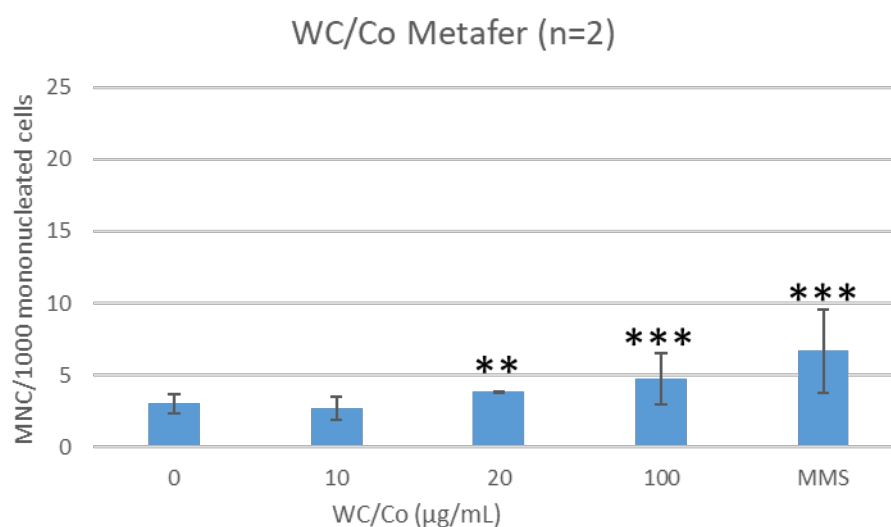


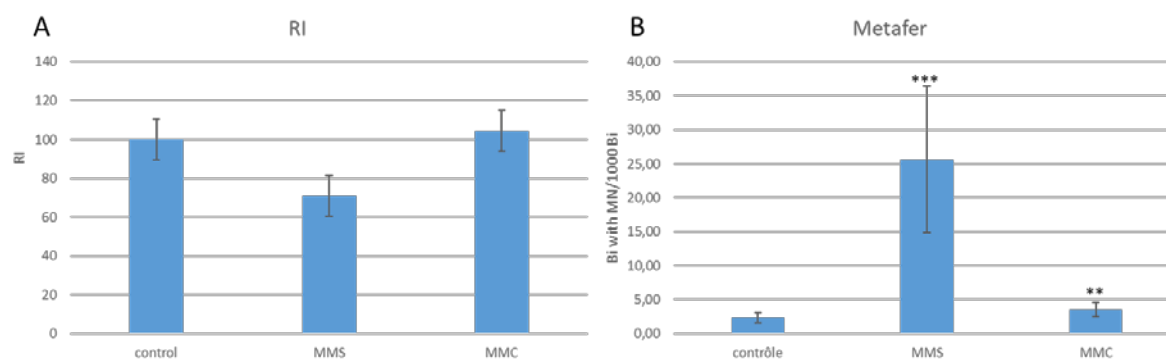
Fig. 88. Micronuclei analysis in mononucleated TK6 cells untreated or treated with WC/Co, using Metafer (n=2). Data was considered statistically significant compared to control when  $p < 0.05$  (\*\*  $p < 0.01$ , \*\*\*  $p < 0.001$ ).

**Table 25: Fold change in micronuclei frequency in mononucleated cells, in the absence of cytochalasin B, upon treatment with positive control MMS (10  $\mu\text{g/mL}$ ) or WC/Co NM.** Data was considered statistically significant compared to control when  $p < 0.05$  (\*\*  $p < 0.01$ , \*\*\*  $p < 0.001$ ) (n=2).

		Fold change in MN frequency compared to control	
		manual counting	Metafer
WC/Co ( $\mu\text{g/mL}$ )	0		
	10	2.02 (***)	0.88
	20	2.07 (***)	1.27 (**)
	100	2.58 (***)	1.56 (***)
	MMS	6.04 (***)	2.21 (***)

#### 4.8.5. Results for Task 5.2: micronucleus assay on TK6 cells using cytochalasin B in a 12-well plate format.

Following the SOP of the micronucleus assay using cytochalasin B in a 12-well plate format, ANSES generated some preliminary data with positive controls. Figure 89B indicates that both positive controls, MMS and MMC, significantly increased the frequency of micronuclei in binucleated cells.



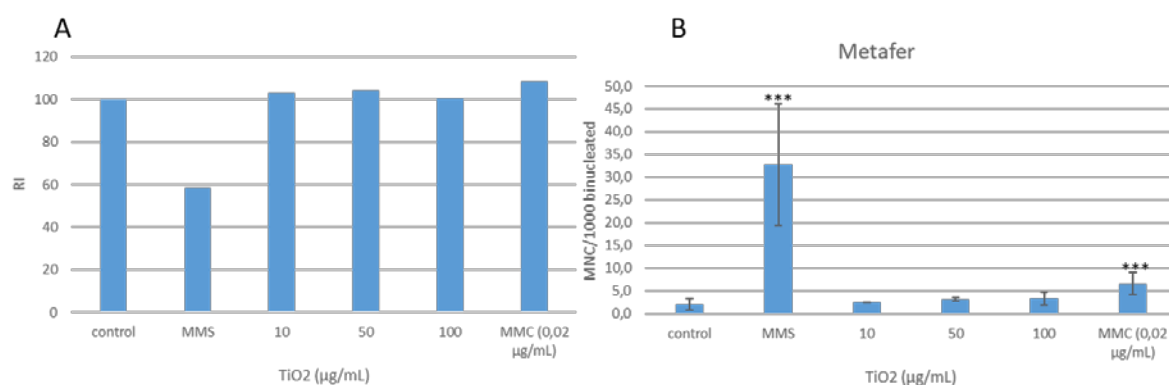
*Fig. 89. Pilot trial using the SOP for the micronucleus assay in a 12-well plate format with cytochalasin B. Replication Index (RI), an indicator for cell proliferation is shown in (A) while the assessment of binucleated cells with micronuclei is displayed in (B). Data was considered statistically significant compared to control when  $p < 0.05$  (\*\*  $p < 0.01$ , \*\*\*  $p < 0.001$ ).*

Table 26 displays critical parameters such as the % binucleated cells and the Cytokinesis-Block Proliferation Index (CBPI). Data from table 6 suggest the assay (cytochalasin B 6  $\mu\text{g}/\text{mL}$ ) is working with enough binucleated cells to perform analysis: more than 60 % binucleated cells in control and a CBPI of 1.8 mean nuclei per cell. Mitomycin C (MMC) used at 0.01  $\mu\text{g}/\text{mL}$  showed a fold change in micronuclei frequency of only 1.5. Importantly, MMS 10  $\mu\text{g}/\text{mL}$  showed large variations in % binucleated cells containing micronuclei (Figures 89B and 90B). These variations could be related to the cytotoxicity observed after 24h incubation with cytochalasin B compared to the results obtained with the same MMS concentration without cytochalasin B and the small percentage of binucleated cells, which makes the analysis of micronuclei less reliable (Table 26).

**Table 26: Critical parameters to assess the reliability of the SOP, displayed in a trial experiment** (duplicates,  $n=1$ ). Methyl methane sulfonate (10  $\mu\text{g}/\text{mL}$ ) and MMC (0.01  $\mu\text{g}/\text{mL}$ ) were used as positive control.

	% Binucleated cells		CBPI		Fold change MN frequency compared to control
	mean	sd	mean	sd	
<b>control</b>	68	0.35	1.8	0.05	
<b>MMS</b>	14	0.14	1.5	0.04	10.91
<b>MMC</b>	69	2.37	1.9	0.06	1.52

Treatment of TK6 cells with nanomaterials was performed only once in duplicates by ANSES for each nanomaterial. Results for  $\text{TiO}_2$  showed no effect on the RI and only a small dose dependent increase in the frequency of micronuclei with  $\text{TiO}_2$  treatment, which was not statistically significant (Figure 32).



**Fig. 90.** Effect of  $TiO_2$  treatment on RI and micronuclei frequency, with the SOP using cytochalasin B. Methyl methanesulfonate (10 µg/mL) was used as a positive control. Results are presented as mean RI (A) and mean frequency of micronuclei in binucleated cells +/- SD (B), from one experiment. Data was considered statistically significant compared to control when  $p < 0.05$  (\*\*\*)  $p < 0.001$ .

The critical parameters of this assay when testing  $TiO_2$  are presented table 27. The % of binucleated cells reached more than 60 % for all conditions tested, except MMS with only 14%.

**Table 27: Critical parameters obtained with the SOP using cytochalasin B in the presence of  $TiO_2$ .** Methyl methanesulfonate (10 µg/mL) was used as a positive control. Results are presented as mean +/- SD of duplicates from one experiment.

		% Binucleated cells	CBPI	RI	Fold change MN frequency compared to control
<b>TiO<sub>2</sub> (µg/mL)</b>	control	64.23	1.86	100.00	
	MMS	14.26	1.50	58.39	15.37
	10	61.67	1.89	103.08	1.15
	50	65.04	1.90	104.23	1.48
	100	62.48	1.86	100.22	1.57
	MMC (0.02 µg/mL)	65.53	1.93	108.39	3.09

The data indicated that ZnO dose dependently reduced the RI suggesting cytostasis and dose dependently increased the frequency of micronuclei in binucleated cells (Figure 91). The effect of ZnO was statistically significant on the duplicates from 1 µg/mL but no significant effect could be observed at 10 µg/mL due to large variations in results, low % of binucleated cells and strong cytotoxicity (Table 28). This negative result at high concentration of ZnO highlight the importance of calculating the RI as an integrated part of the micronucleus assay.



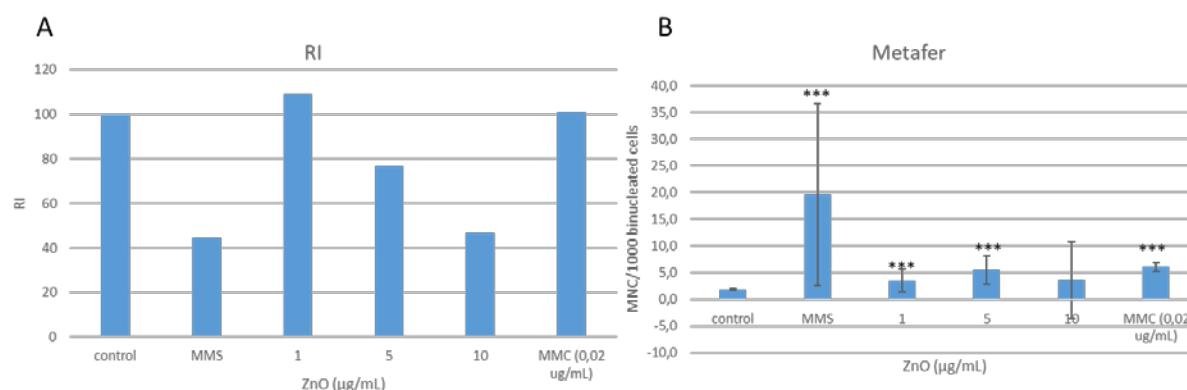


**Fig. 91.** Effect of ZnO treatment on on RI and micronuclei frequency, with the SOP using cytochalasin B. Methyl methanesulfonate (10 µg/mL) was used as a positive control. Results are presented as mean RI (A) and mean frequency of micronuclei in binucleated cells +/- SD (B), from one experiment. Data was considered statistically significant compared to control when  $p < 0.05$  (\*\*\*)  $p < 0.001$ .

**Table 28: Critical parameters obtained with the SOP using cytochalasin B in the presence of ZnO.** Methyl methanesulfonate (10 µg/mL) was used as a positive control. Results are presented as mean +/- SD of duplicates from one experiment.

		% Binucleated cells	CBPI	RI	Fold change MN frequency compared to control
	control	59.02	1.80	100.00	
	MMS	11.62	1.36	44.73	10.74
ZnO (µg/mL)	1	61.99	1.87	108.97	1.93
	5	43.54	1.61	76.57	3.00
	10	31.67	1.37	46.53	1.98
	MMC (0.02 µg/mL)	56.40	1.80	100.99	3.31

WC/Co treatment induced only a small reduction in RI at the highest dose tested (Figure 92A). However, a dose dependent increase in micronuclei frequency was observed, which was significant from 10 µg/mL (Figure 92B). Parameters used to assess the quality of the experiments indicated a good level of binucleated cells to perform analysis (table 29). WC/Co increased by 2.9-fold the frequency of micronuclei at 100 µg/mL compared to control.

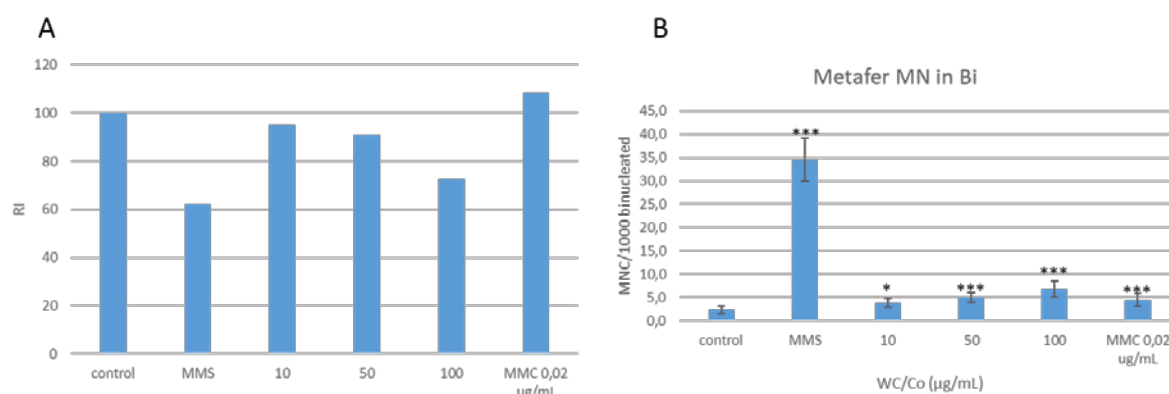


**Fig. 92.** Effect of WC/Co treatment on RI and micronuclei frequency, with the SOP using cytochalasin B. Methyl methanesulfonate (10 µg/mL) was used as a positive control. Results are presented as mean RI (A) and mean frequency of micronuclei in binucleated cells +/- SD (B), from one experiment. Data was considered statistically significant compared to control when  $p < 0.05$  (\*  $p < 0.05$ , \*\*  $p < 0.01$ , \*\*\*  $p < 0.001$ ).

**Table 29: Critical parameters obtained with the SOP using cytochalasin B in the presence of WC/Co.** Methyl methanesulfonate (10 µg/mL) was used as a positive control. Results are presented as mean +/- SD of duplicates from one experiment.

		% Binucleated cells	CBPI	RI	Fold change MN frequency compared to control
	control	57.54	1.85	100.00	
	MMS	15.48	1.53	62.44	14.73
WC/Co (µg/mL)	10	61.69	1.81	95.02	1.65
	50	65.27	1.78	90.90	2.13
	100	55.51	1.62	72.51	2.89
	MMC (0.02 µg/mL)	64.71	1.93	108.56	1.94

From the pilot experiment and the 3 subsequent experiments, data was gathered (Table 30). The % binucleated was superior to 50 % in control cells and MMC-treated cells, while only 14% binucleated cells were seen when treated with MMS (10 µg/mL). Both MMS and MMC significantly increased the frequency of micronuclei in binucleated cells. However, MMS decreased strongly the % of binucleated cells at 10 µg/mL, which can compromise the results. Therefore, it was suggested for the positive controls, to use MMC at a higher concentration to increase the frequency of binucleated cells with micronuclei and to use MMS at a lower concentration (suggested concentration of 1.5 µg/mL) to improve the % of binucleated cells and hence to strengthen the data.

**Table 30: Critical parameters obtained with the SOP using cytochalasin B for control cells or cells treated with positive control MMS or MMC.** Results are presented as mean +/- SEM of a minimum of three independent experiments.

	% Binucleated cells		CBPI		RI		Fold change MN frequency compared to control		% MN cells/1000 Binucleated cells	
	mean	SEM	mean	SEM	mean	SEM	mean	SEM	mean	SEM
control	62.14	2.37	1.83	0.016	100.00	0.000			2.16	0.12
MMS (10 µg/mL)	13.75	0.81	1.48	0.04	59.12	5.46	12.94	1.23	28.14	3.44
MMC (0.02 µg/mL)	62.21	2.92	1.89	0.04	105.98	2.49	2.78	0.43	5.73	0.61

A preliminary study using MMS 1.5 µg/mL and MMC 0.02 µg/mL indicated that MMS at this lower concentration still increase the frequency of micronuclei in binucleated cells, while displaying a good % of nucleated cells (Table 31).

**Table 31: Critical parameters obtained with the SOP using cytochalasin B for control cells or cells treated with positive control MMC or MMS at a lower concentration.** Results are presented as mean of one experiment.

	% Binucleated cells	CBPI	RI	Fold change in MN frequency compared to control
control	57	1.75	100.00	
MMS (1.5 µg/mL)	50	1.70	93.42	4.92
MMC (0.02 µg/mL)	60	1.81	107.88	2.10

As a mean, 15 000 binucleated cells per condition per biological experiment were analysed with Metafer (only 600 for MMS (10 µg/mL due to a low % of binucleated cells), in the micronucleus assay with cytochalasin B, in a 12-well plate format.

#### 4.9. Micronucleus Assay - Results from Swansea University regarding Task 5.2

Task 5.2 which focuses on high throughput and high content analysis was initiated at SU by performing a cytotoxicity screen on a total of 7 ENMs. Five of the ENMs were used in Task 5.1 and the additional two were utilised in the PATROLS project (NM-111 and NM-300k).

##### 4.9.1. *In vitro* micronucleus assay data generated by Swansea University using the ANSES 12-well format SOP on mononucleated TK6 cells

To determine the cytotoxic and genotoxic potential of ZnO, TiO<sub>2</sub> and the WC-Co in TK6 cells, a 12-well version of the *in vitro* micronucleus assay was used with the SOP provided by ANSES. The data shown in **Figure 93** highlights the cytotoxic potential of ZnO with a significant depletion in viability observed initially at 5µg/ml. The ZnO also generated a significant genotoxic response at 10µg/ml which appeared to be concentration dependent. The TiO<sub>2</sub> did not induce any significant cytotoxic or genotoxic responses in the TK6 cells. Finally, the WC-Co whilst not inducing any significant cytotoxicity did induce statistically significant chromosomal damage at 100µg/ml.

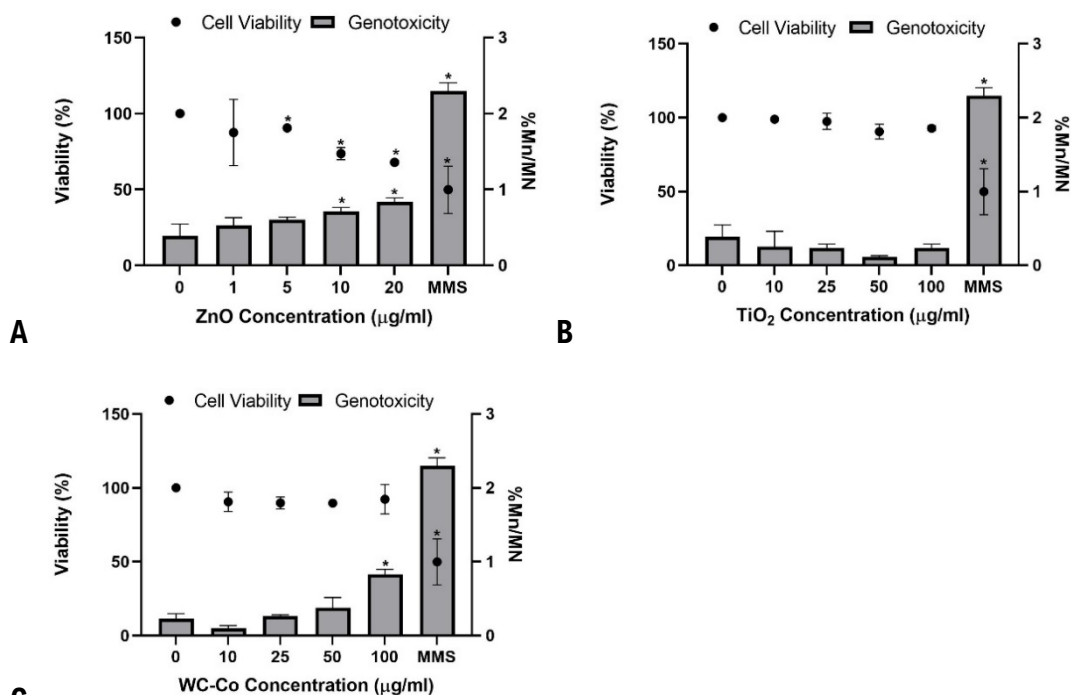


Fig. 93. Cytotoxicity (calculated by RPDs and converted to % cell viability) and chromosomal damage using the 12-well mononucleate version of the micronucleus assay on TK6 cells following a 1.5 cell cycle exposure. Data was considered statistically significant when (\*) was  $p < 0.05$ . Two biological replicates were performed in total to generate this data, two technical replicates were seeded per condition with two slides being prepared from each technical replicate. 1000MN cells were scored per slide for a total of 8000MN (4000MN for biological replicate). MMS was used as the positive control at a concentration of 2μg/ml due to 10μg/ml being too cytotoxic.

#### 4.9.2. *In vitro* cytokinesis-blocked micronucleus assay data generated by Swansea University using the ANSES 12-well SOP with additional cytochalasin B step added.

The final element of experimental work for Task 5.2 was to conduct the 12-well *in vitro* micronucleus assay but to then include the use of cytochalasin B at 3μg/ml. Here, the ZnO induced significant cytotoxicity but at 20 μg/ml and significant genotoxicity at 10- and 20 μg/ml. Once again, the TiO<sub>2</sub> did not induce any statistically significant responses. The WC-Co did mirror the effect seen in the mononucleate 12-well micronucleus assay with just one significant data point for genotoxicity at the highest concentration of 100 μg/ml (Figure 94).

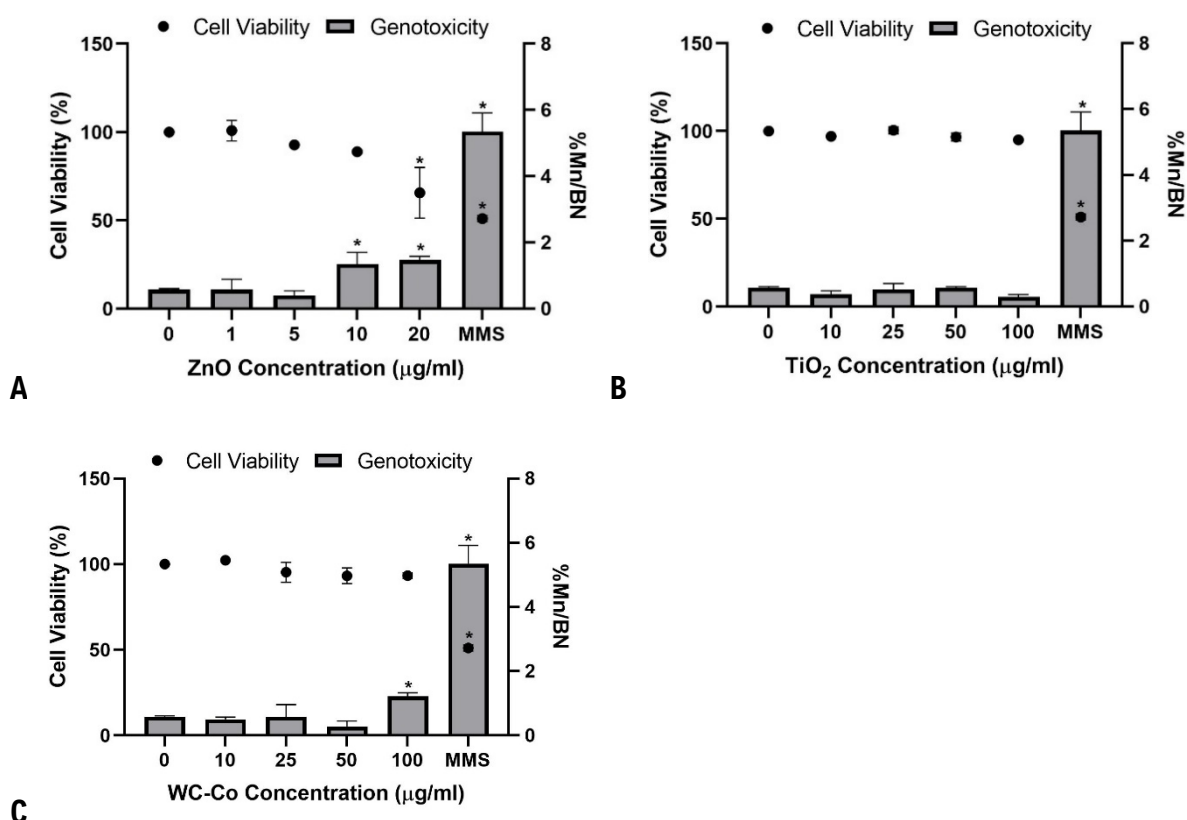


Fig. 94. Cytotoxicity (calculated by RPDs) and chromosomal damage using the 12-well version of the micronucleus assay on TK6 cells following a 1.5 cell cycle exposure. The ANSES protocol was then slightly adapted to include a cytochalasin B step (3 $\mu\text{g/ml}$ ) for 1.5 cell cycles. Data was considered statistically significant when (\*) was  $p < 0.05$ . Two biological replicates were performed in total to generate this data, two technical replicates were seeded per condition with two slides being prepared from each technical replicate. 500BN cells were scored per slide for a total of 4000BN (2000BN for biological replicate). MMS was used as the positive control at a concentration of 2 $\mu\text{g/ml}$  due to 10 $\mu\text{g/ml}$  being too cytotoxic.

#### 4.9.3. Comparison of data obtained from both partners (ANSES and SU) following the SOP from T5.1 and T5.2

##### 4.9.3.1. Task 5.2: SOP for the micronucleus assay in the absence of cytochalasin B

Data gathered from both partners in the SOP using a high throughput approach in the absence of cytochalasin B were compared. Basal levels of micronuclei in mononucleated cells were similar between both partners (4.3 %  $\pm$  0.5 by manual counting and 2.6 %  $\pm$  0.4 (mean  $\pm$  SEM) with Metafer, results of 6 independent experiments at ANSES). TiO<sub>2</sub> did not induce a significant change in frequency of micronuclei in mononucleated cells, for both partners. ZnO induced a dose dependent increase in micronuclei frequency that was significant from 1  $\mu\text{g/ml}$  for ANSES and from 10  $\mu\text{g/ml}$  for SU (the fold change in micronuclei frequency at 10  $\mu\text{g/ml}$  was 6.12 by manual counting for ANSES and 2.84 with Metafer for ANSES, while it was 1.5-fold for SU with Metafer). ANSES could not analyse micronuclei with 20  $\mu\text{g/ml}$  ZnO due to high cytotoxicity, but SU managed to observe a significant increase in micronuclei frequency at that dose. WC/Co induced a significant dose dependent increase in micronuclei frequency that was significant from 10  $\mu\text{g/ml}$  for ANSES by manual counting or 25  $\mu\text{g/ml}$  for ANSES with Metafer, while SU obtained a significant increase in micronuclei frequency at 100  $\mu\text{g/ml}$ . In terms

of fold increase in micronuclei frequency, it reached 2.58 by manual counting and 1.56 with Metafer for ANSES, while it reached 3.7 for SU. This lower fold increase in micronuclei frequency observed with Metafer at ANSES may be due to remaining acridine orange on the slides, hindering their detection.

**Table 32. A summary of the fold-change observed for each ENM tested with TK6 cells**

ENM ( $\mu\text{g/ml}$ )	Concentration	Fold change in MN frequency compared to control			
		ANSES (SOP)		SU	
		manual counting	Metafer	SU (TK6 Manual SOP)	SU (ANSES SOP on Metafer)
TiO <sub>2</sub>	10	0.91	1.02	0.63	0.8
	25	1.00	1.32	0.88	0.55
	50	0.82	1.19	1.1	0.2
	100	1.21	0.90	1.1	0.55
	MMS	3.91 (***)	4.41 (***)	MMC – 10.6*	4.45 (*)
ZnO	1	1.6 (*)	1.31 (***)	0.75	0.9
	5	1.89 (*)	1.68 (**)	1.5	1.25 (*)
	10	6.13 (***)	2.84 (***)	0.75	1.5 (*)
	20				1.75 (*)
	MMS	5.92 (***)	3.85 (***)	MMC – 10.6*	4.45 (*)
WC/Co	10	2.02 (***)	0.88		0.4
	25	2.07 (***)	1.27 (**)	(20 $\mu\text{g/ml}$ ) – 3*	1.2
	100	2.58 (***)	1.56 (***)	3.1*	3.7 (*)
	MMS	6.04 (***)	2.21 (***)	MMC – 10.6*	4.45 (*)

#### 4.9.3.2. Task 5.2: SOP for the micronucleus assay using cytochalasin B

Both partners obtained acceptable level of micronuclei in binucleated cells, for control cells, for this SOP using cytochalasin B (0.22 % binucleated cells +/- 0.01). However, SU used 3  $\mu\text{g/mL}$  cytochalasin B to induce the formation of binucleated cells, while ANSES had to use 6  $\mu\text{g/mL}$  to achieve enough binucleated cells for analysis (more than 50 %). No modification in micronuclei frequency could be observed at SU upon cell treatment with TiO<sub>2</sub>, while ANSES observed a small dose dependent increase in frequency that was not statistically significant. ZnO induced a dose dependent increase in micronuclei frequency in binucleated cells which was statistically significant from 1  $\mu\text{g/mL}$  at ANSES and due to cytotoxicity, no data could be gathered from 20  $\mu\text{g/mL}$  and large variations between duplicate were noted at 10  $\mu\text{g/mL}$ . By contrast, SU observed a significant increase in micronuclei frequency from 10  $\mu\text{g/mL}$  up to 20  $\mu\text{g/mL}$ . For WC/Co, results showed a dose dependent increase in micronuclei frequency, which was significant from 10  $\mu\text{g/mL}$  at ANSES, while SU observed a significant increase in micronuclei only at 100  $\mu\text{g/mL}$ .

**Table 33. A summary of the fold change data generated from the ANSES 12-well SOP this time with cytochalasin B.**

		Fold change MN frequency compared to control	
		ANSES	SU
	MMS	15.37 (***)	9.3 (*)
TiO <sub>2</sub> (µg/mL)	10	1.15	0.65
	50	1.48	1
	100	1.57	0.5
	MMC (0.02 µg/mL)	3.09 (***)	Not tested
	MMS	10.74 (***)	9.3 (*)
ZnO (µg/mL)	1	1.93 (***)	1
	5	3.00 (***)	0.7
	10	1.98	2.3
	MMC (0.02 µg/mL)	3.31	Not tested
	MMS	14.73	9.3 (*)
WC/Co (µg/mL)	10	1.65 (*)	0.87
	50	2.13 (***)	0.47
	100	2.89 (***)	2.1 (*)
	MMC (0.02 µg/mL)	1.94 (***)	Not tested

*4.9.3.3. Task 5.2 : Comparison of the data obtained in a high throughput format in the absence or in the presence of cytochalasin B.*

- TiO<sub>2</sub> was negative in both set-up
- ZnO induced a dose dependent increase in micronuclei frequency in both set-up, which was statistically significant at 1 µg/mL for ANSES and 10 µg/mL for SU.
- WC/Co induced a dose dependent increase in micronuclei frequency in both set-ups. It was statistically significant at 100 µg/mL in the absence of cytochalasin B for both partners and statistically significant from 10 µg/mL for ANSES and 100 µg/mL for SU in presence of cytochalasin B.

#### 4.9.3.4. Comparison of the data obtained in a low or high throughput format in the absence or in the presence of cytochalasin B, from ANSES and SU.

**Table 34. Table presenting all the results obtained by ANSES and SU, when testing the effect of nanomaterials on micronuclei frequency in TK6 cells.** (NS for non-statistically significant, data was considered statistically significant compared to control when  $p < 0.05$  (\*  $p < 0.05$ , \*\*  $p < 0.01$ , \*\*\*  $p < 0.001$ )).

	Increased MN frequency in mononucleated cells (-cyto B)			Increased MN frequency in binucleated cells (+cyto B)		
	ANSES		SU	ANSES	SU SOP Task 5.1	SU SOP Task 5.2
	Manual	Automated	Automated	Automated	Manual	Automated
TiO <sub>2</sub>	NS	NS	NS	NS	NS	NS
ZnO	1µg/mL ***	1µg/mL ***	5µg/ml*	1µg/mL ***	NS	10µg/ml*
WC/Co	10µg/mL ***	25µg/mL **	100µg/ml*	10µg/mL *	100µg/ml *	100µg/ml*

#### 4.9.4. Tests for interferences

Both partners wanted to test the hypothesis that the presence of the respective ENMs in the assay were not hindering the detection of micronuclei. To investigate this possibility, ANSES performed the micronucleus assay in the absence of cytochalasin B and treated cells with a positive control for 24 h (MMS). Cells were then incubated for 30 minutes with nanomaterials at the highest concentration tested and then subsequently harvested and analysed as previously described. The results presented in Figure 95 indicated that the presence of TiO<sub>2</sub> did not alter the value of micronuclei detected in MMS-treated cells. A small reduction in counted micronuclei were observed upon addition of ZnO and WC/Co particles. However, using a Chi-squared test, the difference was significant only for ZnO nanomaterial. Therefore, it could be hypothesised that ZnO and WC/Co may hinder slightly the detection of micronuclei, leading to a slightly under-evaluation of the actual frequency of micronuclei in cells. Importantly, this test for interference evaluates the potential of ENM present with the cells to hinder the detection of cells micronuclei. However, since cells are incubated only for a short amount of time with ENM in this assay, for the ENM not to induce biological effect, they may not be internalised in cells as they would with a longer incubation. Therefore, this test for interference is in some ways limited since it does assess the potential of ENM present in the system to modulate the scoring of micronuclei, but it does not assess the potential of ENM present in cells to have an effect.



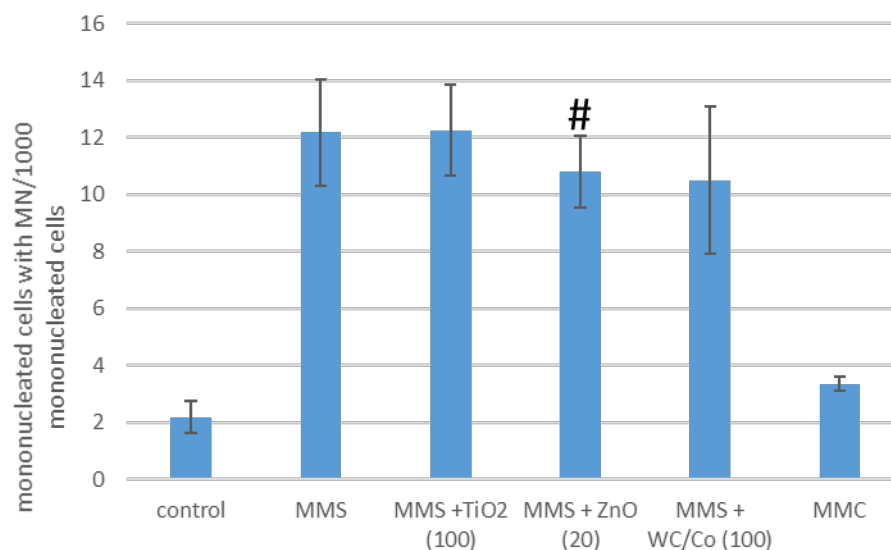


Fig. 95. Test for interference of nanomaterials ( $\mu\text{g}/\text{mL}$ ) in the detection of micronuclei in the micronucleus assay. Values are presented as the mean  $\pm$  SEM of 3 independent experiments. #  $p < 0.05$  compared to MMS alone-treated cells.

#### 4.9.5. Statistical Analysis

The *in vitro* micronucleus data generated in this report was analysed in ANSES and SU using GraphPad Prism version 8.4.3. As the data generated was of two biological replicates / two independent experiments, the Fisher's Exact test was chosen as the most appropriate statistical model for the concentration range. The RPD data generated by SU in the section heading of 6.1 was performed in triplicate (three biological replicates) hence the one-way ANOVA with post-hoc Dunnett's was applied.

#### 4.9.6. Conclusion regarding task 5.2 and the micronucleus assay in a high throughput format

Both partners worked toward the development of a robust SOP for the micronucleus analysis, *in vitro* on TK6 cells, upon treatment with nanomaterials. During task 5.1 and task 5.2, two new SOPs for the micronucleus assay have been proposed by ANSES to increase the high throughput of the initial SOP of task 5.1, one in the absence and one in the presence of cytochalasin B. Preliminary tests with the two SOPs with and without cytochalasin B, as well as including the use of a high throughput counting method showed good data reproducibility between ANSES and SU. Still, some differences in sensitivity have been highlighted between the 2 labs. Issues with interferences should not be neglected although the way of testing them needs to be improved.

## 5. Results analysis

### 5.1. Comparison of the Impedance-based method (xCELLigence) with the HCA testing for cell proliferation and viability assessment (QSAR Lab)

The cell proliferation and viability was assessed by two partners using four different methods: bioimpedance provided by UiB and HCA – cell counts, HCA – nuclear intensity, HCA – nuclear size provided by ANSES. Negative control and three different concentrations (0, 10, 50, and 100  $\mu\text{g}/\text{ml}$ ) of 6 ENMs + 2 diluents: TiO<sub>2</sub> (JRC), ZnO (Sigma Aldrich), CuO (PlasmaChem), MWCNT (Nanocyl), ZnO (JRC), diluent nanocyl, NM-300K (Fraunhofer), and NM-300K dispersion solution were tested on A549 human

lung epithelial cells, and the cytotoxicity was measured as normalized cell index. Concentration-dependent comparison should help to identify methods more, as well as those less prone to ENM interferences. A summary of the materials and methods analyzed here is shown in Table 35.

**Table 35: Overview of the ENMs analyzed and the method used for each ENM**

	BIOIMPEDANCE	HCA - cell count	HCA - nuclear intensity	HCA - nuclear size
TITANIUM DIOXIDE (JRCNM01005A)	+	+	+	+
ZINC OXIDE (SIGMA ALDRICH 721077)	+	+	+	+
CUO 40NM	+	+	+	+
MWCNT 3WT% AQUACYL 0303-NC7000	+	+	+	+
ZINC OXIDE (JRCNM01101A)		+	+	+
NM-300K		+	+	+
DILUENT NANOCYL		+	+	+
NM-300K dispersion medium		+	+	+

### 5.1.1. Presentation of data, summary of data, data analysis, and evaluation

In the case of UiB, in the bioimpedance measurements, human lung epithelial A549 cells, were exposed to 4 different ENMs: TiO<sub>2</sub> (JRC), ZnO (Sigma), CuO (PlasmaChem), MWCNT (Nanocyl). Three independent experiments were conducted for each ENM, with 2 replicate wells for each treatment within each study. The Normalised Cell Index (NCI) was measured and calculated fold-change versus control set to 100% (for details see section 3.3.4). At least three independent measurements in duplicate were performed.

ANSES conducted the analysis using the HCA method in 3 different variants (HCA - cell counts, HCA - nuclear intensity, HCA - nuclear size) in which A549 cells were exposed to the 6 different ENMs + diluents (TiO<sub>2</sub>, two types ZnO, CuO, MWCNT, Tungsten Carbide, NM-300K, NM-300K dispersion medium, Diluent Nanocyl). For HCA two independent experiments were performed for each ENMs, with 3 replicate wells. The results were also calculated relative to the negative control set to 100%. Derived data of NCI obtained by 4 different methods with standard deviation (SD) were summarized and presented in Figure 96.

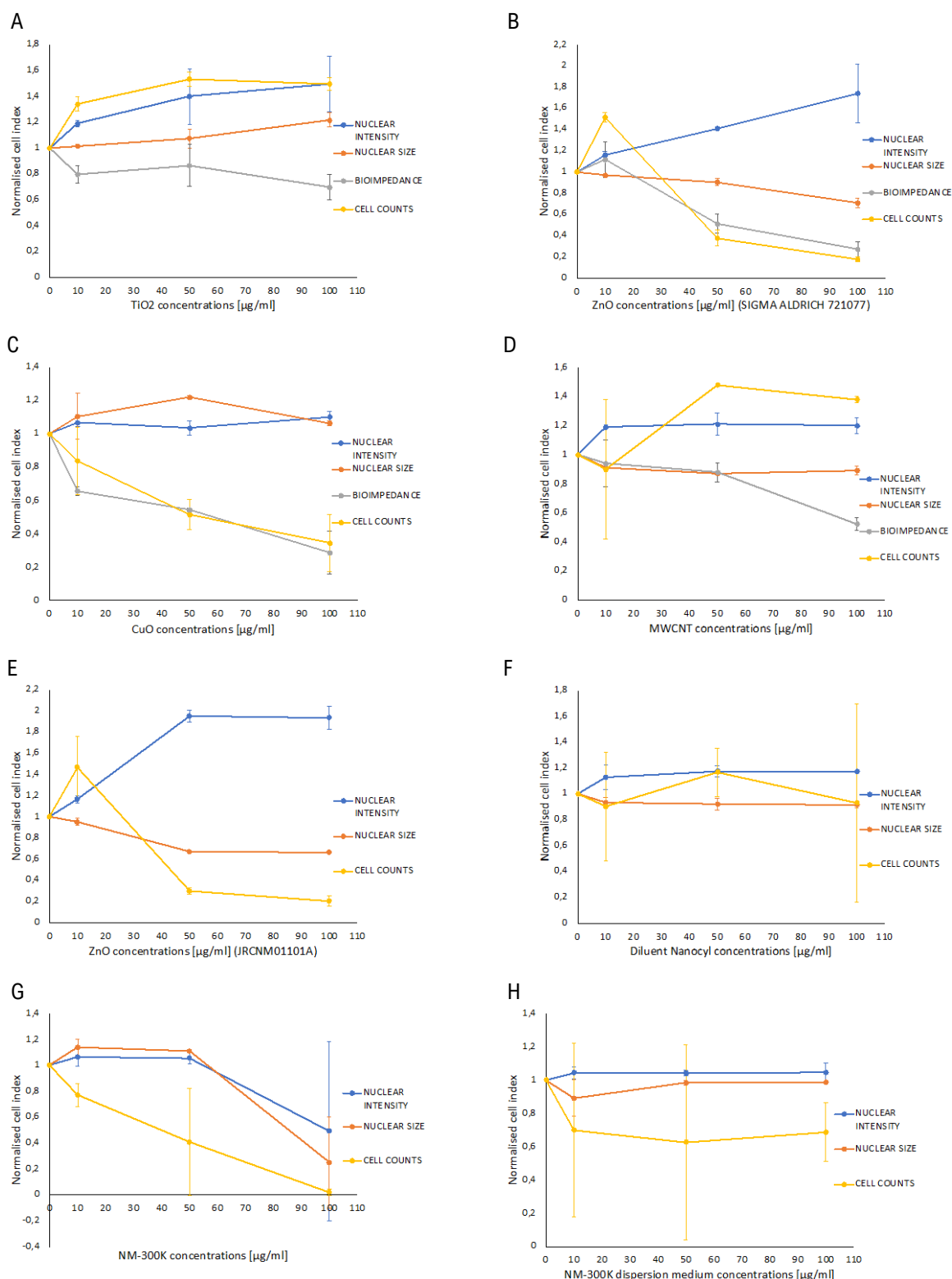


**Fig. 96. HCA vs. Bioimpedance.** A549 cells were exposed to TiO<sub>2</sub> (A), ZnO Sigma 721077 (B), CuO (PlasmaChem) (C), MWCNT (Nanocyl) (D), ZnO JRCNM01101A (E), Diluent Nanocyl (F), NM-300K (G), or NM-300K dispersion medium (H) and cell viability measured as normalized cell index. Cell viability is shown relative to the negative control (set to 100 %) as mean +/- SD from at least 2 independent experiments for HCA- cell counts (yellow), HCA- nuclear intensity (blue), HCA- nuclear size (orange), and at least three independent experiments for bioimpedance (grey),

### 5.1.2. Conclusion on the comparison of impedance-based method with HCA testing for cell proliferation and viability assessment

#### **TiO<sub>2</sub> (JRCNM01005A)**

Generally identified significant discrepancies between the results obtained by different methods. For TiO<sub>2</sub> (Figure 94A.) no significant toxicity was detected taking into account the HCA method. In the case of HCA – cell counts and HCA - intensity, normalized cell index increases when the concentration of ENM increases. HCA – nuclear size method NCI values are slightly higher as the concentration increases. The biggest differences with respect to other methods can be seen for UiB (bioimpedance) where the endpoint values compared to the negative control decrease and are the lowest of all tests for each of the TiO<sub>2</sub> concentrations tested. The series with the largest SD for this sample were measurements at 50 and 100 µg/ml for HCA. - nuclear intensity.

#### **ZnO (SIGMA ALDRICH 721077)**

For the zinc oxide sample (Figure 94B.), the highest cytotoxicity was identified for the HCA - cell counts and bioimpedance methods for concentrations of 50 and 100 µg/ml, in these studies, the endpoint value increased slightly at the lowest concentration value (10 µg/ml) and then decreased sharply. In the case of HCA - nuclear intensity, the NCI value increased with ENM concentration, and in the HCA - nuclear size method, it decreased slightly with increasing concentration.

#### **CuO (PlasmaChem)**

Consecutively, the results for CuO (Figure 1C) show a similar trend for the HCA - nuclear intensity and HCA - size methods where the endpoint value generally increases with increasing ENM concentration. Quite the opposite are the results for the other two approaches (bioimpedance, HCA - cell counts) where the NCI value decreases with CuO concentrations. Here HCA - cell counts method is burdened with the largest standard deviation in each measurement for each of the concentrations.

#### **MWCNT 3WT% AQUACYL 0303-NC7000**

The results for nuclear intensity and nuclear size show a near-constant endpoint value within all 3 concentrations after MWCNT exposure (Figure 94D). For the concentration of 10 µg/ml, similar values are observed across the three methods (HCA - nuclear size, bioimpedance, HCA - cell counts), but the measurement for the cell counts method is subject to a high standard deviation.

#### **ZnO (JRCNM01101A)**

For zinc oxide (JRC) (Figure 94E), the measurement trend for all methods used is the same as for zinc oxide from Sigma Aldrich (Figure 94B), except for a higher value at a concentration of 50 µg/ml for HCA - nuclear intensity.

#### **Diluent nanocyl**

Measurements for diluent nanocyl (Figure 94F) show a similar trend with measurements for MWCNT (Figure 94D) for the HCA – nuclear intensity and HCA - nuclear size methods, in the HCA - cell counts method the results overlap with one of the other methods in a concentration-dependent manner, however, the results are not reliable due to the very high standard deviation values.

#### **NM-300K**

Exposure of cells to two variants of NM300K showed similar results for concentrations of 10 and 50 µg/ml, with the highest concentration (100 µg/ml) of NM-300K (Figure 94G) showing a decrease in

normalized cell index in contrast to NM-300K as a dispersion (Figure 94H) where values at points of all concentrations are almost constant. In these two experiments, it is also the HCA - cell counts method that has the least repeatability of results between independent measurements (highest SD).

## 5.2. Repeatability testing of the Impedance-based method (xCELLigence): Data from UiB, NILU, and CEA (QSAR lab)

### 5.2.1. Summary of results

The results for Normalised cell index (NCI) obtained by UiB, NILU and CEA, using the same impedance-based method (xCELLigence) were compared. Tests were conducted by UiB, NILU, and CEA for 3 ENMs: ZnO NM-110 (JRC), NM-200 (JRC), and NM-300K (Fraunhofer). Negative control (unexposed cells) + four different concentrations of ENMs (0, 2, 20, 50, and 100 µg/ml) were tested on A549 human lung epithelial cells.

The statistical analysis was used to determine if reached measurements between the three labs (NILU, CEA, and UiB) are consistent. A single analysis consisted of comparing results between two labs in every possible combination: NILU-CEA, NILU-UiB, and CEA-UiB. The analysis also included determining the precision and accuracy of the obtained measurements.

Precision is the degree to which future measurements or calculations yield the same or similar results — it is a measure of the spread of repeated measurement results and depends only on the distribution of random errors – it does no indication of how close those results are to the true value. To compare the precision of two independent measurements obtained during the analysis of samples with the same level of analyte content, we use the F-Snedecor test. The critical value for the cases under consideration depends on the number of tested concentrations for each particular experiment. Its values are presented in Table 36.

Accuracy refers to the degree of conformity of a measured or calculated quantity to an actual (true) value. Accuracy is closely related to precision, but it's not the same thing. A result is said to be accurate when it matches to a particular target. In the analysis, we investigated the differences between the experiments performed in two labs with a pairwise t Student's test for each ENM concentration.

Critical values depend on the number of variables presented in Table 1, the values used in the following analysis have been highlighted.

### 5.2.2. Conclusion on repeatability testing of the impedance-based method

#### ZnO NM-110 (JRCNM01101A)

**Precision (F-Snedecor test):** Determined F is lower than  $F_{crit}$  ( $F < F_{crit}$ ) for all pairs to comparison (NILU-CEA, NILU-UiB, CEA-UiB), therefore, the obtained values of standard deviations do not differ statistically significantly between laboratories.

**Accuracy (t Student test):** In the case of comparison for NILU-CEA or CEA-UiB the determined t statistic is lower than  $t_{crit}$  and the p-value is higher than 0.05. This proves that the measurements do not differ from each other in accuracy. Statistics between NILU and UiB specified t lower than  $t_{crit}$ , but the p-value does not exceed 0.05, which makes the research differ in terms of accuracy.

#### SiO<sub>2</sub> NM-200 (JRC)

**Precision (F-Snedecor test):** The compared measurements between NILU and CEA or UiB differ statistically significantly of precision because determined F statistics are higher than  $F_{crit}$  in mentioned cases ( $F > F_{crit}$ ). Due to the value of F being lower than the  $F_{crit}$  in the case of the CEA-UiB comparison, it can be stated that the obtained values of standard deviations do not differ statistically significantly between laboratories.

**Accuracy (t Student test):** A comparison of the NILU measurements and those of the two other partners (CEA and UiB) shows a t-value above the critical value ( $t > t_{crit}$ ) and a p-value is lower than 0.05, indicating a difference in measurements in terms of accuracy. Between the CEA and UiB laboratories, it can be concluded that there is no difference in the accuracy of the tests, as explained by t lower than the  $t_{crit}$  and a p-value above 0.05.

### NM-300K (JRC)

**Precision (F-Snedecor test):** There was no difference in the precision of the tests performed given the comparisons between all laboratories, as confirmed by the F value below the critical value ( $F < F_{crit}$ ).

**Accuracy (t Student test):** Based on the t-value not exceeding the critical t and a p-value above 0.05, it can be concluded that there are no differences between the accuracy of the measurements, considering all partners (NILU-CEA, NILU-UiB, CEA-UiB).

**Table 36. Critical values of the F distribution and t distribution for different degrees of freedom** (significance level = 5%)

Degrees of freedom	F distribution	t distribution
2	19.00	4.3029
3	9.28	3.1824
4	6.39	2.7764
5	5.05	2.5706
6	4.28	2.4469
7	3.79	2.3646
8	3.44	2.3060

The F-Snedecor test ( $F_{crit} = 6.39$ ) and pairwise t Student's test ( $t_{crit} = 2.7764$ ) were performed to determine the precision and accuracy of the measurements. The results are presented in Table 37.

**Table 37. Comparison of the statistical parameters from measurements from different labs.**

		BIOIMPEDANCE		
		NILU-CEA	NILU-UIB	CEA-UIB
NM-110	F statistic			
	Test statistic			
	p value			
NM-200	F statistic			
	Test statistic			
	p value			
NM-300K	F statistic			
	Test statistic			
	p value			

The Colour red corresponds to the results of F and t values higher than the critical F and t statistics and  $p < 0.05$ .

The Colour green corresponds to the results of F and t values lower than the critical F and t statistics and  $p > 0.05$ .

### 5.3 SOPs

The SOPs for the methods that were also used in Task 5.1, can be found in the Deliverable 5.1. The SOPs that were developed in Task 5.2 and used in the interlaboratory method comparison, can be found in Annex. 1

## 6. Final conclusions

- The number of papers obtained from the literature review that satisfied the GuideNano guidelines and a Q score  $\geq 0.8Q$  was too low to provide a solid basis for the identification of the most reliable, reproducible, and promising HTS and HCA methods for nanotoxicity testing. It was therefore decided to compare the methods available at the Task 5.2 partners' laboratories. The methods were grouped according to the biological endpoints they address and then compared for reliability, taking into account possible ENM interferences.
- Colorimetric assays, such as AB and WST-1, are more prone to ENM interferences. Washing steps after exposure and proper controls to identify possible interferences with the ENMs, need to be included. The coupling of colorimetric tests with methods that do not employ colorimetry or fluorescence is recommended to ensure that the results obtained are correct.
- For the HCA methods used in T5.2, ENM interferences were noted in some cases. A potential mitigation measure could be the use of a different combination of antibodies that work at a different wavelengths.

- The CA is compatible with the genotoxicity testing of ENMs, but proper interference testing is needed for each ENM. A cut-off for cytotoxic response and titration of concentrations of the ENM to be tested is needed. Positive controls, such as H<sub>2</sub>O<sub>2</sub>, are also necessary. The throughput of CA can be easily increased.
- For the micronucleus assay in the absence and in the presence of cytochalasin B, good data reproducibility was obtained between ANSES and SU. However, some differences in sensitivity have been highlighted between the 2 labs. Issues with interferences should not be neglected, however the way of identifying them needs to be improved.
- With regards to accuracy, differences were noted for impedance measurements only between NILU and UiB for ZnO NM-110 and NILU and UiB for SiO<sub>2</sub> NM-200.
- With regards to precision, no differences could be noted between the results obtained by the laboratories that did impedance-based testing (UiB, NILU, CEA).
- Bioimpedance has emerged from the interlaboratory comparison of methods as a promising HTS method for proliferation and viability screening. It has the advantage of being label-free and thus, less prone to ENM interference. It monitors cells in real-time, making it easy to identify timepoints and concentrations of interest. Other significant advantages are cost-, time-, and personnel-efficiency and being less pollutant for the environment.
- A general recommendation is to use at least two different methods that are based on different principles for each biological endpoint tested, in order to ensure that the results are reliable.



## 7. References

- Aimonen, K., K. Huuonen, Savukoski, S., H. Lindberg, A. Schoonenberg, K. Valimaki, S. Libertini, H. Wolff, J. Catalan and H. Norppa (2019). "In situ detection of DNA double strand breaks by immunofluorescent gamma-H2AX staining in mice exposed to multiwalled carbon nanotubes." *Toxicology Letters* 314: S122-S122.
- Almutary, A., Sanderson, B.J. The MTT and Crystal Violet Assays: Potential Confounders in Nanoparticle Toxicity Testing. (2016) *Int J Toxicol.* 35(4):454–62. Epub 2016/05/22. 10.1177/1091581816648906.
- Armstead, A. L., C. B. Arena and B. Li (2014). "Exploring the potential role of tungsten carbide cobalt (WC-Co) nanoparticle internalization in observed toxicity toward lung epithelial cells in vitro." *Toxicol Appl Pharmacol* 278(1): 1-8.
- Armstead, A. L. and B. Li (2016). "Nanotoxicity: emerging concerns regarding nanomaterial safety and occupational hard metal (WC-Co) nanoparticle exposure." *Int J Nanomedicine* 11: 6421-6433.
- Azqueta, A., Stopper, H., Zegura, B., Dusinska, M., and Møller, P. (2022). Do cytotoxicity and cell death cause false positive results in the in vitro comet assay? *Mutation Research/Genetic Toxicology and Environmental Mutagenesis*, 503520. doi: 10.1016/J.MRGENTOX.2022.503520
- Azqueta, A., Gutzkow, K. B., Priestley, C. C., Meier, S., Walker, J. S., Brunborg, G., & Collins, A. R. (2013). A comparative performance test of standard, medium- and high-throughput comet assays. *Toxicol In Vitro*, 27(2), 768-773. doi:10.1016/j.tiv.2012.12.006
- Bastian, S., W. Busch, D. Kühnel, A. Springer, T. Meissner, R. Holke, S. Scholz, M. Iwe, W. Pompe, M. Gelinsky, A. Potthoff, V. Richter, C. Ikonomidou and K. Schirmer (2009). "Toxicity of tungsten carbide and cobalt-doped tungsten carbide nanoparticles in mammalian cells in vitro." *Environ Health Perspect* 117(4): 530-536.
- Bonner, W.M., Redon, C.E., Dickey, J.S., Nakamura, A.J., Sedelnikova, O.A., Solier, S., Pommier, Y. GammaH2AX and cancer. *Nat Rev Cancer* 2008, 8:957-967.
- Cerioti, L., et al. Assessment of cytotoxicity by impedance spectroscopy. *Biosens Bioelectron* (2007)
- Cheung, K.C., Di Berardino, M., Schade-Kampmann, G., Hebeisen, M., Pierzchalski, A., Bocsi, J., Mittag, A. and Tárnok, A. (2010), Microfluidic impedance-based flow cytometry. *Cytometry*, 77A: 648-666. <https://doi.org/10.1002/cyto.a.20910>
- Chevion, S., et al. The use of cyclic voltammetry for the evaluation of antioxidant capacity. *Free Radic Biol Med* (2000) 28(6): 860-70.
- Chevion, S., et al., Evaluation of Plasma Low Molecular Weight Antioxidant Capacity by Cyclic Voltammetry. *Free Radical Biology and Medicine* (1997) 22(3): 411-421.
- Chevion, S., et al., Antioxidant Capacity of Edible Plants: Extraction Protocol and Direct Evaluation by Cyclic Voltammetry. *Journal of Medicinal Food* (1999) 2(1): 1-10.
- Cimpan, M. R., et al. An impedance-based high-throughput method for evaluating the cytotoxicity of nanoparticles. *J. Phys.: Conf. Ser.* (2013) 429 012026. DOI 10.1088/1742-6596/429/1/012026.
- Collins, A. R., et al. High throughput toxicity screening and intracellular detection of nanomaterials. *Wiley Interdiscip. Rev. Nanomedicine Nanobiotechnology* (2016) 9, e1413.

Collins A, Møller P, Gajski G, Vodenková S, Abdulwahed A, Anderson D, Bankoglu EE, Bonassi S, Boutet-Robinet E, Brunborg G, Chao C, Cooke MS, Costa C, Costa S, Dhawan A, de Lapuente- J, Bo' CD, Dubus J, Dusinska M, Duthie SJ, Yamani NE, Engelward B, Gaivão I, Giovannelli L, Godschalk R, Guilherme S, Gutzkow KB, Habas K, Hernández A, Herrero O, Isidori M, Jha AN, Knasmüller S, Kooter IM, Koppen G, Kruszewski M, Ladeira C, Laffon B, Larramendy M, Hégarat LL, Lewies A, Lewinska A, Liwszyc GE, de Cerain AL, Manjanatha M, Marcos R, Milić M, de Andrade VM, Moretti M, Muruzabal D, Novak M, Oliveira R, Olsen AK, Owiti N, Pacheco M, Pandey AK, Pfuher S, Pourrut B, Reisinger K, Rojas E, Rundén-Pran E, Sanz-Serrano J, Shaposhnikov S, Sipinen V, Smeets K, Stopper H, Teixeira JP, Valdiglesias V, Valverde M, van Acker F, van Schooten FJ, Vasquez M, Wentzel JF, Wnuk M, Wouters A, Žegura B, Zikmund T, Langie SAS, Azqueta A. (2023). Measuring DNA modifications with the comet assay: a compendium of protocols. *Nat Protoc.* 18(3):929-989. doi: 10.1038/s41596-022-00754-y.

Condello, M., B. De Berardis, M. G. Ammendolia, F. Barone, G. Condello, P. Degan and S. Meschini (2016). "ZnO nanoparticle tracking from uptake to genotoxic damage in human colon carcinoma cells." *Toxicol In Vitro* 35: 169-179.

Cummings, B. S. and R. G. Schnellmann (2021). "Measurement of Cell Death in Mammalian Cells." *Curr Protoc* 1(8): e210.

Cveticanin, J., G. Joksic, A. Leskovac, S. Petrovic, A. V. Sobot and O. Neskovic (2010). "Using carbon nanotubes to induce micronuclei and double strand breaks of the DNA in human cells." *Nanotechnology* 21(1): 015102.

Davoren, M., Herzog, E., Casey, A., Cottineau, B., Chambers, G., Byrne, H. J., & Lyng, F. M. (2007). In vitro toxicity evaluation of single walled carbon nanotubes on human A549 lung cells. *Toxicol In Vitro*, 21(3), 438-448. doi:10.1016/j.tiv.2006.10.007

DeLoid, G.M., et al., Preparation, characterization, and in vitro dosimetry of dispersed, engineered nanomaterials. *Nat Protoc* (2017). 12(2): 355-371.

Di Bucchianico S, Cappellini F, Le Bihanic F, Zhang Y, Dreij K, Karlsson HL. Genotoxicity of TiO<sub>2</sub> nanoparticles assessed by mini-gel comet assay and micronucleus scoring with flow cytometry. (2017) *Mutagenesis*. 32(1):127-137. doi: 10.1093/mutage/gew030.

Drasler, B.; et al. In vitro approaches to assess the hazard of nanomaterials. *NanoImpact* (2017) 8: 99-116. <https://doi.org/10.1016/j.impact.2017.08.002>.

Dušinská M, Collins A. (1996) Detection of Oxidised Purines and UV-induced Photoproducts in DNA of Single Cells, by Inclusion of Lesion-specific Enzymes in the Comet Assay. *Alternatives to Laboratory Animals*. 24(3):405-411. doi:10.1177/026119299602400315

Dusinska, M., Boland, S., Saunders, M., Juillerat-Jeanneret, L., Tran, L., Pojana, G., . . . Worth, A. (2015). Towards an alternative testing strategy for nanomaterials used in nanomedicine: lessons from NanoTEST. *Nanotoxicology, 9 Suppl 1*, 118-132. doi:10.3109/17435390.2014.991431

Eidet, J. R., L. Pasovic, R. Maria, C. J. Jackson and T. P. Utheim (2014). "Objective assessment of changes in nuclear morphology and cell distribution following induction of apoptosis." *Diagn Pathol* 9: 92.

Elgrishi, N., et al., A Practical Beginner's Guide to Cyclic Voltammetry. *Journal of Chemical Education* (2018) 95(2): 197-206.



El Yamani, N., Mariussen, E., Gromelski, M., Wyrzykowska, E., Grabarek, D., Puzyn, T., . . . Rundén-Pran, E. (2022). Hazard identification of nanomaterials: In silico unraveling of descriptors for cytotoxicity and genotoxicity. *Nano Today*, 46, 101581. doi:<https://doi.org/10.1016/j.nantod.2022.101581>

El Yamani, N., Rundén-Pran, E., Collins, A. R., Longhin, E. M., Elje, E., Hoet, P., . . . Dusinska, M. (2022). The miniaturized enzyme-modified comet assay for genotoxicity testing of nanomaterials. *Frontiers in Toxicology*, 4. doi:10.3389/ftox.2022.986318

Eskandani, M., H. Hamishehkar and J. Ezzati Nazhad Dolatabadi (2013). "Cyto/Genotoxicity study of polyoxyethylene (20) sorbitan monolaurate (tween 20)." *DNA Cell Biol* 32(9): 498-503.

Fadeel., B., et al. Advanced tools for the safety assessment of nanomaterials. *Nat Nanotechnol.* (2018) 13(7): 537-543. doi: 10.1038/s41565-018-0185-0.

Fahmy, H. M., N. M. Ebrahim and M. H. Gaber (2020). "In-vitro evaluation of copper/copper oxide nanoparticles cytotoxicity and genotoxicity in normal and cancer lung cell lines." *J Trace Elem Med Biol* 60: 126481.

Fernández-Cruz, L., Hernández-Moreno, L. D., Catalán, J., Cross, R. K., Stockmann-Juvala, H., Cabellos, J., Lopes, V. R., Matzke, M., Ferraz, N., Izquierdo, J. J., Navas, J. M., Park, M., Svendseng, C., Janer, G. (2018) Quality evaluation of human and environmental toxicity studies performed with nanomaterials – the GUIDEnano approach M. e: *Environ. Sci.: Nano* 5, 38. doi:<https://doi.org/10.1039/C7EN00716G>

Fernández-Bertólez, N., Brandão, F., Costa, C., Pásaro, E., Teixeira, J. P., Laffon, B., & Valdíglesias, V. (2021). Suitability of the In Vitro Cytokinesis-Block Micronucleus Test for Genotoxicity Assessment of TiO<sub>2</sub> Nanoparticles on SH-SY5Y Cells. *International journal of molecular sciences*, 22(16), 8558. doi:10.3390/ijms22168558

Ghasemi, M., Turnbull, T., Sebastian, S., and Kempson, I. (2021). The mtt assay: Utility, limitations, pitfalls, and interpretation in bulk and single-cell analysis. *International Journal of Molecular Sciences* 22. doi: 10.3390/IJMS222312827/S1.

Guadagnini, R., Halamoda Kenzaoui, B., Walker, L., Pojana, G., Magdolenova, Z., Bilanicova, D., Saunders, M., Juillerat-Jeanneret, L., Marcomini, A., Huk, A., et al. (2015). Toxicity screenings of nanomaterials: challenges due to interference with assay processes and components of classic in vitro tests. *Nanotoxicology*, 9 Suppl 1:13-24.

Gutzkow, K. B., Langleite, T. M., Meier, S., Graupner, A., Collins, A. R., & Brunborg, G. (2013). High-throughput comet assay using 96 minigels. *Mutagenesis*, 28(3), 333-340. doi:10.1093/mutage/get012

Hamid, R., Rotshteyn, Y., Rabadi, L., Parikh, R., and Bullock, P. (2004). Comparison of alamar blue and MTT assays for high through-put screening. *Toxicology in Vitro* 18, 703–710. doi: 10.1016/J.TIV.2004.03.012.

Hansjosten, I., J. Rapp, L. Reiner, R. Vatter, S. Fritsch-Decker, R. Peravali, T. Palosaari, E. Joossens, K. Gerloff, P. Macko, M. Whelan, D. Gilliland, I. Ojea-Jimenez, M. P. Monopoli, L. Rocks, D. Garry, K. Dawson, P. J. F. Röttgermann, A. Murschhauser, J. O. Rädler, S. V. Y. Tang, P. Gooden, M. A. Bellinga-Desaunay, A. O. Khan, S. Briffa, E. Guggenheim, A. Papadiamantis, I. Lynch, E. Valsami-Jones, S. Diabaté and C. Weiss (2018). "Microscopy-based high-throughput assays enable multi-parametric analysis to assess adverse effects of nanomaterials in various cell lines." *Arch Toxicol* 92(2): 633-649.

He, H., Z. Zou, B. Wang, G. Xu, C. Chen, X. Qin, C. Yu and J. Zhang (2020). "Copper Oxide Nanoparticles Induce Oxidative DNA Damage and Cell Death via Copper Ion-Mediated P38 MAPK Activation in Vascular Endothelial Cells." *Int J Nanomedicine* 15: 3291-3302.

Hondroulis, E., et al. Whole cell based electrical impedance sensing approach for a rapid nanotoxicity assay. *Nanotechnology* (2010) 21: 315103

Islaih, M., Halstead, B. W., Kadura, I. A., Li, B., Reid-Hubbard, J. L., Flick, L., . . . Watson, D. E. (2005). Relationships between genomic, cell cycle, and mutagenic responses of TK6 cells exposed to DNA damaging chemicals. *Mutat Res*, 578(1-2), 100-116. doi:10.1016/j.mrfmmm.2005.04.012

Jensen, A. K. NANoREG D2.08 SOP 02 for measurement of hydrodynamic Size-Distribution and Dispersion Stability by DLS, (2017) <https://www.rivm.nl/sites/default/files/2018-11/NANoREG%20D2.08%20SOP%2002%20For%20measurement%20of%20hydrodynamic%20Size-Distribution%20and%20Dispersion%20Stability%20by%20DLS.pdf>.

Kaiser, J. P., Wessling, F., Fischer, K., Roesslein, M., Wick, P., & Krug, H. F. (2011). A novel comprehensive evaluation platform to assess nanoparticle toxicity <i>in vitro</i>. *Journal of Physics: Conference Series*, 304(1). doi:<http://dx.doi.org/10.1088/1742-6596/304/1/012053>

Kalaiarasi, A., R. Sankar, C. Anusha, K. Saravanan, K. Aarthy, S. Karthic, T. L. Mathuram and V. Ravikumar (2018). "Copper oxide nanoparticles induce anticancer activity in A549 lung cancer cells by inhibition of histone deacetylase." *Biotechnol Lett* 40(2): 249-256.

Kansara, K., P. Patel, D. Shah, R. K. Shukla, S. Singh, A. Kumar and A. Dhawan (2015). "TiO<sub>2</sub> nanoparticles induce DNA double strand breaks and cell cycle arrest in human alveolar cells." *Environ Mol Mutagen* 56(2): 204-217.

Karlsson HL, Di Bucchianico S, Collins AR, Dusinska M. Can the comet assay be used reliably to detect nanoparticle-induced genotoxicity? (2015) *Environ Mol Mutagen*. Mar;56(2):82-96. doi: 10.1002/em.21933. Epub 2014 Dec 8. PMID: 25488706.

Kroll, A., et al. (2012). Interference of engineered nanoparticles with in vitro toxicity assays. *Arch Toxicol* 86: 1123-1136.

Kühnel, D., K. Scheffler, P. Wellner, T. Meißner, A. Potthoff, W. Busch, A. Springer and K. Schirmer (2012). "Comparative evaluation of particle properties, formation of reactive oxygen species and genotoxic potential of tungsten carbide based nanoparticles in vitro." *J Hazard Mater* 227-228: 418-426.

Landry, M., D. Nelson, E. Choi, A. DuRoss and C. Sun (2022). Development of a G2/M arrest high-throughput screening method identifies potent radiosensitizers. *Transl Oncol* 16: 101336.

Leng, Y., *Materials Characterization: Introduction to Microscopic and Spectroscopic Methods*. 2013: Wiley.

Liu, J., Y. Zhao, W. Ge, P. Zhang, X. Liu, W. Zhang, Y. Hao, S. Yu, L. Li, M. Chu, L. Min, H. Zhang and W. Shen (2017). "Oocyte exposure to ZnO nanoparticles inhibits early embryonic development through the  $\gamma$ -H2AX and NF- $\kappa$ B signaling pathways." *Oncotarget* 8(26): 42673-42692.

Longhin, E. M., El Yamani, N., Rundén-Pran, E., & Dusinska, M. (2022). The alamar blue assay in the context of safety testing of nanomaterials. *Front Toxicol*, 4, 981701. doi:10.3389/ftox.2022.981701

Magdolenova, Z., Lorenzo, Y., Collins, A., & Dusinska, M. (2012). Can standard genotoxicity tests be applied to nanoparticles? *J Toxicol Environ Health A*, 75(13-15), 800-806. doi:10.1080/15287394.2012.690326.

Mah, L.-J., A. El-Osta and T. C. Karagiannis (2010). "γH2AX as a molecular marker of aging and disease." *Epigenetics* 5(2): 129-136.

Moche, H., D. Chevalier, N. Barois, E. Lorge, N. Claude and F. Nessler (2014). "Tungsten carbide-cobalt as a nanoparticulate reference positive control in in vitro genotoxicity assays." *Toxicol Sci* 137(1): 125-134.

Moche, H., D. Chevalier, H. Vezin, N. Claude, E. Lorge and F. Nessler (2015). "Genotoxicity of tungsten carbide-cobalt (WC-Co) nanoparticles in vitro: mechanisms-of-action studies." *Mutat Res Genet Toxicol Environ Mutagen* 779: 15-22.

Morris, S. M., O. E. Domon, L. J. McGarrity, R. L. Kodell, D. A. Casciano and W. F. Morgan (1991). "Flow cytometric evaluation of cell-cycle progression in ethyl methanesulfonate and methyl methanesulfonate-exposed P3 Cells: Relationship to the induction of sister-chromatid exchanges and cellular toxicity." *Environmental and Molecular Mutagenesis* 18(2): 139-149.

Mukherjee, B., C. Kessinger, J. Kobayashi, B. P. Chen, D. J. Chen, A. Chatterjee and S. Burma (2006). DNA-PK phosphorylates histone H2AX during apoptotic DNA fragmentation in mammalian cells. *DNA Repair (Amst)* 5(5): 575-590

OCDE. (2016a). *Test No. 474: Mammalian Erythrocyte Micronucleus Test*.

OCDE. (2016b). *Test No. 487: In Vitro Mammalian Cell Micronucleus Test*.

OECD (2018). Guidance Document on Good In Vitro Method Practices (GIVIMP). *OECD Series on Testing and Assessment* 286. doi: 10.1787/9789264304796-en.

O'Driscoll, M., Jeggo, P.A. The role of double-strand break repair - insights from human genetics. *Nat Rev Genet* 2006, 7:45-54.

Ostermann, M., et al. Label-free impedance flow cytometry for nanotoxicity screening. *Sci Rep* (2020) 10, 142. <https://doi.org/10.1038/s41598-019-56705-3>.

Paget, V., H. Moche, T. Kortulewski, R. Grall, L. Irbah, F. Nessler and S. Chevillard (2015). "Human cell line-dependent WC-Co nanoparticle cytotoxicity and genotoxicity: a key role of ROS production." *Toxicol Sci* 143(2): 385-397.

Paszowski, J.J. and A. Dardik. (2003). Arterial Wall Shear Stress: Observations from the Bench to the Bedside. *Vascular and Endovascular Surgery*, 37(1): p. 47-57

Pliquett, U. Bioimpedance: A Review for Food Processing. *Food Engineering Reviews* (2010) 2: 74-94.

Prodan, E., et al. The Dielectric Response of Spherical Live Cells in Suspension: An Analytic Solution. *Biophysical Journal* (2008) 95: 4174-4182.

Psotová, J., et al., Determination of total antioxidant capacity in plasma by cyclic voltammetry. Two case reports. *Biomedical Papers* (2001) 145(2): 81-83.

Rahimi Kalateh Shah Mohammad, G., M. Homayouni-Tabrizi, A. Ghahremanloo and N. Yazdanbakhsh (2021). "Cytotoxic effect, apoptotic activity, hematological and histological alterations induced by green

synthesized ZnO nanoparticles applying *Hyssopus officinalis* leaves." *Inorganic and Nano-Metal Chemistry* 51(11): 1560-1569.

Riss, T. L., Moravec, R. A., Niles, A. L., Duellman, S., Benink, H. A., Worzella, T. J., et al. (2016). Cell Viability Assays. *Assay Guidance Manual*. Available at: <https://www.ncbi.nlm.nih.gov/books/NBK144065/> [Accessed June 25, 2022].

Riss, T., Niles, A., Moravec, R., Karassina, N., and Vidugiriene, J. (2019). Cytotoxicity Assays: In Vitro Methods to Measure Dead Cells. *Assay Guidance Manual*. Available at: <https://www.ncbi.nlm.nih.gov/books/NBK540958/> [Accessed May 10, 2022].

Ruzycka, M., et al. Microfluidics for studying metastatic patterns of lung cancer. *J Nanobiotechnol* (2019) 17: 71. <https://doi.org/10.1186/s12951-019-0492-0>.

Savvina Chortarea, F. Z., Hana Barosova, Dedy Septiadi, Martin J.D. Clift, Alke Petri-Fink, and Barbara Rothen-Rutishauser (2019). "Profibrotic Activity of Multiwalled Carbon Nanotubes Upon Prolonged Exposures in Different Human Lung Cell Types." *Applied In Vitro Toxicology* 5(1): 47-61.

Scarcello, E., Lambremont, A., Vanbever, R., Jacques, P.J., Lison, D. Mind your assays: Misleading cytotoxicity with the WST-1 assay in the presence of manganese. *PLoS One*. 2020 Apr 16;15(4):e0231634. doi: 10.1371/journal.pone.0231634. PMID: 32298350; PMCID: PMC7161962.

Seiffert, J. M., et al. Dynamic monitoring of metal oxide nanoparticle toxicity by label free impedance sensing. *Chem Res Toxicol* (2012) 25(1): 140–152.

Sorrell, J.M., Baber, M.A., and Caplan, A.I. (2007). A Self-Assembled Fibroblast-Endothelial Cell Co-Culture System That Supports in vitro Vasculogenesis by both Human Umbilical Vein Endothelial Cells and Human Dermal Microvascular Endothelial Cells. *Cells Tissues Organs*. 186(3): p. 157-168.

Stearns, R. C., J. D. Paulauskis and J. J. Godleski (2001). "Endocytosis of ultrafine particles by A549 cells." *Am J Respir Cell Mol Biol* 24(2): 108-115.

Strauch, B. M., R. K. Niemand, N. L. Winkelbeiner and A. Hartwig (2017). "Comparison between micro- and nanosized copper oxide and water soluble copper chloride: interrelationship between intracellular copper concentrations, oxidative stress and DNA damage response in human lung cells." *Part Fibre Toxicol* 14(1): 28.

Sun, T., Y. Yan, Y. Zhao, F. Guo and C. Jiang (2012). "Copper oxide nanoparticles induce autophagic cell death in A549 cells." *PLoS One* 7(8): e43442.

Thongkam, W., K. Gerloff, D. van Berlo, C. Albrecht and R. P. F. Schins (2016). "Oxidant generation, DNA damage and cytotoxicity by a panel of engineered nanomaterials in three different human epithelial cell lines." *Mutagenesis* 32(1): 105-115.

Toyooka, T., T. Amano and Y. Ibuki (2012). "Titanium dioxide particles phosphorylate histone H2AX independent of ROS production." *Mutat Res* 742(1-2): 84-91

Vandebriel, R. J. and W. H. De Jong (2012). "A review of mammalian toxicity of ZnO nanoparticles." *Nanotechnol Sci Appl*. 2012 Aug 15;5:61-71. doi: 10.2147/NSA.S23932.


Vinkovic Vrcek, I., et al. Does surface coating of metallic nanoparticles modulate their interference with *in vitro* assays? *RSC Adv*. (2015) 5: 70787–70807.

Zhao, X., F. Takabayashi and Y. Ibuki (2016). "Coexposure to silver nanoparticles and ultraviolet A synergistically enhances the phosphorylation of histone H2AX." *Journal of Photochemistry and Photobiology B: Biology* 162: 213-222.

Zhao, X., G. Yang, T. Toyooka and Y. Ibuki (2015). "New mechanism of  $\gamma$ -H2AX generation: Surfactant-induced actin disruption causes deoxyribonuclease I translocation to the nucleus and forms DNA double-strand breaks." *Mutat Res Genet Toxicol Environ Mutagen* 794: 1-7.

Zhu, L., D. W. Chang, L. Dai and Y. Hong (2007). "DNA damage induced by multiwalled carbon nanotubes in mouse embryonic stem cells." *Nano Lett* 7(12): 3592-3597.

## ANNEX 1

 anses Agence nationale de sécurité sanitaire alimentaire, vétérinaire, rurale Connaître, évaluer, protéger Laboratoire de Fougères	<b>Riskgone SOP for Task 5.2: High Content Analysis of active caspase-3 and <math>\gamma</math>H2AX in A549 cells</b>	REFERENCE :
		VERSION : V1
		DATE D'APPLICATION : P_APPLICATION_DATE

Rédacteur (s) : <b>J. VARET, S. HUET</b>	Approbateur (s) : <b>K. HOGVEEN, V. FESSARD</b>
---	--

Laboratoire ANSES de Fougères, Toxicology of Contaminants Unit, France.

**Cell culture:****A549 (adherent cell) – from ATCC**

A549 cells are grown in DMEM (low glucose with 4 mM L-glutamine) (Sigma D6046), 9 % Fetal Bovine Serum (FBS) (26140-079, ThermoFisher), 100 U/ml penicillin/100  $\mu$ g/ml streptomycin solution (15140-122, ThermoFisher).

Cells were grown in 75 cm<sup>2</sup> flasks and sub-cultured twice a week. Flasks were seeded at a density of 3000 cells per mL, in a total of 25 mL of complete cell culture medium. Cells were maintained at 37°C and 5 % CO<sub>2</sub>.

**Day 1: Cell seeding**

Cells are seeded in black 96-well plates (clear flat bottom plates, reference 655090, GREINER) 24 h before treatment.

Seed 25 000 cells per cm<sup>2</sup> (8000 cell per well), with 150  $\mu$ L of complete cell culture medium per well.

To study :

- all NMs at the three concentrations chosen (which concentrations?) and the positive and negative controls (in triplicates)
- and the respective tests for interference (1 well)

Prepare 4 96-well plates, prepare 50 mL of cell culture medium containing 4 million cells.

Cells are incubated for 24h at 37°C and 5% CO<sub>2</sub>.

**Day 2: Cell treatment**

Negative control and the various treatments are prepared in complete cell culture medium immediately prior to treatment.

For a description of the preparation of the treatments, please see annex.

The medium is removed and replaced by 150  $\mu$ L/well of cell culture medium without or with the various treatments.

Negative control: complete cell culture medium

Positive controls:

- Methylmethane sulfonate (Sigma, 129925): 0.2 mM (positive control for  $\gamma$ H2AX)
- Staurosporine (Sigma, S5921): 0.8 $\mu$ M (positive control for active caspase-3)

Nanomaterials:

- TiO<sub>2</sub> JRC NM 1005a
- Zinc oxide (Sigma) (20 wt/v % in water)



- Zinc oxide NM111 (JRCNM01101a)
- WC/Co (NanoAmor, ref 5561HW)
- Aquacyl AQ0303 (NC7000) (Nanocyl, 3 % w/v NC7000 in Nanocyl dispersant)
- Nanocyl dispersant
- CuO (Palsmached)
- NM-300K (Silver <20 nm) (Fraunhofer, 10.16 % w/w in NM-300kDIS)
- NM-300KDIS (Fraunhofer)

All NMs (and corresponding diluents) were tested at 10, 50 and 100 µg/mL.

Cells are treated for 24h at 37°C and 5% CO<sub>2</sub>.

### Day 3: Cell staining

For cell staining, the antibodies used are described in the following table:

#### PRIMARY ANTIBODIES

Anti-	clone	Host	Supplier	ref	Conc	Dilution
Active Caspase 3	Polyclonal	Rabbit	Abcam	ab13847	1 mg/mL	1:1500
γH2AX	Monoclonal	Mouse	Abcam	ab26350	1 mg/mL	1:2000

#### SECONDARY ANTIBODIES

Anti-	Conjugation	Host	Supplier	reference	Conc	Dilution
Mouse (IgG)	480 nm	goat	Abcam	Ab150113	2mg/mL	1:2000
Rabbit (IgG)	647 nm		Abcam	ab150079	2mg/mL	1:2000

#### Fixation:

Remove medium

Rinse cells once with PBS 1 X (100µL per well)

Fixation with formaldehyde 4% in PBS, 50µL per well

**Incubate 10 minutes at room temperature (RT)**

Rinse 3 X with PBS 1X (100µL per well)

**Once fixed, sealed plates can be stored at 4°C with 100 µl PBS per well**

#### Permeabilisation:

After having removed the PBS, add a solution of Triton X100 0.2% in PBS, 100 µL per well

**Incubate 10 minutes at RT**

#### Immunofluorescence Staining:

- Rinse cells 2X with PBS Tween 0.05% (100µL per well)

- Block plates with PBS Tween 0.05%, BSA 1% (100 $\mu$ L per well)
- **Incubate 30 minutes at RT**
- Remove the blocking solution
- Add 50 $\mu$ L per well of a solution of :
  - o both primary antibodies prepared at their respective dilution in PBS Tween 0.05%, BSA 1%, for test wells
  - o only PBS Tween 0.05%, BSA 1% for control wells without primary antibody
  - o only one primary antibody, at its respective dilution in PBS Tween 0.05%, BSA 1%, for tests for interference wells.
- **Incubate 2 hours at RT**
- Rinse cells 3X in PBS Tween 0.05%
- Following the plate scheme described previously, add 50  $\mu$ L per well of a solution of :
  - o both secondary antibodies prepared at their respective dilution in PBS Tween 0.05%, BSA 1%, for test wells
  - o only PBS Tween 0.05%, BSA 1% for control wells without secondary antibody
  - o only one secondary antibody, at its respective dilution in PBS Tween 0.05%, BSA 1%, for tests for interference wells.
- **Incubate 1 hour at RT in the dark**
- Rinse 2X with PBS Tween 0.05%
- Add 50  $\mu$ L per well of a solution of DAPI 1 $\mu$ g/mL in PBS Tween 0.05%
- **Incubation 5 min at RT in the dark**
- Rinse 1 X with PBS
- Add 100  $\mu$ L PBS per well and store plates covered with film and foil at 4°C, until HCA analysis.

#### HCA analysis

Cellular imaging was performed with an Arrayscan VTi High Content Imaging platform. Ten fields per well were imaged with a 10X objective. Images were analyzed with the Target Activation BioApplication of the HCS Studio software. Briefly, individual cells were identified based on DAPI staining and regions of interest for fluorescence quantification were selected in each channel based on the localization of the marker to be analyzed. When applicable, positive cells were defined as cells with fluorescence 2 standard deviations above the mean fluorescence of negative control cells.

**Annex:** Description of the preparation of the various treatments on Day 2.

Note:

- All described sonications were performed in ice with a Branson sonicator equipped with a 13 mm probe diameter, at 400 W with 10 % amplitude.
- The NANOGENOTOX protocol consists in pre-wetting nanomaterials in 0.5% absolute ethanol in a scintillation vial and to disperse the suspension at a final concentration of 2.5 mg/mL in 0.05% BSA in ultra-pure water and to sonicate for 16 min.

#### **Methylmethane sulfonate (MMS) 0.2 mM**

Prepare a solution at 10 mM = 1.1 mg/mL by weighing around 15 mg MMS and resuspend at 1.1 mg/mL in complete cell culture medium.

Prepare 5 mL of working solution of MMS at 0.2 mM by diluting 100  $\mu$ L of the 10 mM solution in 5 mL of cell culture medium.

#### **Staurosporine 0.8 $\mu$ M**

From a stock solution at 0.4 mM (in DMSO) (-20°C), dilute 10  $\mu$ L of stock solution in 5 mL cell culture medium.

#### **NM and their diluents:**

##### **TiO<sub>2</sub>**

Weight around 15 mg TiO<sub>2</sub> and prepare a stock suspension at 2.5 mg/mL in ultra pure water.

Sonication 5 min, according to Riskgone SOP.

Prepare working dilutions in cell culture medium.

##### **ZnO Sigma**

The stock suspension of ZnO was provided as a 20 % w/v suspension in water .

Vortex stock suspension and prepare a working suspension at 2.5 mg/mL in ultra pure water (using up to 50  $\mu$ L stock suspension).

Prepare working dilutions in cell culture medium.

##### **NM111**

Weight around 15 mg NM111 and prepare a stock suspension at 2.5 mg/mL, according to the Nanogenotox protocol (in 0.5% Ethanol and 0.05% BSA diluted in ultra pure water) (Sonication 16 min).

Prepare working dilutions in cell culture medium.

##### **MWCNT Nanocyl**

Stock suspension at 3 wt % NC7000 (3 g pour 100 ml)

Vortex and prepare a working suspension at 2.5 mg/mL by diluting 416.7  $\mu$ L of the stock suspension (3% w/v) in 4.6 mL of ultra pure water.

Prepare working dilutions in cell culture medium.

#### Nanocyl diluent

From the stock diluent, prepare a stock solution equivalent to 2.5 mg/mL by mixing 416.7  $\mu$ L of the stock suspension in 4.6 mL of ultra pure water.

Prepare working dilutions in cell culture medium.

#### CuO

Weigh around 15 mgCuO NM and prepare a stock suspension at 2.5 mg/mL in ultra pure water.

Sonication 5 min according to Riskgone SOP.

Prepare working dilutions in cell culture medium.

#### WC/Co

Weigh around 15 mg WC/Co and prepare a stock suspension at 2.5 mg/mL, according to Nanogenotox protocol.

Prepare working dilutions in cell culture medium.

#### NM300K

From the stock suspension, using around 100  $\mu$ L prepare a working suspension at 2.5 mg/mL, according to Nanogenotox protocol.

Prepare working dilutions in cell culture medium.

#### NM300KDIS

Similarly to NM300K, prepare a corresponding working solution of NM300KDIS, following the Nanogenotox protocol.

Prepare working dilutions in cell culture medium.

## Standard Operating procedure

### Impedance-based ENM toxicity testing on adherent cells (UiB)

#### Cell culture

Human lung carcinoma epithelial cells (A549) and human monoblastoid cells (U937) were purchased from ATTC (Manassas, USA). The proliferation and viability was tested using the xCELLigence RTCA SP instrument (Agilent, Santa Catalina, CA, USA) system. The cells were cultured in T75 flasks (Nunc, Roskilde, Denmark) in Duplecco's modified eagle medium (DMEM) supplemented with 10% FBS and 1% P/S Sigma-Aldrich in an incubator at 37°C and 5% CO<sub>2</sub>.

A549 cells were passaged at approximately 80% confluency by trypsinization, i.e., the flask was washed twice with phosphate buffered saline (PBS) before adding 2 mL of trypsin-verse EDTA (Sigma-Aldrich). The cells were incubated for 5 min before the cell suspension was mixed with 8 mL of completed culture medium, then transferred to a 15 mL tube, which was centrifuged at 250 g for 5 min. The supernatant was discarded and afterwards the cell pellet was resuspended in 10 mL CCM. Trypan blue 0.4% was used to assess the viability of the cells. Cells in passage 4-15 with viability higher than 90% were used for testing.

#### **Trypan blue exclusion test of cell viability**

A volume of 10 µL of trypan-blue 0.4% (ThermoFisher, Waltham, MA, USA) and 10 µL of cell suspension were placed in a 500 µL Eppendorf tube and thoroughly mixed. Out of the mixture, 10 µL were pipetted to both chambers of an Invitrogen Countess chamber (ThermoFisher, Waltham, MA, USA). The automatic cell counter was then used to count cells and assess cell viability.

#### **Nanomaterials and dispersion protocols**

An overview of the ENMs and the dispersion protocols is given in Table 4. A 130-Watt probe sonicator (VCX130, Vibra-Cell, 130W, Sonic & Materials, Newtown, USA) was used at 22% amplitude of the maximum amplitude, equipped with a 12.8 mm probe with a replaceable tip to prepare particle dispersions. The sonicator was calibrated to ensure that the desired energy was delivered to the systems. The power (P) was found to be 6.1919 J for the DeLoid-protocol (DeLoid 2017) and 8.41 J for the NANOGENOTOX-protocol (Jensen et al. 2011). By implementing the referenced critical delivered sonication energy (DSE<sub>cr</sub>) and Equation 1 the sonication time (t<sub>cr</sub>) needed to disperse the ENMs was calculated.

$$t_{cr} = \frac{DSE_{cr}}{P} V \quad (1)$$

t<sub>cr</sub> = critical sonication time (s)

DSE<sub>cr</sub> = Referenced delivered sonication energy (J/mL)

P = Sonicator power (J/s)

V = Volume of dispersion (mL)



- **DeLoid-protocol**

A mass of 15 mg of ENM powder was carefully weighed in a 20 mL scintillation vial by using a disposable plastic antistatic spatula. MilliQ water was added drop-by-drop to the glass scintillation vial while tilting and swirling the vial, so that a concentration of 5 mg/mL was reached. After swirling the vial containing ENM and milliQ water, the sonication started. Without touching the sides of the vial, the tip of the sonicator probe was placed inside the vial. The tip was submerged at 2/3 of the height of the vial carefully, not touching the bottom. The ENM was then sonicated according to the  $DSE_{cr}$ -values specified in the LIST-protocol. The amount of time calculated as necessary to sonicate the dispersion was 19 sec for CuO, 93,5 sec for TiO<sub>2</sub> (Sigma-Aldrich) and 156,2 sec for TiO<sub>2</sub> (JRC). To protect it against light, the dispersion was sealed and covered with aluminum foil.

- **NANOGENOTOX-protocol**

A mass of 15.36 mg of ENM powder was weighed in a 20 mL scintillation vial by using a disposable plastic antistatic spatula. The vial was tilted at a 45° angle and tapped gently on the side to gather the material. A volume of 30 µL EtOH (96%) was added drop-by-drop onto the raw material and mixed gently. A volume of 970 µL of 0.05% BSA water was added slowly to avoid foaming. Lastly, an additional 5 mL of 0.05% BSA water was added slowly along the walls of the vial to collect any powder that might have deposited on the walls. A stock concentration of 2.56 mg/mL was made. The vial was sealed with a cap and placed on ice for at least 5 min, while the sonicator was prepared. The sonicator probe was carefully submerged in the scintillation so that to avoid touching any of the sides. The ENM dispersion was sonicated according to the  $DSE_{cr}$ -values specified in the NANOGENOTOX-protocol. The time calculated to sonicate the WC-Co dispersion was 2 sec. Afterwards, the dispersion was sealed with a cap and covered with aluminum foil and placed on ice to rest.

- **Vortexing: Multi-Walled Carbon Nano Tubes (AQUACYL 3 wt. % NC7000) dispersion by vortexing**

The MWCNT (AQUACYL 3 wt. % NC7000) were provided by Nanocyl (Sambreville, Belgium). The MWCNT (AQUACYL 3 wt. % NC7000) dispersion was a pitch-black dense viscous solution, which was vortexed vigorously for 30 sec. An intermediate suspension was made by extracting a quantity of 1 mL of stock dispersion and diluting it at 1:6 ration in the proprietary dispersant (1 mL AQUACYL 3 wt.% dispersion + 5 mL Dispersant). Thus, a concentration of 5 mg/mL was obtained.

- **Vortexing: Zinc Oxide (ZnO)**

ZnO was provided by Sigma-Aldrich (Darmstadt, Germany) as a powder suspension. The density of the ZnO bottled in suspension was estimated at 240 mg/mL. A volume of 1 mL was removed from the bottle and the ZnO suspension was vortexed vigorously for 30 sec. before further dilution in cell culture medium and before cell exposure.

### **Preparation of ENM dispersions in cell culture medium**

The ENM to be tested was dispersed in a 15 mL tube cell culture medium at required concentrations by adding fresh vortexed ENM dispersions to complete the cell culture medium. The tube with the solution was then rotated in the tube rotator ISB3 (Bibby Scientific, Staffordshire, England) at 40 rpm for 2 minutes and mixed with a pipet. When multiple concentrations were prepared, a high concentration tube (100 µg/mL or 50 µg/cm<sup>2</sup>) was used for serial dilution. In each dilution series step, the solution was mixed by pipetting and vortexed for 5 seconds. Before exposure to cells, the solution was mixed by pipetting.

## **ENM characterization in exposure media**

### **Dynamic light scattering**

Dynamic light scattering (DLS) using a Zetasizer Nano ZSP (Malvern Instruments, Malvern, England) was employed to measure the hydrodynamic diameter (HDD) of the batch dispersions and of ENMs in complete cell culture medium. For the latter, the highest exposure concentration (100 µg/mL) was used. Three measurements of the HDD and polydispersity index (PDI) were performed for each sample at the beginning and end of exposure to ENM dispersions.

### **Zeta potential**

The Zeta potential (ZP) was measured for the ENMs dispersed in complete CCM (with 10% FBS and 1% P/S). In a prewetted folded capillary zeta cell (DTS1070, Malvern Instrument), 800 µL of the highest ENM concentration used in experiments (100 µg/mL which corresponds to 50 µg/cm<sup>2</sup>) was pipetted. The ZP was measured using a Zetasizer Nano ZSP at the temperature corresponding to that used during ENM exposure in the toxicity tests.

## **Impedance-based toxicity testing using the xCELLigence system**

For the interlaboratory comparison of methods assessing proliferation and viability, the following ENMs were used: ZnO from Sigma (ERM00000063), TiO<sub>2</sub> from JRC (ERM00000064), CuO (ERM00000088), Nano Tungsten (ERM00000089), MWCNTs (ERM00000325), Ag NM-300K (JRC), and ZnO NM-111 (JRC).

For interlaboratory reproducibility testing of impedance-based nanotoxicity testing, the following set of sENMs were used by UiB and NILU: Ag NM-300K (JRC- Fraunhofer), ZnO NM-110 (JRC) and NM-200 (JRC). As NILU or other partners in RiskGone, other than UiB, do not possess an xCELLigence system, the instrument was transported to NILU and training was provided by UiB to NILU colleagues. The results obtained by UiB and NILU were also compared with those obtained in the FP7 project NANoREG by CEA (Commissariat à l'Énergie Atomique) for the same set of ENMs.

The impedance-based measurements were performed using an xCELLigence RTCA SP instrument (Agilent, Santa Catalina, CA, USA) with 16-well E-plates for label-free, real-time monitoring of A549 cell proliferation, adherence and viability. This is achieved by measuring the difference in impedance at the gold-plated electrodes that cover 70-80% of the bottom of the wells onto which cells are seeded. The experiments using xCELLigence followed three main steps: preparation of the E-plate, seeding of cells and exposure of A549 cells to ENM dispersions.

The xCELLigence (RTCA) instrument measures the electrical impedance under static exposure conditions. For each timepoint, the software provides the measured impedance as a Cell Index (CI), which is a nondimensional quantity. In both the presence and absence of cells, the CI is a measurement of electrical impedance normalized by a frequency factor,  $Z_n$  (equation 2):

$$CI = \frac{Z_t - Z_0}{Z_n} \quad (2)$$

Where  $Z_t$  = Impedance at time t

$Z_0$  = Impedance at time 0 (background)

$Z_n$  = Frequency factor

Increase of cell proliferation and attachment are indicated by a rise in the CI, whereas detachment, loss of membrane integrity, and cell death are indicated by a reduction in the CI.

All the experiments were done in triplicates or duplicates and in three independent experimental repetitions. In these experiments, A549 cells were exposed to ENMs after an initial seeding and proliferation for 24 h in the E-plates. The CIs were normalized to the value measured right before the cells were exposed to the ENMs, i.e., at 24 h after seeding. The normalization is given as equation 3; the normalization was performed to correct for possible differences in cell numbers between the wells at the time of exposure.

$$NCI = \frac{CI_t - CI_{med}}{CI_{t=24}} \quad (3)$$

$CI_t$  = Cell Index at timepoint t.

$CI_{med}$  = Cell index of the referenced medium, without cells.

$CI_{t=24}$  = Cell index at timepoint 24-hours, last timepoint before exposure of cells to ENM

In order to evidence the interference that the ENMs might have with impedance-based readings, the CI of wells containing cell culture medium with the highest concentration of ENMs (i.e., 100  $\mu\text{g}/\text{mL}$ ) was also measured. The calculation of NCI gives real time information about whether there is a proliferation or decrease of viability of cells.

The fold-change vs control (FC) represents the ratio between the cells exposed to ENMs and control cells at the measured timepoints. The FC was calculated for the cells at 48 h after seeding, i.e., 24 h after exposure to ENMs. The FC is given in **equation 4** and the FC of control = 1. Consequently,  $FC > 1$  at a specific concentration of ENM solution indicates increase of proliferation/viability compared to the control and  $FC < 1$  indicates a decrease.

$$FC = \frac{CI_{t=24}}{CI_{control}} \quad (4)$$

$CI_{t=48}$  = Cell index of exposed cells at timepoint t = h.

$CI_{control}$  = Cell index of control group at timepoint t = 48 h.

For every experiment, the cells were seeded and left to attach to the electrode surface and proliferate for 24 h before exposure to ENMs. After 24h, the cells were exposed to five different concentrations of ENMs (2, 10, 20, 50, 100  $\mu\text{g}/\text{mL}$ ).

### **16-well E-plate preparation and treatment**

The 16-well E-plates were prepared by filling the sides around each well with sterile water to maintain humidity in the E-plate while inside the incubator. Then 100  $\mu\text{L}$  of fresh complete DMEM was pipetted



into each well and then kept at room temperature for 30 min, before placing them in the xCELLigence RTCA SP for a background measurement. The seeding of the cells happened immediately after the background measurement. A549 cells were added to each well resulting in a density of 25.000 cells/cm<sup>2</sup> (5.000 cells/well) for a total volume of 200 µL in each well. For the wells without cells, complete medium alone was added. The plate was then incubated at 37°C at 5% CO<sub>2</sub> for 30 min before insertion into the xCELLigence system located in an incubator with the same parameters. The CI was measured every 15 min for the next 24 h.

After 24 h, the E-plate was taken out of the xCELLigence system, 100 µL of cell culture medium were removed and replaced by the ENM dispersions in complete cell culture medium at different concentrations. In the wells not containing any cells and the control group, 100 µL of fresh complete medium were added. In the wells with cells, 100 µL of ENM dispersions at concentrations 1, 2, 5, 10, 25 and 50 µg/cm<sup>2</sup> (corresponding to 2, 10, 20, 50, and 100 µg/mL) were added. For ENM interference control, 100 µL of the highest concentration (100 µg/mL) were added in wells with medium only (without cells). Then the CI was measured every 15 min for an additional 24 h. Each measurement was performed in duplicate and repeated at least three times. The plate layout for the experiments is shown below.

#### Overview of the 16-well plate experimental showing the contents of the wells.

	1	2	3	4	5	6	7	8
A	M	M+100	C	2	10	20	50	100
B	M	M+100	C	2	10	20	50	100

<b>M: DMEM only (no cells)</b>	<b>C: Cells only (control)</b>
<b>M+100: DMEM with NM at 100 µg/mL (no cells)</b>	<b>X: Cells + NM at concentration X</b>



[www.riskgone.eu](http://www.riskgone.eu) | [riskgone@nilu.no](mailto:riskgone@nilu.no)

**BERGEN, 27 05 2023**

*The publication reflects only the author's view and the European Commission is not responsible for any use that may be made of the information it contains.*

